Processes essential for *Physcomitrium patens* protonemal development require distinct levels of total activity provided by functionally redundant PpROP GTPases

Aude Le Bail[1,2,*], Benedikt Kost[1,*], Janina Nüssel[1], Tamara Isabeau Lolis[1], David Koch[1], Hildegard Voll[1], Sylwia Schulmeister[1], Karin Ljung[3], Maria Ntefidou[1,#]

[1]Cell Biology, Department of Biology, Friedrich-Alexander-University Erlangen-Nürnberg, 91058 Erlangen, Germany

[2]Present address: Sorbonne Université, CNRS, Laboratoire de Biologie Intégrative des Modèles Marins, LBI2M, F-29680 Roscoff, France

[3]Umeå Plant Science Centre, Department of Forest Genetics and Plant Physiology, Swedish University of Agricultural Sciences, 90183 Umeå, Sweden

*contributed equally

[#]Corresponding author: maria.ntefidou@fau.de

Running title:

ROP GTPase functions in *P. patens* development

One-sentence summary:

Knock-out, complementation, and overexpression experiments further defined PpROP functions in *P. patens* development, and demonstrated their dependence on distinct levels of total PpROP activity.

The author responsible for the distribution of materials integral to the findings presented in this article in accordance with the policy described in the Instructions for Authors (https://academic.oup.com/plcell) is: Maria Ntefidou (maria.ntefidou@fau.de)

Abstract

RHO GTPases are key regulators of cellular and developmental processes in most eukaryotic organisms. ROPs (RHO of plants) constitute a plant-specific RHO subfamily. ROP families expanded and functionally diversified during the evolution of structurally complex vascular plants, but generally contain few members in non-vascular plants with ancient features. In vascular and non-vascular plants, ROP proteins are required for cell polarization, directional cell expansion, and mitotic cell plate positioning. All these processes are impaired by the disruption of PpROP activity in the non-vascular moss *Physcomitrium patens*. The aim of the study presented here was to further characterize PpROP functions during *P. patens* protonemal development by a) knocking out individually or in all possible combinations each of the four Rp*ROP* genes, which encode nearly identical proteins, b) complementing knock-out mutants with WT or mutant PpROP isoforms, or with heterologous homologs, and c) performing overexpression experiments. PpROPs were found to have additional previously unknown functions in the regulation of cell proliferation, caulonema differentiation, and gametophore formation. Furthermore, different cellular and developmental processes were shown to require distinct levels of total PpROP activity, rather than individual PpROP isoforms. Implications of the remarkable sequence conservation and functional integration within the PpROP protein family are discussed.

Keywords *Physcomitrium patens*, RHO/ROP GTPases, GTP/GDP cycling, polarity, directional cell expansion, cell plate positioning, cell proliferation, caulonema differentiation, gametophore development, apical initial cells, plant evolution

Introduction

RHO (RAS homologous) family small GTPases (guanosine triphosphate hydrolases) are expressed in most eukaryotic organisms (Boureux et al., 2007) and play key roles in the regulation of essential cellular processes with important functions in the development of multicellular tissues and organs (Etienne-Manneville and Hall, 2002; Kawano et al., 2014). Most RHO GTPases are associated with the plasma membrane (PM) based on posttranslational prenylation, interact with different effectors to trigger downstream signaling specifically in the GTP-bound confirmation, and are inactive when bound to

59 GDP after GTP hydrolysis. While regulatory factors that control RHO activity by
60 promoting GDP for GTP exchange, by stimulating GTP hydrolysis or by modulating PM-
61 association are closely related in different organisms (Berken et al., 2005; Kost, 2010;
62 Hodge and Ridley, 2016), RHO-dependent downstream signaling appears to be much
63 less conserved. Different families of RHO effectors are controlling similar cellular
64 processes in animals and in plants (Heasman and Ridley, 2008; Yalovsky et al., 2008;
65 Müller, 2023; Ntefidou et al., 2023). Furthermore, RHO effectors playing key roles in the
66 regulation of important cellular processes in complex vascular plants are either entirely
67 missing (Eklund et al., 2010; Ou and Yi, 2022) or have completely different functions in
68 non-vascular plants with more ancient features (Ntefidou et al., 2023).

69 RHO functions in the control of developmentally relevant cellular processes including
70 polarization, directional growth, motility, and division have been extensively
71 characterized both in animals and in plants. However, the direct demonstration of RHO
72 functions in tissue and organ development based on the investigation of loss-of-function
73 mutants has been hampered by substantial redundancy within large families of RHO
74 proteins typically expressed in complex multicellular organisms and, possibly, by
75 essential roles of at least some of these proteins in the development of such organisms
76 (Mulvey and Dolan, 2023b).

77 ROP (RHO of Plants) functions have been most extensively studied in *Arabidopsis*
78 *thaliana*, a complex flowering plant with an elaborate vascular system, which expresses
79 11 AtROPs sharing 80-98 % amino acid sequence identity (Li et al., 1998; Winge et al.,
80 2000). The functional characterization of these proteins largely depended on the
81 investigation 1) of loss-of-function mutants, and 2) of effects of overexpressing either
82 wild type (WT) AtROPs, or mutant versions of these proteins locked in the GTP-bound
83 conformation (constitutively active) or displaying reduced nucleotide affinity (moderate
84 reduction: fast-cycling, strong reduction: dominant negative). Different AtROPs were
85 determined to play distinct but partially overlapping (Feiguelman et al., 2018) essential
86 roles in the control of the following cellular processes: 1) extremely polarized tip growth
87 displayed by pollen tubes (Li et al., 1999; Luo et al., 2017) and root hairs (Molendijk et
88 al., 2001; Denninger et al., 2019), 2) diffuse directional expansion of leaf epidermal
89 pavement cells (Fu et al., 2005; Lauster et al., 2022), 3) morphogenesis of single-celled

90 trichomes (Liu et al., 2023), and 4) mitotic cell plate positioning required for tissue
91 patterning in developing roots (Roszak et al., 2021).

92 Interestingly, Arabidopsis mutants disrupted in the expression of multiple At*ROP* genes
93 show severely aberrant root hair and/or epidermal leaf pavement cells morphogenesis,
94 but no substantial defects in tissue organization and organ development (Fu et al., 2005;
95 Ren et al., 2016). Similarly, the development of the liverwort *Marchantia polymorpha* is
96 not strongly affected by knocking out the single Mp*ROP* gene identified in this non-
97 vascular plant, even though defects in the formation of selected tissues and organs were
98 observed (Mulvey and Dolan, 2023b). The relatively weak phenotype of *M. polymorpha*
99 *rop* knock-out mutants obviously cannot be attributed to genetic redundancy. ROP
100 signaling therefore only appears to play a minor role in controlling the development in
101 this liverwort, which displays ancient features presumably similar to those of extinct
102 common ancestors of all land plants. By contrast, growth and development of the closely
103 related non-vascular moss *P. patens* are severely disrupted in knock-out or knock-down
104 mutants completely lacking or displaying minimal ROP activity (Burkart et al., 2015;
105 Cheng et al., 2020; Yi and Goshima, 2020; Bao et al., 2022). These mutants only form
106 tiny colonies of irregularly shaped cells, which are unable to directionally expand,
107 differentiate or form organized tissues. The phenotype of these mutants established that
108 *P. patens* development strictly depends on the total activity of the four nearly identical
109 PpROPs expressed in this moss, which share 99.5-100 % amino acid identity and
110 display sequence variability only outside of known functional domains at positions 148
111 and 149 (Eklund et al., 2010). However, currently available data concerning PpROP
112 functions leave several important questions unanswered: 1) does PpROP activity only
113 exert previously identified functions in the control or cell polarization, directional cell
114 expansion and mitotic cell plate positioning, or is this activity also required for other
115 cellular and developmental processes?, 2) are different processes controlled by
116 individual ROP isoforms or by the combined activity of multiple PpROPs?, 3) are the four
117 PpROPs functionally redundant or do they differentially contribute to total PpROP
118 activity?, and 4) which evolutionary mechanisms may account for the origin and
119 maintenance of the PpROP protein family with its exceptionally high amino acid
120 sequence conservation?

121 The development of haploid *P. pates* gametophytes, which are composed of protonemal
122 filaments and gametophores, is an ideal system to further characterize PpROP
123 functions. This process 1) dominates the *P. patens* life cycle, 2) relies on cell
124 polarization, tip growth, strictly controlled cell plate positioning, and additional cellular or
125 developmental processes, and 3) is highly amenable to genetic manipulation based on
126 homologous recombination and CRISPR/Cas (Schaefer and Zrÿd, 1997; Cove, 2005;
127 Collonnier et al., 2017; Rensing et al., 2020). Gametophyte development starts with the
128 germination of haploid spores, which results in the formation of branched filamentous
129 protonemata. These structures can also be induced to develop *in vitro* from isolated
130 protonemal protoplasts or explants, with protoplast-derived colonies more closely
131 recapitulating normal development (Grimsley et al., 1977; Kofuji and Hasebe, 2014). A
132 single apical initial cell at the tip of each protonemal filament expands by tip growth and
133 regularly divides transversely, resulting in filament elongation. The association of
134 different PpROPs with the PM of apical initial cells specifically at the tip, as well as
135 underneath the transversal cell wall separating these cells from subapical cells, is
136 consistent with essential functions of PpROP activity in tip growth and cell plate positing
137 (Le Bail et al., 2019; Cheng et al., 2020; Yi and Goshima, 2020). While young
138 protonemal filaments display chloronemal characteristics, the initial cells at their tips
139 undergo gradual caulonema differentiation, which is associated with 1) an increased rate
140 of tip growth and proliferation, 2) a reduction in chloroplast size and number, and 3) the
141 formation of oblique rather than perpendicular transversal cell walls (Jaeger and Moody,
142 2021). Interestingly, caulonema differentiation is stimulated by the phytohormone auxin
143 (Jang and Dolan, 2011) and has recently been demonstrated to be effectively blocked by
144 the RpROP effector PpRIC downstream of auxin-induced changes in gene expression
145 (Ntefidou et al., 2023). Filament branching as well as the formation of lateral buds
146 developing into gametophores are initiated by the asymmetric division of subapical
147 caulonemal cells. As this process is defective in mutants lacking 3 of the four PpROPs, it
148 also appears to be controlled by PpROP activity (Yi and Goshima, 2020). Mature
149 gametophores are composed of leafy shoots with leaf-like phyllids and filamentous
150 rhizoids, which are free of chloroplasts but otherwise closely resemble caulonemal
151 filaments and elongate based on the same mechanisms. Reproductive organs produced
152 at the tip of mature gametophores mediate sexual reproduction, which initiates

153 sporophyte development that corresponds to the short diploid phase of the life cycle. To
154 address open questions concerning PpROP functions during different phases of *P.*
155 *patens* gametophyte development, systematic knock-out, complementation and
156 overexpression experiments were performed.

157 **Results**

158 **Individual Pp*ROP* genes are not essential for protonemal development**

159 Previously reported quantitative polymerase chain reaction (RT-qPCR) and RNA-
160 sequencing data demonstrated similar expression levels of all four Pp*ROP* genes in
161 developing protonemata (Perroud et al., 2018, Ntefidou et al., 2023). RT-qPCR analyses
162 performed here essentially confirmed these observations, although Pp*ROP4* was found
163 to display about 2x higher transcript levels as compared to the other three genes
164 (Supplementary Fig. S1). Based on these data, all four PpROPs appear to contribute to
165 the control of protonemal growth and/or differentiation.

166 To systematically investigate PpROP functions in protonemal development, homologous
167 recombination (Schaefer et al., 1991) was employed to replace all Pp*ROP* genes
168 individually and in every possible combination by antibiotic resistance genes. Knockout
169 (KO) lines obtained were verified by PCR genotyping (Supplementary Figs. S2A and B,
170 S3 and S4). Higher order mutants were generated sequentially, starting with *rop1*, *rop2*,
171 *rop3*, and *rop4* single KO lines (Supplementary Fig. S2C, upper panel). To enable
172 comparative quantitative characterization of KO phenotypes, protonemata regenerated
173 from isolated protoplasts were investigated at defined developmental stages. At least
174 two independent lines per genotype were generally characterized, except for the *rop2*,
175 *rop4*, r*op4/1* and *rop2/4/1* genotypes, which were only obtained once. Independently
176 generated genotypically identical lines in all cases displayed indistinguishable
177 phenotypes.

178 None of the four single *rop* KO mutants (*rop*^{1xKO}) displayed detectable defects in a) the
179 length of fully expanded subapical chloronemal or caulonemal cells (Supplementary Fig.
180 S5A), b) the morphology of the tips of chloronemal or caulonemal filaments
181 (Supplementary Fig. S5B), c) the rate of caulonema differentiation (Supplementary Fig.
182 S5C), which is enhanced in a KO mutant lacking the PpROP effector PpRIC (*ric-1*^{KO},

183 Ntefidou et al., 2023), or d) the size or morphology of 5-day-old protonemata or of 5
184 week-old colonies (Supplementary Fig. S5D-F). These observations establish that each
185 individual *ROP* gene is dispensable for cell expansion and differentiation during
186 protonemal development.

187 **Mutants lacking any combination of two Pp*ROP* genes display enhanced**
188 **caulonema differentiation**

189 The six *rop*^{2xKO} mutants lacking two Pp*ROP* genes in all possible combinations did not
190 show detectable defects in cell expansion or morphology in 5-day-old protonemata,
191 except for an apparent minor decrease in the size of *rop4/1* protonemata (Fig. 1A, B, D
192 and F). However, at the same developmental stage caulonema differentiation was
193 substantially enhanced to a similar extent in all *rop*^{2xKO} mutants (Fig. 1C), establishing
194 an essential function of PpROP activity in the inhibition of this process. Caulonema
195 differentiation was proposed to be triggered when elongating apical chloronemal cells
196 reach a threshold length (Jang and Dolan 2011). Since the length of chloronemal cells
197 was not affected in *rop*^{2xKO} mutants (Fig. 1A), enhanced caulonema differentiation
198 displayed by these mutants is not a secondary effect of altered cell expansion, but
199 appears to be a direct consequence of reduced PpROP activity.

200 As none of the *rop*^{1xKO} mutants showed enhanced caulonema differentiation
201 (Supplementary Fig. S5C), any combination of three Pp*ROP* genes evidently is sufficient
202 for the inhibition of this process in normally developing protonemata, which has
203 previously been shown to also require the PpROP effector PpRIC (Ntefidou et al., 2023).
204 PpRIC was demonstrated to inhibit caulonema differentiation downstream of gene
205 expression controlled by indole-3-acetic acid (IAA), an auxin-family phytohormone with a
206 key role in the stimulation of this process (Jaeger and Moody, 2021). To further
207 investigate whether PpROP activity and PpRIC act together in the same pathway to
208 inhibit caulonema differentiation as proposed by Ntefidou et al. (2023), IAA levels, a
209 marker for auxin transport and auxin dependent-gene expression were analyzed in
210 *rop*^{2xKO} mutants. Like *ric-1*^{KO} mutants (Ntefidou et al., 2023), all *rop*^{2xKO} mutants were
211 found a) to contain wild-type IAA levels (Supplementary Fig. S6A), b) to display normal
212 accumulation of the key auxin transporter PpPINA (PIN-FORMED A auxin efflux carrier;
213 Viaene et al., 2014) specifically in the PM at the tip of apical protonemal cells

214 (Supplementary Fig. S6B), and c) to express at normal levels different auxin-responsive
215 genes (Supplementary Fig. S6C), which are required for auxin-induced caulonema
216 differentiation (Pp*RSL1*; *ROOTHAIR DEFECTIVE SIX-LIKE1*; Jang et al., 2011), or have
217 essential functions in auxin biosynthesis (Pp*SHI1*; *SHORT INTERNODES1*; Eklund et
218 al., 2010b), transport (Pp*PINA*) or signaling (Pp*AUX1*; *AUXIN RESISTANT 1*; Lavy et
219 al., 2016). These observations establish that PpROP activity, like PpRIC, inhibits
220 caulonema differentiation without affecting auxin-controlled gene expression, supporting
221 the notion that PpROP activity regulates this process via PpRIC stimulation.

222 Consistent with a considerably higher growth rate of caulonemal as compared to
223 chloronemal filaments (Cove and Knight, 1993), enhanced caulonema differentiation
224 substantially enlarged the size of 5-week-old *ric-1*^{KO} colonies (Ntefidou et al., 2023). By
225 contrast, despite enhanced caulonema differentiation, the size of 5-week-old *rop*^{2xKO}
226 colonies was significantly reduced (Fig. 1E and G), although as discussed above, 5-day-
227 old *rop*^{2xKO} protonemata did not display substantial growth defects (Fig. 1A, B, D and F).
228 Based on these observations, PpRIC appears to be exclusively required for the
229 inhibition of caulonema differentiation, whereas RpROP activity, as previously
230 demonstrated, also promotes cell and protonemata expansion, evidently by stimulating
231 other effectors. However, it is important to note that *rop*^{2xKO} protonemata displayed
232 minimal growth defects, which only became apparent late during development and did
233 not prevent the detection of enhanced caulonema differentiation at an earlier stage.

234 **Cell and protonemal expansion are severely disrupted in mutants lacking any**
235 **combination of three Pp*ROP* genes**

236 Consistent with a previously reported phenotypic analysis of *P. patens rop1/2/3* and
237 *rop2/3/4* triple KO mutants (Yi and Goshima, 2020), 5-day-old protonemata of each of
238 the four *rop*^{3xKO} mutants lacking three Pp*ROP* genes in all possible combinations
239 displayed severe growth defects (Fig. 2A, B, D and G). Already at this early
240 developmental stage, the length of apical and subapical chloronemal and caulonemal
241 cells (Fig. 2A and B), as well as the size of protonemata (Fig. 2D and G), were
242 substantially decreased. Interestingly, at the same developmental stage and by contrast
243 to *rop*^{2xKO} mutants, *rop*^{3xKO} mutants did not display enhanced caulonema differentiation
244 (Fig. 2C). As caulonema differentiation seems to depend on a cell length threshold (Jang

245 and Dolan, 2011), reduced cell expansion appears to inhibit this process in *rop*^{3xKO}
246 protonemata.

247 The analysis of 5-week-old *rop*^{3xKO} colonies revealed even more pronounced growth
248 defects (Fig. 2E and H). Interestingly and consistent with previously reported
249 observations (Yi and Goshima, 2020), at this developmental stage *rop*^{3xKO} colonies
250 formed gametophores with small but morphologically essentially normal leafy shoots
251 and even more severely stunted rhizoids (Fig. 2F, H and I), which like protonemata are
252 composed of filaments that elongate based on apical tip growth. The phenotypic
253 characterization of *rop*^{3xKO} protonemata and gametophores therefore not only confirms
254 essential functions of PpROP activity in the control of tip growth but also suggests less
255 important roles of this activity in other forms of directional cell expansion, which are
256 required for leafy shoot development. Whereas tip growth is strongly reduced in all
257 *rop*^{3xKO} mutants (Fig. 2), this process is only marginally affected in all *rop*^{2xKO} mutants
258 (Fig. 1). The expression of any combination of two PpROPs therefore appears to be
259 sufficient to support nearly normal tip growth.

260 **All four PpROPs are equally capable of promoting tip growth**

261 Amino acid sequence identities of at least 99.5 % within the PpROP protein family,
262 together with highly similar phenotypes of all *rop*^{2xKO} (Fig. 1) and *rop*^{3xKO} (Fig. 2) mutants
263 revealed by quantitative characterization, suggest essentially equivalent functions in all
264 four PpROPs in developing protonemata. However, cell and protonema expansion was
265 reduced to a remarkably variable extent in *rop*^{3xKO} mutants expressing distinct single
266 PpROP family members (Fig. 2B, D and E), indicating that these proteins may differ in
267 their ability to promote tip growth. Alternatively, the observed phenotypic variability of
268 *rop*^{3xKO} mutants may be caused a) by differential up- or down-regulation of the
269 expression of the remaining Pp*ROP* gene after the disruption of the other members of
270 the Pp*ROP* gene family, b) by different genetic backgrounds resulting from multiple
271 rounds of gene replacement based on homologous recombination, and/or c) by the
272 expression of variable sets of selectable marker genes resulting from this procedure.

273 RT-qPCR analysis established that in all four *rop*^{3xKO} mutants the remaining Pp*ROP*
274 gene was expressed at the same level as the corresponding gene in the wild type

275 background (Fig. 3A). This demonstrates that the phenotypic variability displayed by
276 *rop*^{3xKO} mutants is not caused by differential feed-back control of transcript levels within
277 the Pp*ROP* gene family. To distinguish between the other possible causes of phenotypic
278 variability displayed by *rop*^{3xKO} mutants, the activity of all PpROP family members was
279 directly compared by individually expressing each of them under the control of the same
280 promoter in an identical genetic background. To this end, based on homologous
281 recombination the coding sequence (exons and introns) and 3′ untranslated region
282 (UTR) of the endogenous Pp*ROP1* gene in the *rop3/2/4* background was replaced by
283 CDS (coding sequence) fragments encoding PpROP1, PpROP2, or PpROP3, which
284 were attached to the Pp*ROP1*, Pp*ROP2*, or Pp*ROP3* 3′ UTR, respectively
285 (Supplementary Fig. S2A and C: lower panel). As PpROP1 and PpROP4 share identical
286 amino acid sequences, the Pp*ROP4* CDS was not included in this analysis. Resulting
287 *rop*^{4xKO}/*ROP1*^{pro}:*ROPX* lines (at least two per genotype) were confirmed by PCR
288 genotyping (Supplementary Fig. S2B) and in essence represent *rop*^{4xKO} mutants sharing
289 an identical genetic background, which are complemented by the expression of different
290 single PpROPs under the control of the endogenous Pp*ROP1* promoter. RT-qPCR
291 analysis confirmed that each of the *ROP1*^{pro}:*ROPX* genes was expressed in the *rop*^{4xKO}
292 background at a similar level as the endogenous Pp*ROP1* gene in the *rop3/2/4* mutant
293 or in WT protonema (Fig. 3B). Size and morphology of 5-day-old protonemata as well as
294 of 5-week-old colonies formed by all *rop*^{4xKO}/*ROP1*^{pro}:*ROPX* lines were found to be
295 indistinguishable (Fig. 3C-E), establishing that all four 4 PpROPs are equally capable of
296 promoting tip growth.

297 **Disruption of all four Pp*ROP* genes completely abolishes polarized cell expansion**
298 **and affects cell division**

299 Two independent *rop*^{4xKO} lines were generated (Supplementary Fig. S2C: upper panel)
300 by knocking out based on homologous recombination either Pp*ROP1* in the *rop3/2/4*
301 background (*rop3/2/4/1*; Supplementary Fig. S2A and B) or Pp*ROP2* in the *rop3/4/1*
302 background (*rop3/4/1/2*; Supplementary Fig. S3A and B). Both *rop*^{4xKO} lines displayed
303 the same phenotype (Fig. 4A) as previously described *P. patens* mutants, in which the
304 expression of all 4 *PpROP* genes was disrupted either by RNAi/microRNA-mediated
305 downregulation (Burkart et al., 2015; Bao et al., 2022), by CRISPR/Cas9 (clustered

306 regularly interspaced short palindromic repeats/CRISPR-associated nuclease 9)-
307 mediated KO (Cheng et al., 2020), or by a combination of these approaches (Yi and
308 Goshima, 2020). Mutants entirely or nearly completely lacking PpROP activity form tiny
309 colonies of irregularly shaped cells (Fig. 4A). By contrast to cells containing at least one
310 functional PpROP gene (*rop*^{3xKO}), protonemal *rop*^{4xKO} cells were unable a) to undergo
311 normal polarization, b) to maintain parallel orientation of cell division planes required for
312 the development of linear filaments, or c) to directionally expand (Fig. 4A and B). When
313 cultured for prolonged periods of time, *rop*^{4xKO} colonies continued to slowly grow based
314 on cell division but failed to differentiate and did not develop gametophores.
315 Interestingly, *rop*^{4xKO} lines essentially phenocopy *P. patens* KO mutants lacking
316 geranylgeranyltransferase type I activity (Thole et al., 2014), suggesting that PpROPs
317 require prenylation by this activity to be functional (Bao et al., 2022).

318 In addition to the defects described in the previous paragraph, quadruple Pp*ROP* RNAi
319 knock-down mutants were demonstrated to also display reduced cell adhesion and
320 altered cell wall composition (Burkart et al., 2015; Bao et al., 2022). Consistent with
321 these observations, protoplasts could not be isolated from colonies formed by the two
322 different *rop*^{4xKO} mutants described here, hampering the comparative quantitative
323 phenotypic characterization of these mutants. To circumvent this issue, conditionally
324 complemented *rop*^{4xKO} lines were generated. Based on homologous recombination the
325 coding sequence (exons and introns) and 3′ UTR of the Pp*ROP3* gene in the *rop2/4/1*
326 background was replaced by a CDS fragment encoding PpROP2, which was fused at 5'-
327 end to an estradiol-inducible lexa/35S promoter (Kubo et al., 2013) and at the other end
328 to the Pp*ROP2* 3′ UTR (Supplementary Figs. S2C: lower panel; and S3C). The two
329 independent *rop*^{4xKO}/*ind*^{pro}:*ROP2* lines obtained based on this procedure were confirmed
330 by PCR genotyping (Supplementary Fig. S3D). In the absence of estradiol, these lines
331 produced Pp*ROP2* transcripts at substantially lower levels as compared to the *rop3/4/1*
332 mutant (Fig. 4C), and displayed a typical *rop*^{4xKO} phenotype after 5 days and after 5
333 weeks in culture (Fig. 4D). Adding 10^{-3} µM estradiol to the culture medium resulted in
334 partial complementation of the *rop*^{4xKO} phenotype, which enabled protoplast isolation.

335 Quantitative comparison of protoplast-derived 5-day-old protonemata growing on
336 estradiol-free culture medium confirmed that *rop*^{4xKO}/*ind*^{pro}:*ROP2* colonies displaying a

337 *rop*^{4xKO} phenotype were significantly smaller than *rop3/4/1* colonies (Fig. 4E), which
338 showed the strongest growth defects of all *rop*^{3xKO} mutants when compared to WT (Fig.
339 2D and E). Remarkably, counting DAPI (4′,6-diamidino-2-phenylindole)-labeled nuclei in
340 protoplast-derived protonemata grown for 4 days in the absence of estradiol (Fig. 4F)
341 established that the observed stepwise reduction of the size of WT, *rop3/4/1* and
342 *rop*^{4xKO}/*ind*^{pro}:*ROP2* (*rop*^{4xKO} phenotype) protonemata (Fig. 4E) is a consequence not
343 only of inhibited cell expansion but also of a similar stepwise decrease in the rate of cell
344 division (Fig. 4G). The cell division rate of apical protonemal cells is enhanced by
345 caulonema differentiation (Cove and Knight, 1993; Jang and Dolan, 2011) and possibly
346 by rapid cell expansion (Fantes and Nurse, 1977; Jones et al., 2017). The complete
347 disruption of both these processes in *rop*^{4xKO} mutants (Fig. 4) and the partial inhibition of
348 cell expansion in *rop*^{3xKO} mutants (Fig. 2), therefore appear likely to be partially
349 responsible for the reduced cell proliferation displayed by these mutants. However, like
350 related mammalian RHO GTPases (Coleman et al., 2004), PpROPs may also directly
351 target cell cycle regulation to enhance the rate of cell division, in addition to promoting
352 cell expansion and differentiation.

353 Comparing the phenotypes of *rop*^{4xKO} mutants and of the four *rop*^{3xKO} mutants
354 expressing distinct individual PpROPs (Figs. 2-4) establishes that each of these proteins
355 alone is capable of inducing not only normal polarization and directional expansion
356 (albeit at the reduced rate) of protonemal cells, but also parallel cell division plane
357 positioning, which is required for the development of linear filaments. Consistent with an
358 important role of PpROP activity in cell division plane positioning, defects in this process
359 were also observed a) in asymmetrically dividing cells in Arabidopsis roots
360 overexpressing constitutively active mutant AtROP9 (Roszak et al., 2021) or in maize
361 leaves lacking functional Zm*ROP2* and Zm*ROP9* genes (Humphries et al., 2011), b)
362 during branch formation in *P. patens rop*^{3xKO} protonemata (Yi and Goshima, 2020), and
363 c) in different tissues of the closely related liverwort *Marchantia polymorpha* after the
364 disruption of the single Mp*ROP* gene expressed in this organism (Mulvey and Dolan,
365 2023b). Interestingly, quantitative phenotypic characterization of *rop*^{3xKO} and *rop*^{4xKO}
366 mutants further demonstrated that PpROP activity directly and/or indirectly promotes the
367 rate of cell division in growing protonemata. In summary, based on the investigation of

368 these mutants PpROP activity was determined to control protonemal morphogenesis by
369 promoting cell polarization, parallel cell division plane positioning, cell proliferation, and
370 directional cell expansion.

371 **Estradiol-induced Pp*ROP2* expression at increasing levels progressively**
372 **complements different defects displayed by *rop*^{4xKO} mutants**

373 Data generated by the quantitative phenotypic characterization of *rop*^{KO} mutants (Figs.
374 1,2 and 4), and by the investigation of the ability of different PpROPs to complement
375 *rop*^{4xKO} phenotypes (Fig. 3), strongly suggests that a) the four nearly identical PpROPs
376 are functionally redundant, and b) increasing levels of total PpROP activity in apical
377 protonemal cells are required for the normal polarization, division, expansion and
378 differentiation of these cells (in this order). To further support these findings, the
379 phenotypes of *rop*^{4xKO}/*ind*^{pro}:*ROP2* protonema were investigated, in which Pp*ROP2*
380 expression was gradually induced by increasing estradiol concentrations in the culture
381 medium. Estradiol concentrations eliciting striking phenotypic alterations were selected
382 for this analysis (Fig. 5A). Control experiments confirmed that estradiol at these
383 concentrations did not affect the development of WT protonemata (Supplementary Fig.
384 S7).

385 At concentrations of up to $4x10^{-4}$ µM, estradiol-induced Pp*ROP2* expression remained
386 much lower as compared to the WT expression level of this gene (Fig. 5B), which also
387 corresponds to the level of total Pp*ROP* gene expression in *rop3/4/1* and in other *rop*^{3xKO}
388 mutants (Fig. 3A, Supplementary Fig. S1). A linear correlation between estradiol
389 concentrations of up to $4x10^{-4}$ µM and resulting minimal levels of Pp*ROP2* expression,
390 which were near the detection limit, could not be established based on RT-qPCR
391 analysis (Fig. 5B). Pp*ROP2* expression induced by $9x10^{-4}$ µM estradiol was about 2.3x
392 stronger than in WT protonemata (Fig. 5B) and thus reached a level comparable to total
393 Pp*ROP* gene expression in *rop*^{2xKO} mutants (2-3x WT Pp*ROP2* expression level;
394 Supplementary Fig. S1). Unfortunately, higher estradiol concentrations failed to further
395 enhance Pp*ROP2* expression to levels comparable to total Pp*ROP* gene expression in
396 normally developing *rop*^{1xKO} or WT protonemata (3-4x or 5x WT Pp*ROP2* expression
397 level, respectively; Supplementary Fig. S1).

398 As already shown above (Fig. 4D), in the absence of estradiol *rop*^{4xKO}/*ind*^{pro}:*ROP2*
399 protonema displayed a typical *rop*^{4xKO} phenotype after 5 days and after several weeks in
400 culture (Fig. 5). Remarkably, induction of Pp*ROP2* expression at the lowest level by
401 2x10^{-5} µM estradiol partially restored cell polarization and parallel cell division plane
402 positioning required for filament formation (Fig. 5A), without substantially promoting
403 directional cell expansion (Fig. 5C and E, Supplementary Table S1) or supporting
404 caulonema differentiation (Fig. 5D). These observations demonstrate that cell
405 polarization and parallel cell division plane positioning can be uncoupled from directional
406 cell expansion, and that these processes depend on different levels of total PpROP
407 activity.

408 On solid culture medium containing 2x10^{-4} µM estradiol, at low frequency chloronemal
409 filaments were formed, which elongated based on directional cell expansion (Fig. 5A,
410 Supplementary Table S1). However, this process was not fully restored, as subapical
411 cells in these filaments were much shorter than corresponding WT cells (Fig. 5C), and
412 colony growth remained strongly restricted (Fig. 5A and E). Caulonema differentiation
413 (Fig. 5A and D) or gametophore formation (Fig. 5A) was not observed under these
414 conditions. Interestingly, colonies growing for 4 weeks in liquid medium containing
415 estradiol at the same concentration, and displaying an otherwise indistinguishable
416 phenotype, frequently developed small gametophore-like structures, which contained
417 two to four rudimentary phyllids, but failed to form stems or rhizoids (Fig. 5A). This
418 finding is consistent with previous reports demonstrating that liquid culture can promote
419 gametophore formation (Reski and Abel, 1985). As similar gametophore-like structures
420 were never formed by *rop*^{4xKO}/*ind*^{pro}:*ROP2* colonies growing in liquid medium containing
421 estradiol at lower concentrations, PpROP activity at minimal levels appears to be able to
422 induce the formation of gametophore-like structures even in the absence of caulonema
423 differentiation. Furthermore, PpROP activity at these levels evidently is sufficient for the
424 development of rudimentary phyllids.

425 Pp*ROP2* expression induced by 4x10^{-4} µM estradiol further promoted directional cell
426 expansion (Fig. 5A and C; Supplementary Table S1) and partially rescued caulonema
427 differentiation (Fig. 5A and D). This led to a substantial increase in the size of 4-week-old
428 colonies (Fig. 5A and E) and was accompanied by the frequent development of regular

429 gametophores with a reduced size and severely stunted rhizoids on solid culture
430 medium (Fig. 5A). However, the length of subapical protonemal cells, the rate of
431 caulonema differentiation, as well as the size of 5-days-old and 4-weeks-old colonies
432 remained significantly decreased. Interestingly, essentially the same developmental
433 defects are shown by *rop*^{3xKO} mutants (Fig. 2), although the phenotype of these mutants
434 appears to be somewhat weaker, as they display caulonema differentiation at WT rates,
435 which are significantly reduced only in comparison to *rop*^{2xKO} mutants.

436 Finally, *rop*^{4xKO}/*ind*^{pro}:*ROP2* protonemata growing in medium containing 9x10^{-4} µM
437 estradiol essentially phenocopied *rop*^{2xKO} mutants (Figs. 1 and 5, Supplementary Table
438 S1), which as discussed above exhibit similar levels of total Pp*ROP* gene expression. As
439 compared to WT protonemata, *rop*^{4xKO}/*ind*^{pro}:*ROP2* protonemata expressing Pp*ROP2* at
440 this level of induction displayed significantly enhanced caulonema differentiation (Fig.
441 5D), while subapical cell length in 5-day-old protonemata was not detectably affected
442 (Fig. 5C), and colony size after 5 days or after 4 weeks in culture as well as
443 gametophore growth were only weakly reduced (Figs. 5A and E).

444 Data presented in this section demonstrate that PpROP2, a single member of the
445 PpROP family, can effectively complement different severe defects displayed by *rop*^{4xKO}
446 mutants. Partially interdependent developmental processes disrupted in these mutants
447 were progressively restored by increasing levels of estradiol-induced Pp*ROP2*
448 expression, indicating that these processes require distinct levels of total PpROP
449 activity, rather than specific individual ROPs. Listed in the order of their increasing
450 requirement for total PpROP activity, the following processes were restored by estradiol-
451 induced PpROP2 expression: a) cell polarization and parallel cell division plane
452 positioning required for filament formation, b) directional cell expansion, and c)
453 development of gametophore-like structures or small gametophores, and d) caulonema
454 differentiation.

455 **Pp*ROP* overexpression inhibits caulonema differentiation and depolarizes**
456 **directional cell expansion**

457 To investigate effects of PpROP overexpression, based on homologous recombination a
458 CDS fragment encoding PpROP1, which was fused at the 5'-end to the estradiol-

459 inducible lexa/35S promoter and at the other end to the Pp*ROP1* 3′ UTR, was
460 introduced into a neutral region (Schaefer et al., 1991) of the WT genome
461 (Supplementary Fig. S2D). One of the resulting WT/*ind*^{pro}:*ROP1* lines, which displayed
462 massive estradiol-inducible Pp*ROP1* overexpression, was confirmed by PCR
463 genotyping (Supplemental Fig. S2E) and selected for phenotypic characterization. In the
464 absence of estradiol, protoplast-derived protonemata of this line expressed Pp*ROP1* at
465 WT level (Fig. 6A) and displayed no developmental defects (Fig. 6B-H). Growing these
466 protonemata on solid medium containing 10^{-3} µM estradiol resulted in Rp*ROP1*
467 expression at a more than 150x higher level (Fig. 6A), which roughly corresponds to a
468 30x increase in total Pp*ROP* gene expression as compared to WT protonemata (total
469 Pp*ROP* gene expression ca. 5x stronger than Pp*ROP1* expression; Supplementary Fig.
470 S1). Control experiments showed that estradiol at this concentration did not affect
471 Pp*ROP1* expression or developmental processes in WT protonemata (Supplementary
472 Fig. S7).

473 As discussed above, PpROP activity was concluded to directly inhibit caulonema
474 differentiation based on the observation that this process is enhanced in otherwise
475 essentially normally developing *rop*^{2xKO} protonemata (Fig. 1). Further supporting this
476 conclusion, Pp*ROP1* overexpression effectively disrupted caulonema differentiation (Fig.
477 6B). In angiosperm pollen tubes and root hairs excess ROP activity strongly depolarizes
478 tip growth and results in massive apical ballooning (Chen et al., 2003; Gu et al., 2003a;
479 Klahre and Kost, 2006; Kost, 2008). Overexpression of a fluorescent PpROP2 fusion
480 proteins was reported to have similar but comparably weaker effects on directional
481 expansion at the tip of *P. patens* protonemata (Ito et al., 2014). Quantitative analysis of
482 protoplast-derived WT/*ind*^{pro}:*ROP1* protonemata revealed that high-level Pp*ROP1*
483 overexpression strongly reduced the length and enhanced the width of subapical cells in
484 chloronemal filaments (Fig. 6C-E), which indicates massive depolarization of tip growth
485 displayed by adjacent apical cells. Interestingly, PpPOP1 overexpression caused the
486 apical dome of these cells to oscillate at irregular intervals between a wide flattened and
487 a narrow pointed morphology (Fig. 6E). Together, inhibited caulonema differentiation and
488 defective cell expansion strongly reduced the size of Pp*ROP1*-overexpressing 5-day-old
489 protonemata and of 4-week-old colonies (Fig. 6F-H). Remarkably, WT/*ind*^{pro}:*ROP1*

490 protonemata never developed gametophores when growing on solid or in liquid medium
491 containing 10^{-3} µM estradiol, demonstrating that PpPOP1 overexpression effectively
492 blocked the formation of these structures (Fig. 6H).

493 In summary, consistent with and further defining PpROP functions identified by the
494 phenotypic characterization of *rop*^{KO} mutants, PpROP1 overexpression prevented
495 caulonema differentiation, effectively depolarized cell expansion at the tip of protonemal
496 filaments, strongly reduced protonemal growth, and completely blocked gametophore
497 formation. Overexpression of the PpROP effector PpRIC (ca. 40x WT Pp*RIC* expression
498 level) also strongly inhibited caulonema differentiation and gametophore formation, but
499 did not depolarize directional cell expansion and, consequently, only weakly reduced
500 protonemal growth (Ntefidou et al., 2023). These observations strongly suggest that
501 PpROP inhibits caulonema differentiation via PpRIC activation, but interacts with other
502 effectors to control directional cell expansion. As discussed above, this conclusion is
503 further supported by the increase or decrease in colony size displayed by *ric-1*^{KO} and
504 *rop2x*^{KO} mutants, respectively. PpROP and PpRIC may also act together in a common
505 pathway to directly inhibit gametophore formation, as this process is completely blocked
506 by the overexpression of either of these two proteins. However, chloronemal filaments
507 were proposed to lack competence for gametophore formation during normal
508 protonemal development (Cove and Knight, 1993; Schumaker and Dietrich, 1997; Brun
509 et al., 2003; Harrison et al., 2009), indicating that PpROP or PpRIC overexpression may
510 indirectly block gametophore formation by inhibiting caulonema differentiation.
511 Consistent with this interpretation, increasing ROP activity progressively stimulates the
512 formation of gametophore-like structures and the development of gametophores (Figs. 2
513 and 5), suggesting that ROP activity promotes rather than inhibits these processes.

514 **PpROP functions in fundamental developmental processes depend on GDP/GTP**
515 **cycling**

516 Highly conserved amino acid residues can be mutated to alter the intrinsic rate of GDP/
517 GTP cycling displayed by RHO GTPases (Aspenström, 2019). These proteins are
518 locked in the GTP-bound state by mutations corresponding to the Q61L exchange in H-
519 RAS, which disrupt GTPase activity (GTP-locked). By contrast, mutations equivalent to
520 the F28L exchange in H-RAS reduce nucleotide-binding affinity and enhance intrinsic

521 GDP/GTP exchange (fast-cycling). Fast-cycling RHO mutants are preferentially GTP-
522 bound at high GTP/GDP concentration ratios typically observed in the cytoplasm of
523 eukaryotic cells. Like GTP-locked mutants, fast-cycling mutants are therefore
524 considered to be constitutively active. To assess the importance of GDP/GTP cycling for
525 PpROP functions in protonemal development, based on homologous recombination the
526 coding sequence (exons and introns) and 3′ UTR of the endogenous Pp*ROP1* gene in
527 the *rop3/2/4* background was replaced by CDS fragments encoding GTP-locked
528 PpROP1^{Q64L} or fast-cycling PpROP1^{F31L}, which were attached to the Pp*ROP1* 3′ UTR
529 (Supplementary Fig. S2A and C: lower panel). Resulting *rop*^{4xKO}/*ROP1*^{pro}:*ROP1*^{Q64L} and
530 *rop*^{4xKO}/*ROP1*^{pro}:*ROP1*^{F31L} lines were confirmed by PCR genotyping (Supplementary
531 Fig. S2B). Based on RT-qPCR analysis of 1-week-old protonemata, lines expressing
532 mutated Pp*ROP1* genes at the same level as Pp*ROP1* expression in WT plants and in
533 *rop3/2/4* mutants were identified (Fig. 7A) and selected for phenotypic characterization
534 (Fig. 7B-D).

535 Even after prolonged culture on solid medium, *rop*^{4xKO}/*ROP1*^{pro}:*ROP1*^{Q64L} colonies
536 displayed a typical *rop*^{4xKO} phenotype (Fig. 7B). As this phenotype includes cell wall
537 defects preventing protoplast isolation, *rop*^{4xKO}/*ROP1*^{pro}:*ROP1*^{Q64L} colonies shown were
538 grown from tissues explants. This remarkable observation established that GDP/GTP
539 cycling is strictly required for PpROP functions in fundamental developmental
540 processes, including cell polarization and parallel division plane positioning required for
541 filament formation. It remains to be determined whether GDP/GTP exchange is also
542 essential for ROP functions in directional cell expansion and other processes, which
543 appear to directly or indirectly depend on cell polarization and/or parallel division plane
544 positioning. Interestingly, like *rop*^{4xKO}/*ind*^{pro}:*ROP2* colonies in the presence of estradiol at
545 low concentration ($2x10^{-4}$ µM; Fig. 5A), *rop*^{4xKO}/*ROP1*^{pro}:*ROP1*^{Q64L} colonies frequently
546 formed gametophore-like structures exclusively when grown in liquid medium (Fig. 7C).
547 The induction of gametophore formation in the absence of caulonema differentiation, as
548 well as the promotion of rudimentary phyllid development by low-level PpROP activity,
549 therefore does not require GDP/GTP cycling.

550 Protoplast-derived 5-day-old and 5-week-old *rop*^{4xKO}/*ROP1*^{pro}:*ROP1*^{F31L} and *rop3/2/4*
551 protonemata displayed indistinguishable phenotypes (Fig. 7B). As compared to WT

552 protonemata, colony size was similarly reduced (Fig. 7D), caulonema differentiation was
553 not significantly affected (Fig. 7E), and gametophores with small but morphologically
554 essentially normal leafy shoots and severely stunted rhizoids were formed (Fig. 7C).
555 These data establish that by contrast to GTP-locked PpROP1^{Q64L}, which is severely
556 functionally impaired, fast-cycling PpROP1^{F31L} displays essentially the same ability as
557 WT PpROP1 to promote protonemal development. However, it remains to be
558 demonstrated that PpROP1^{F31L} is also capable of inhibiting caulonema differentiation
559 when expressed at endogenous level in a *rop*^{2xKO} mutant, or upon overexpression.

560 **Overexpression of heterologous RHO GTPases in the *rop*^{4xKO} background**
561 **suggests limited evolutionary conservation of PpROP downstream signaling**
562 To test the ability of heterologous RHO GTPases to complement total loss of PpROP
563 activity, AtROP7, the closest Arabidopsis PpROP homologue (Eklund et al., 2010), and
564 human HsRHOA, one of the most extensively characterized RHO GTPases (Bishop and
565 Hall, 2000), were overexpressed in the *rop*^{4xKO} background. To this end, based on
566 homologous recombination, the coding sequence (exons and introns) of the
567 endogenous Pp*ROP4* gene in the *rop3/1/2* background was replaced by CDS fragments
568 encoding AtROP7 or HsRHOA, which were fused at 5'-end to the estradiol-inducible
569 lexa/35S promoter (Supplementary Fig. S4A). Resulting *rop*^{4xKO}/*ind*^{pro}:At*ROP7* and
570 *rop*^{4xKO}/*ind*^{pro}:Hs*RHOA* lines were confirmed by PCR genotyping (Supplementary Fig.
571 S4B). Based on RT-qPCR analysis of 1-week-old protonemata (Fig. 8A), lines displaying
572 maximal At*ROP7* or Hs*RHOA* transcript levels upon estradiol-induction were selected
573 for phenotypic characterization (Fig. 8B and C). Maximal At*ROP7* and Hs*RHOA*
574 transcript levels obtained were about 40x or more than 500x, respectively, higher than
575 Pp*ROP4* transcript levels in WT plants and in *rop3/1/2* mutants (Fig. 8A), which roughly
576 corresponds to 16x or more than 200x higher transcript levels as compared to total
577 Pp*ROP* gene expression in WT protonemata (ca. 2,5x stronger than Pp*ROP4*
578 expression; Supplementary Fig. S1). Control experiments showed that estradiol at
579 concentrations of 10^{-3} µM or 1 µM, which maximally induced At*ROP7* or Hs*RHOA*
580 expression, respectively, did not affect developmental processes in WT protonemata
581 (Supplementary Fig. S7).

582 Remarkably, massive At*ROP7* or Hs*RHOA* over-expression complemented the *rop*^{4xKO}
583 phenotype to a similar extent (Fig. 8B and C) as estradiol-induced Pp*ROP2* expression
584 at minimal level (2x10^{-5} µM; Fig. 5). Cell polarization and parallel cell division plane
585 positioning required for filament formation were restored, whereas directional cell
586 expansion was not substantially promoted and caulonema differentiation was never
587 induced (Fig. 8B). Furthermore, even on solid culture medium, small gametophore-like
588 structures occasionally developed, which contained a few rudimentary phyllids, but
589 unlike regular WT or *rop*^{3xKO} gametophores failed to form stems or rhizoids (Fig. 8C).
590 These observations establish that massive overexpression of heterologous flowering
591 plant and mammalian RHO GTPases can restore fundamental developmental
592 processes in *rop*^{4xKO} mutants, which require minimal levels of total PpROP activity.
593 Consequently, PpROP downstream signaling controlling these processes appears to be
594 evolutionary conserved at least to some extent. Supporting this conclusion, in *P. patens*
595 KO mutants lacking geranylgeranyltransferase type I activity, which as discussed display
596 a *rop*^{4xKO} phenotype, cell polarization and parallel cell division plane positioning could be
597 restored by a YFP-AtROP1 fusion protein mutated to enable prenylation by
598 farnesyltransferases. However, when tested using the same approach, human HsRAC1
599 or HsKRAS4b did not show a similar ability to complement loss of PpROP activity (Bao
600 et al., 2022).

601 **Discussion**

602 PpROP functions in protonemal development were systematically investigated based on
603 quantitative phenotypic characterization a) of KO mutants lacking single Pp*ROP* genes
604 or multiple such genes in all possible combinations, b) of complemented *rop*^{4xKO} lines
605 expressing WT PpROPs, constitutively active PpROP1 mutants or heterologous RHO
606 GTPases either at endogenous or different estradiol-titrated levels, and c) of lines
607 displaying PpROP1 overexpression in the WT background. The results of these
608 analyses firmly establish a) that the four nearly identical PpROPs, which are co-
609 expressed at similar levels in protonemata, are functionally redundant, and b) that
610 different developmental processes depend on distinct levels of total PpROP activity,
611 rather than on specific individual ROPs (Fig. 9).

612 **PpROP activity induces cell polarization and parallel division plain positioning at**
613 **minimal levels, and increasingly promotes tip growth when further enhanced**
614 Low levels of total PpROP activity induce cell polarization and parallel cell division plane
615 positioning, which enables filament formation, but are insufficient for the promotion of
616 directional cell expansion. Tip growth of apical protonemal cells is induced at somewhat
617 higher total PpROP activity and is further promoted by increasing levels of this activity
618 until it reaches WT rates in *rop*^{1xKO} mutants (Fig. 9). High-level PpROP overexpression
619 massively depolarizes tip growth, similar to what has been observed in vegetative pollen
620 tube cells and in root hairs (Chen et al., 2003; Gu et al., 2003a; Klahre and Kost, 2006;
621 Kost, 2008). However, unlike these other cell types apical protonemal cells
622 overexpressing PpROP activity do not simply swell at the tip, but display complex growth
623 behavior that warrants further investigation (Fig. 6E). Despite these somewhat different
624 overexpression effects, ROP functions in the control of tip growth appear to be
625 essentially conserved from mosses to flowering plants. Yeast and mammalian RHO
626 GTPases also have well-characterized functions in the regulation of directional cell
627 expansion and related processes (Hall and Lalli, 2010; Ou and Yi, 2022).

628 **PpROP activity at WT and somewhat lower levels blocks caulonema**
629 **differentiation via PpRIC stimulation**
630 As caulonema differentiation is substantially enhanced both in *rop*^{2xKO} and *in ric-1*^{KO}
631 mutants, total PpROP activity at levels reached in *rop*^{1xKO} and in WT protonemata
632 appears to inhibit caulonema differentiation by stimulating the effector protein PpRIC
633 (Fig. 9; Ntefidou et al., 2023). This conclusion is further supported by the recent
634 demonstration that inhibition of PpROP activity by upstream regulators of the PpGAP
635 (GTPase activating proteins) and PpREN (ROP Enhancer) families also promotes
636 caulonema differentiation (Ruan et al., 2023). Consistent with these findings, caulonema
637 differentiation is almost completely blocked by PpROP1 (Fig. 9) or PpRIC (Ntefidou et
638 al., 2023) overexpression. However, as discussed above, apical chloronemal cells were
639 proposed to undergo caulonema differentiation after reaching a threshold length (Jang
640 and Dolan, 2011). Whereas PpRIC overexpression (ca. 40x WT Pp*RIC* expression level)
641 does not substantially affect directional cell expansion (Ntefidou et al., 2023) and
642 therefore appears to directly block caulonema differentiation, PpROP1 overexpression

643 (ca. 30x increase in total Pp*ROP* gene expression as compared to WT; Fig. 6A)
644 presumably interferes with this process also indirectly by disrupting tip growth. Similarly,
645 the inhibition of caulonema differentiation observed at PpROP activity levels lower than
646 those displayed by *rop*^{2xKO} mutants appears more likely to be a consequence of severely
647 reduced directional cell expansion (Fig. 9) than to indicate a direct role of low-level
648 PpROP activity in the stimulation of caulonema differentiation.

649 **PpROP activity contributes to the maintenance of apical initial cell identity**

650 Protonemal filaments elongate based on tip growth and regular division of apical initial
651 cells, which undergo gradual caulonema differentiation. PpROP activity appears to play
652 an important role in the maintenance of apical initial cell identity not only by stimulating
653 tip growth and by inhibiting caulonema differentiation as discussed above, but also by
654 promoting the rate of cell division. Supporting this notion and consistent with previously
655 reported functions of mammalian RHO GTPases in stimulating cell proliferation
656 (Coleman et al., 2004), cell division rates were increasingly reduced in *rop*^{3xKO} and in
657 *rop*^{4xKO} mutants (Fig. 9). As rapid cell expansion was proposed to enhance the
658 proliferation of apical protonemal cells (Fantes and Nurse, 1977; Jones et al., 2017),
659 PpROP activity may promote the division of these cells indirectly by increasing the rate
660 of tip growth, rather than directly by accelerating cell cycle progression. Alternatively,
661 PpROP activity may stimulate both these processes.

662 **PpROP activity induces the formation of gametophore-like structures and**
663 **promotes the growth of regular gametophores**

664 Regular gametophore formation was entirely abolished by high-level PpROP
665 overexpression, as well as at levels of total PpROP activity lower than those displayed
666 by *rop*^{3xKO} mutants (Fig. 9). The same conditions also completely blocked caulonema
667 differentiation (Fig. 9), which was proposed to be essential for regular gametophore
668 formation (Cove and Knight, 1993; Schumaker and Dietrich, 1997; Brun et al., 2003;
669 Harrison et al., 2009). Strongly enhanced or reduced PpROP activity therefore appears
670 to indirectly prevent regular gametophore formation by disrupting caulonema
671 differentiation. However, in liquid culture medium estradiol-induced PpROP2 expression
672 at low levels insufficient for regular gametophore formation, or PpROP1^{Q64L} expression
673 at endogenous level, induced and supported the development of gametophore like-

674 structures composed of rudimentary phyllids without rhizoids, which were never formed
675 in the complete absence of PpROP activity (Fig. 9). Whereas regular gametophores
676 develop from caulonema cells undergoing a well-defined series of asymmetric and
677 symmetric cell divisions (Moody et al., 2018), gametophore like-structures emerged from
678 undifferentiated or chloronemal cells dividing in a comparably random fashion (Fig. 9;
679 Supplementary Fig. S8). Despite these differences, the observation that low-level
680 PpROP activity can induce the formation of aberrant gametophore-like structures
681 suggests that at higher levels enabling caulonema differentiation, this activity may also
682 play an important role in initiating regular gametophore development. Furthermore,
683 regular gametophore growth clearly depends on PpROP activity, since *rop*^{2xKO} *and*
684 *rop*^{3xKO} mutants, as well as complemented *rop*^{4xKO} mutants displaying similar levels of
685 total PpROP activity, formed gametophores with small leafy shoots and stunted rhizoids
686 (Fig. 9). These observations demonstrate that PpROP activity not only has essential
687 functions in promoting tip growth responsible for the elongation of protonemal filaments
688 and rhizoids, but also plays an apparently somewhat less important role in stimulating
689 other forms of directional cell expansion, which are required for the growth of leafy
690 shoots.

691 **GDP/GTP cycling is essential for PpROP functions in fundamental developmental**
692 **processes**

693 When expressed at endogenous level in *rop*^{4xKO} mutants, both WT PpROP2 and fast-
694 cycling PpROP1^{F31L} restored the *rop*^{3xKO} phenotype. By contrast, at the same
695 expression level GTP-locked PpROP1^{Q64L} was unable to complement defects in cell
696 polarization and parallel cell plate positioning displayed by *rop*^{4xKO} mutants, but induced
697 the formation of gametophore-like structures by these mutants in liquid medium (Fig. 9).
698 These observations demonstrate that GDP/GTP cycling is essential for PpROP
699 functions in fundamental developmental processes underlying filament formation, but is
700 not necessary for the induction of gametophore-like structures or directional cell
701 expansion responsible for the growth of these structures. Further investigations are
702 required to determine, whether GDP/GTP cycling is also essential for other PpROP
703 functions such as the promotion of tip growth, which requires cell polarization, or the
704 inhibition of caulonema differentiation, which depends on the formation of elongating

705 filaments. While RHO GTPase functions generally appear to depend on GDP/GTP
706 cycling, in animals atypical endogenous RHO GTPase have been identified, which like
707 PpROP1^{Q64L} regulate selected cellular or developmental processes in a constitutively
708 GTP-bound conformation (Hodge and Ridley, 2016; Aspenström, 2022).

709 **Evolutionary origin and maintenance of the Pp*ROP* gene family**

710 *P. patens* protonemata express at similar levels four Pp*ROP* genes encoding nearly
711 identical proteins, which as demonstrated by data presented here have essentially
712 redundant functions and together provide total PpROP activity that governs key
713 processes underlying protonemal development. A similar degree of sequence
714 conservation and functional integration is not generally observed in eukaryotic gene
715 families and raises questions concerning origin and maintenance of the Pp*ROP* gene
716 family during evolution.

717 At least one *ROP* gene is generally expressed in all plants (viridiplantae) with the
718 exception of some green algae of the chlorophyte group (Mulvey and Dolan, 2023b, a;
719 Ntefidou et al., 2023). Interestingly, *ROP* gene families typically have between four and
720 more than ten members in ferns, gymnosperm, and flowering plants, but are much
721 smaller with only one or two members in most plants displaying more ancient features,
722 which include lycophytes, the simplest vascular plants, along with mosses and all other
723 non-vascular plants (Mulvey and Dolan, 2023a). Similarly, *RIC* gene families also
724 substantially expanded and structurally differentiated with the emergence of flowering
725 plants (Ntefidou et al., 2023). These observations suggest a) that the evolution of
726 structurally increasingly complex vascular plants was accompanied by the diversification
727 of ROP functions, and b) that one or two ROP isoforms are generally sufficient to exert
728 comparably simple functions in plants with more ancient features. Consequently, total
729 PpROP activity regulating *P. patens* protonematal development, which is provided by
730 four co-expressed, nearly identical and functionally redundant PpROP family members,
731 appears to correspond to the activity of one or two ROP isoforms in other non-vascular
732 plants and in lycophytes.

733 The four members of the Pp*ROP* family are likely to have originated from a single
734 ancient ROP gene as a consequence of two rounds of whole genome duplications

735 (WGDs), which have occurred during the evolution of the *P. patens* genome (Rensing et
736 al., 2007; Lang et al., 2018; Leebens-Mack et al., 2019; Gao et al., 2022). Supporting
737 this notion, two consecutive WGDs and *ROP* gene families with four members have also
738 been identified in mosses of the genus *Sphagnum*, whereas more than one WGD
739 seems to have rarely occurred during the evolution of non-vascular plants with smaller
740 *ROP* gene families (Supplementary Table S2; Lang et al., 2018; Leebens-Mack et al.,
741 2019; Gao et al., 2022; Mulvey and Dolan, 2023b, a). The four *Sphagnum fallax* ROPs
742 and all ROPs expressed in a number of mosses with smaller *ROP* gene families share
743 at least 93 % identical amino acids with PpROP1 (Supplementary Table S2), suggesting
744 that ROP functions are highly conserved in all mosses, which is in line with the
745 hypothesis formulated at the end of the previous paragraph.

746 Remarkably, the four Pp*ROP* genes encoding nearly identical proteins, which apparently
747 derived from genome duplications, were maintained in *P. patens* evidently in the
748 absence of selective pressure driving their functional diversification. Although some
749 degree of functional redundancy commonly appears to be evolutionary stable,
750 particularly in gene families with important signaling functions (Vieten et al., 2005; Cevik
751 et al., 2023; Kumar and Ruiz, 2023), the selective advantage of this phenomenon is not
752 fully understood (Dean et al., 2008) and subject of ongoing further investigation (Nowak
753 et al., 1997; Raval et al., 2023). Genomic functional redundancy can provide resilience
754 against loss-of-function mutations (Gu et al., 2003b), as exemplified by the essentially
755 normal development of *P. patens rop*^{1xKO} mutants. Furthermore, it increases gene
756 dosage, which was proposed to enhance plant adaptability to changing environmental
757 conditions (Kondrashov et al., 2002).

758 **Outlook**

759 Evolutionary conserved essential functions of ROP GTPases in cell polarization,
760 directional cell expansion and cell plate positioning have previously been established
761 based on the investigation of defects caused by loss-of-function or gain-of-function
762 mutations in the moss *P. patens* (Burkart et al., 2015; Cheng et al., 2020; Yi and
763 Goshima, 2020; Bao et al., 2022), in the closely related non-vascular liverwort *M.*
764 *polymorpha* (Mulvey and Dolan, 2023b), as well as in the flowering plants *A. thaliana*
765 (Roszak et al., 2021) and *Z. mays* (Humphries et al., 2011). Data shown here

766 demonstrate that during *P. patens* protonemal development PpROP activity has
767 additional important functions in inhibiting caulonema differentiation, in controlling
768 gametophore development, and in the direct or indirect regulation of cell proliferation.
769 Whether ROP GTPases have similar or related functions also in other plants represents
770 an important area of future research.

771 The discoveries summarized in the previous paragraph have provided an increasingly
772 detailed understanding of ROP functions in the control of different cellular and
773 developmental processes in plants. However, the signaling network stimulated by ROP
774 activity to regulate these processes has not been well characterized. Compared to ROP
775 and RHO GTPase functions, this network appears to be much less evolutionary
776 conserved. In line with this notion, data presented here demonstrate that AtROP7 and
777 HsRHOA can only complement the *rop*^{4xKO} phenotype to a very limited extent. Although
778 these heterologous RHO GTPases are closely related to PpROPs (85.2-85.7 %
779 [AtROP7] and 49.7 % [HsRHOA] amino acid identity) even upon massive
780 overexpression they are only able to restore developmental processes in *rop*^{4xKO}
781 mutants, which require minimal PpROP activity. Consistent with this finding, homologs of
782 key animal RHO downstream effectors such as PAKs or ROCKs seem to be generally
783 missing in plants. Instead, plant-specific ROP effectors including RICs, ICR/RIPs and
784 RISAPs were shown to control directional cell expansion in flowering plants (Lavy et al.,
785 2007; Yalovsky et al., 2008; Stephan et al., 2014). Interestingly, the *P. patens* genome
786 encodes no ICR/RIP or RISAP homologs and only a single member of the RIC family
787 (Eklund et al., 2010; Ntefidou et al., 2023). Furthermore, the single PpRIC protein is
788 structurally very different from all its 11 *A. thaliana* homologs, and unlike several of these
789 proteins does not regulate directional cell expansion, but inhibits caulonema
790 differentiation (Ntefidou et al., 2023). Consequently, nothing is currently known about the
791 effectors regulating tip growth downstream of PpROP activity in *P. patens*, and PpRIC is
792 the only PpROP effector with a demonstrated function in the control of other cellular or
793 developmental processes in this moss (Fig. 9). To further characterize the signaling
794 network activated by PpROPs, it will be essential to identify and functionally characterize
795 novel interaction partners and potential effectors of these proteins. The same approach

796 will also provide important insights into the adaptation of ROP downstream signaling
797 during plant evolution.

798 **Materials and Methods**

799 **Plant materials and culture conditions**

800 *P. patens* ecotype Gransden wild-type (WT) strain (2012) (Ashton and Cove, 1977) and
801 transgenic lines (Supplementary Table S3) were grown axenically at 25°C under
802 continuous white light illumination with fluorescent tubes (Philips Master TL-D Super 80
803 58 W, cool white) at an intensity of 50 µmol m^{-2} s^{-1}. Unless otherwise stated, moss
804 protonemata were cultivated and analyzed in 9-mm Petri dishes on BCDA medium (1
805 mM $MgSO_4$, 1.84 mM KH_2PO_4, 10 mM KNO_3, 5 mM ammonium-tartrate, 1 mM $CaCl_2$,
806 45 µM $FeSO_4$, 9.9 µM H_3BO_3, 2 µM $MnCl_2$, 116 nM $AlK[SO_4]_2$, 424 nM $CoCl_2$, 220 nM
807 $CuSO_4$, 235 nM KBr, 168 nM KI, 660 nM LiCl, 124 nM $SnCl_2$, and 191 nM $ZnSO_4$)
808 (Ashton and Cove, 1977) solidified with 0.7% (w/v) agar and supplemented with 100
809 µg/mL vancomycin (Duchefa Biochemie) unless other antibiotics were used for
810 transgene selection. Solidified medium was covered with cellophane discs (AA
811 Packaging) (Grimsley et al., 1977) except for long-term cultivation of moss cultures
812 consisting of small clumps of round cells. Protonemata were sub-cultured every 7 days
813 and regenerated every 6 weeks from gametophores by homogenization (OMNI
814 International) in Milli-Q H_2O (Merck). Gametophore-forming colonies were cultivated and
815 analyzed on BCD medium (BCDA without ammonium-tartrate, supplemented with 100
816 µg/ml vancomycin) solidified with 0.7% (w/v) agar or in liquid BCD medium. Titratable
817 expression of RHO GTPases was induced by adding β-estradiol (Sigma), dissolved in
818 DMSO at concentrations from $2x10^{-5}$ µM to 1 µM to BCDA or BCD medium after
819 autoclaving. The culture conditions used in each experiment are listed in Supplementary
820 Table S4.

821 **Phenotypic analysis of protonemata regenerated from protoplasts**

822 Protonemata regenerated from protoplasts were prepared as described previously (Le
823 Bail et al., 2019) based on Cove et al. (Cove et al., 2009). In brief, 4 to 7-day-old
824 protonemata were digested with 0.5% (w/v) driselase (Sigma) in 8.5% mannitol and
825 regenerated on PRMB medium (supplemented with 100 µg/ml vancomycin) solidified

826 with 0.7 % agar in Petri dishes covered with cellophane for 2 days, followed by transfer
827 of the cellophane disc to BCDA medium (supplemented with 100 µg/ml vancomycin).
828 BCDA medium was treated with ≤ 1 µM β-estradiol for Pp*ROP1* overexpression
829 (WT/*ind*^{pro}:*ROP1*) or complementation of *rop*^{4xKO} with an inducible *ROP* or *RHO*
830 expression construct (*rop*^{4xKO}/*ind*^{pro}:ROPX or *rop*^{4xKO}/*ind*^{pro}:*RHO*). Nuclei were counted 4
831 days after protoplast preparation. Cell length, caulonema differentiation and protonemal
832 area were measured at 5 days. To analyze the gametophore stage, individual
833 protonemal colonies, having regenerated for 5 days on BCDA were transferred to BCD
834 medium without cellophane and supplemented with 100 µg/ml vancomycin, and the
835 colony area was measured 4 or 5 weeks after protoplast preparation. The culture
836 conditions used in each experiment are listed in Supplementary Table S4. Experiments
837 were repeated three times. The cell length and the area of 5-day-old and 5-week-old
838 colonies in Figures 1, 2, 4, and Supplementary Figure S5 were analyzed simultaneously.

839 **Bright field microscopy of cell length, caulonema differentiation, and colony size**

840 To determine the cell length and caulonema differentiation, filaments with three or more
841 cells of 5-day-old protonemata regenerated from protoplasts were imaged using a wide-
842 field microscope (DMI4000B, Leica). The length of subapical cells was analyzed using
843 Fiji software (ImageJ 1.54f; Schindelin et al., 2012), and caulonema differentiation was
844 assessed by optical inspection of apical cells. The colony size was determined based on
845 chlorophyll autofluorescence (excitation, 470 nm; emission, 500 nm long-pass) images
846 obtained with a fluorescence stereo microscope (M205 FA, Leica) and analyzed using a
847 Fiji macro (Vidali et al., 2007). 4 to 5-week-old colonies were imaged using the stereo
848 microscope (M205 FA, Leica), and the area was determined by applying thresholding to
849 convert reflected light 8-bit images to 1-bit images and analyzed using Fiji software
850 (ImageJ 1.54f; Schindelin et al., 2012).

851 **Generation of knockout constructs**

852 Molecular cloning was performed with standard methods (Green and Sambrook, 2012)
853 using Phusion DNA polymerase (ThermoFisher Scientific), primers listed in
854 Supplementary Data Set S1 (Eurofins Genomics), restriction enzymes and T4 Ligase
855 (New England Biolabs). The resulting constructs (Supplementary Data Set S2) were

856 verified by Sanger sequencing (Eurofins Genomics). To knock out Pp*ROP*s (*rop1*, *rop2*,
857 *rop3*, and *rop4*) based on homologous recombination, genomic fragments of 0.7 to 1.0
858 kb upstream of the start codon (5′ target) and downstream of the stop codon (3′ target)
859 were cloned flanking a resistance marker. The backbone of pMT123 (Thelander et al.,
860 2004) was used for cloning into the XhoI/HindIII and SpeI/NotI sites, resulting in pSLU33
861 for knockout of Pp*ROP1* (Supplementary Fig. S2A and B); the p35S-Zeo backbone
862 (Hiwatashi et al., 2008) was used for cloning pSLU34 for knockout of Pp*ROP2*
863 (Supplementary Fig. S3A and B), the p35S-loxP-BSD backbone (Li et al., 2017) was
864 used for cloning pSLU35 for knockout of Pp*ROP3* (Supplementary Fig. S3C and D), and
865 the pMT164 backbone (Thelander et al., 2007) was used for cloning pSLU36 for
866 knockout of Pp*ROP4* (Supplementary Fig. S4). Multiple Pp*rop* knockouts (rop^{2xKO},
867 rop^{3xKO}, rop^{4xKO}) were generated through sequential knockout of single PpROPs in the
868 order listed in Supplementary Fig. S2C. For each knockout, at least two lines were
869 obtained except for *rop2*, *rop4*, and *rop4/1*, which had only one line each
870 (Supplementary Table S3). All lines for each genotype showed the same phenotype, and
871 the results of only one transgenic line are presented.

872 **Generation of expression constructs**

873 To complement rop^{4xKO} with Pp$ROP1^{Q64L}$ or Pp$ROP1^{F31L}$ expressed by the endogenous
874 Pp*ROP1* promoter, the Pp*ROP1* coding and 3'UTR sequence were amplified from cDNA
875 and cloned into pENTR™/D-Topo (Thermo Fisher Scientific) yielding pFAU253 and
876 mutated using PCR-based site-directed mutagenesis followed by DpnI digestion
877 generating pFAU256 (Pp$ROP1^{Q64L}$) or pFAU417 (Pp$ROP1^{F31L}$). The Pp$ROP1^{Q64L}$ or
878 Pp$ROP1^{F31L}$ fragments were transferred into the SalI/HindIII sites of pMT123 (Thelander
879 et al., 2004) and flanked by 0.7 to 1.0 kb regions upstream of the start codon (5′ target)
880 or downstream of the stop codon (3′ target) of Pp*ROP1* enabling the replacement of the
881 Pp*ROP1* locus in *rop3/2/4* through homologous recombination yielding pFAU306
882 (rop^{4xKO}/$ROP1^{pro}$:$ROP1^{Q64L}$) or pFAU421 (rop^{4xKO}/$ROP1^{pro}$:$ROP1^{F31L}$) (Supplementary
883 Fig. S2A and B; Supplementary Data Set S2).

884 To complement rop^{4xKO} with a single Pp*ROP* under the control of the Pp*ROP1* promoter,
885 the full-length coding sequences of Pp*ROP2* or Pp*ROP3,* including the respective 3′
886 UTR, were amplified from cDNA and cloned into pENTR™/D-Topo, generating pFAU269

887 (Pp*ROP2*) and pFAU270 (Pp*ROP3*). Each Pp*ROP* fragment was then transferred from
888 pFAU253 or pFAU269 or pFAU270 into the SalI/HindIII sites of pFAU306 which enabled
889 the replacement of the Pp*ROP1* locus in *rop3/2/4* through homologous recombination,
890 yielding pFAU508 (rop^{4xKO}/$ROP1^{pro}$:*ROP1*), pFAU509 (rop^{4xKO}/$ROP1^{pro}$:*ROP2*), and
891 pFAU517 (rop^{4xKO}/$ROP1^{pro}$:*ROP3*) respectively (Supplementary Fig. S2A and B).
892 To complement rop^{4xKO} with a titratable expression of a *ROP* or *RHO GTPase*, the lexA
893 operator and the XVE chimeric sequence were amplified by PCR from pGX8 (Kubo et
894 al., 2013) and cloned into the NotI/EcoRV sites of pSLU35, yielding pFAU425, and into
895 the SpeI/PmeI/PmlI sites of pSLU36, yielding pFAU391. The coding and 3' UTR
896 sequence of Pp*ROP2* were transferred from pFAU269 to pFAU425 by Gateway LR
897 reaction (Thermo Fisher Scientific) (Katzen, 2007) generating pFAU431
898 (rop^{4xKO}/ind^{pro}:*ROP2*) (Supplementary Fig. S3C and D) that was used for replacement of
899 the Pp*ROP3* locus based on homologous recombination in *rop2/4/1*. The full-length
900 At*ROP7* and Hs*RHOA* coding sequences were amplified from Arabidopsis or *Homo*
901 *sapiens* cDNA, respectively, and cloned into pENTR/D-Topo (Thermo Fisher Scientific),
902 yielding pFAU290 (At*ROP7*) and pFAU294 (Hs*RHOA*), followed by Gateway LR reaction
903 (Thermo Fisher Scientific) (Katzen, 2007) with pFAU391 generating pFAU398
904 (rop^{4xKO}/ind^{pro}:At*ROP7*) or pFAU402 (rop^{4xKO}/ind^{pro}:Hs*RHOA*) for gene replacement
905 based on homologous recombination of the Pp*ROP4* locus in *rop3/1/2* (Supplementary
906 Fig. S4A and B).
907 To overexpress Pp*ROP1* (WT/ind^{pro}:*ROP1*) from the β-estradiol-inducible promoter, the
908 coding sequence of Pp*ROP1*, including the 3′ UTR, was transferred from pFAU253 by
909 Gateway LR reaction (Thermo Fisher Scientific) (Katzen, 2007) into pGX8 (Kubo et al.,
910 2013) generating pFAU461 (Supplementary Fig. S2D) used for transgene integration
911 based on homologous recombination into the neutral genomic region of PIG1b (Okano
912 et al., 2009).
913 To express Pp*PINA-eGFP* under the endogenous Pp*PINA* promoter, the pFAUobt63
914 vector was obtained from Mattias Thelander (Viaene et al., 2014) for integration of
915 $PINA^{pro}$*:PINA-eGFP* into the neutral genomic region Pp108 (Schaefer and Zrÿd, 1997) of
916 *P. patens* WT and *rop1/2* double knockout.

917 ***P. patens* transformation**

918 Gene targeting into the *P. patens* genome by homologous recombination was previously
919 described for polyethylene glycol PEG-mediated transformation (Le Bail et al., 2019)
920 based on the method by Schaefer and Zrÿd (Schaefer and Zrÿd, 1997). In brief, 1.6 x
921 10^6 protoplasts were transformed with 15 µg of linearized vector and allowed to
922 regenerate for 5 days on PRMB medium, followed by two rounds of selection alternating
923 between BCDA medium containing the appropriate antibiotic (30 µg/mL hygromycin B
924 [Carl Roth], 20 µg/mL G418 [Merck], 50 µg/mL zeocin [Thermo Fisher Scientific], or 75
925 µg/mL blasticidin [InvivoGen]) according to the transformed resistance cassette and
926 BCDA medium (supplemented with 100 µg/ml vancomycin). Transgenic lines were
927 genotyped through PCR using primers indicated in Supplementary Data Set S1 and
928 Supplementary Fig. S2-S4.

929 **Gene expression analysis by RT-qPCR**

930 Total RNA was extracted from 1-week-old protonemata cultivated through
931 homogenization or from 7 to 10-day-old protonemata regenerated from protoplasts.
932 Samples were frozen in liquid nitrogen and lysed with glass beads using TissueLyser II
933 (Qiagen). Total RNA was isolated using a Nucleospin RNA Plus™ Kit (Macherey-Nagel),
934 and RNA integrity was assessed using agarose gel electrophoresis. First-strand cDNA
935 was synthesized from 1 µg of total RNA using iScript™ Reverse Transcription Supermix
936 for RT-qPCR (Bio-Rad) and diluted 1:20 in Milli-Q H_2O. RT-qPCR was conducted using
937 SscAdvanced™ Universal SYBR Green Supermix (Bio-Rad) and a CFX96TM thermal
938 cycler (Bio-Rad). Total RNA was prepared from three moss samples (biological
939 replicates), and each cDNA sample was measured in two RT-qPCR reactions (technical
940 replicates). Absolute transcript levels were quantified with standard curves prepared
941 from a 10-fold dilution series of genomic DNA from 1-week old protonemata using the
942 PhytoPure DNA Extraction kit (Cytiva). Pp*UBIQUITIN-E2* served as a reference gene
943 (Le Bail et al., 2013). Primers used for RT- qPCR are listed in Supplementary Data Set
944 S1. Experiments were repeated two times.

945 **Quantification of free IAA**

946 7-day-old protonemata tissues (around 15-30 mg fresh weight per sample) were
947 extracted after addition of 500 pg ^{13}C6-IAA internal standard per sample, purified and

948 analyzed for free IAA concentration using combined gas chromatography-tandem mass
949 spectrometry as described (Andersen et al., 2008).

950 **Confocal microscopy and staining of nuclei and cell walls**

951 A Leica TCS SP8 DIVE-FALCON inverted confocal laser scanning microscope with an
952 HC PL APO CS2 20X/0.75 NA water immersion lens was used for confocal imaging,
953 operated by Application Suite X software. GFP fluorescence was imaged through
954 excitation using an argon laser at 488 nm and emission at 500-550 nm. The cell number
955 was determined by counting nuclei in 4-day-old cells, or protonemata regenerated from
956 protoplasts, stained according to the method of Vidali et al. (Vidali et al., 2010). In brief,
957 moss samples were fixed for 30 min in a staining solution of 100 mM PIPES, pH 6.8,
958 0.1% (v/v) Nonidet P-40, 2% (w/v) paraformaldehyde, and 0.1 µg/mL 4′,6-diamidino-
959 2phenylindole (DAPI). The fluorescence was detected through excitation using an argon
960 laser at 360 nm and emission at 460 nm. Cell walls of gametophores were stained with
961 10 µg/mL propidium iodide solution (Merck), and the fluorescence was excited using a
962 DPSS 561 laser (excitation, 536 nm; emission, 617 nm) and recorded using Z-stacks of
963 optical sections at 2-µm spacing. Fiji software (Schindelin et al., 2012) was used to
964 generate maximum Z-stack projections.

965 **Alignment analysis**

966 A protein alignment of full-length PpROPs, AtROP7, and HsRHOA sequences and the
967 protein identity matrix were obtained using Uniprot (The UniProt Consortium, 2024).

968 **Statistical analysis**

969 GraphPad Prism (Version 10.3.1, GraphPad software) was used for data analysis.
970 Unpaired Student's *t*-tests were used to determine significant differences between two
971 genotypes and one-way analysis of variance (ANOVA, Welch's ANOVA) or two-way
972 ANOVA followed by pairwise multiple comparison tests (Tukey's/Dunnett's) between
973 three or more genotypes as indicated in the figure legends. Significance to WT and
974 comparisons relevant to data interpretation are indicated in graphs, and all statistical
975 results are given in Supplementary Data Set S3.

Accession numbers

Sequence data were analyzed by BLAST (Altschul et al., 1990) and are available in the data libraries of Phytozome *P. patens* V6.1 (Joint Genome Institute) (Goodstein et al., 2012; Bi et al., 2024), TAIR (Arabidopsis Information Resource) (Berardini et al., 2015), ONEKP CNGBdb (Leebens-Mack et al., 2019), and GenBank (Clark et al., 2016) under the following accession numbers: Aa*ROP* (onekp|ZTHV_scaffold_2084304 Atrichum_angustatum, CNGBdb); Aat*ROP1* (onekp|QMWB_scaffold_2004844 Anomodon_attenuatus, CNGBdb); Aat*ROP2* (onekp|QMWB_scaffold_2004846 Anomodon_attenuatus, CNGBdb); Aat*ROP3* (onekp|QMWB_scaffold_2004845 Anomodon_attenuatus, CNGBdb); Ar*ROP* (gnl|onekp|WOGB_scaffold_2094631 Andreaea_rupestris, CNGBdb); At*ROP7* (At5g45970, TAIR); Ba*ROP* (gnl|onekp|JMXW_scaffold_2006533 Bryum_argenteum, CNGBdb); Bap*ROP* (gnl|onekp|HRWG_scaffold_2070290 Buxbaumia_aphylla, CNGBdb); Cc*ROP* (gnl|onekp|TAVP_scaffold_2005151 Calliergon_cordifolium, CNGBdb); Cd*ROP* (gnl|onekp|MIRS_scaffold_2008952 Climacium_dendroides, CNGBdb); Cp*ROP1* (gnl|onekp|FFPD_scaffold_2008289 Ceratodon_purpureus, CNGBdb); Cp*ROP2* (gnl|onekp|FFPD_scaffold_2009252 Ceratodon_purpureus, CNGBdb); Df*ROP* (gnl|onekp|AWOI_scaffold_2072508 Diphyscium_foliosum, CNGBdb); Fa*ROP* (gnl|onekp|DHWX_scaffold_2074728 Fontinalis_antipyretica, CNGBdb) Hs*RHOA* (NM_001664.4, GenBank); La*ROP* (gnl|onekp|VMXJ_scaffold_2010101 Leucobryum_albidum, CNGBdb); Ol*ROP1* (gnl|onekp|CMEQ_scaffold_2011516 Orthotrichum_lyellii, CNGBdb); Ol*ROP2* (gnl|onekp|CMEQ_scaffold_2013049 Orthotrichum_lyellii, CNGBdb); Pf*ROP* (gnl|onekp|ORKS_scaffold_2003761 Philonotis_fontana, CNGBdb); Pc*ROP* (onekp|SZYG_scaffold_2042265 Polytrichum_commune, CNGBdb); Pp*AUX1* (Pp6c16_1210, Phytozome); Pp*PINA* (Pp6c23_4450, Phytozome); Pp*ROP1* (Pp6c14_2140, Phytozome); Pp*ROP2* (Pp6c2_11900, Phytozome); Pp*ROP3* (Pp6c1_11060, Phytozome); Pp*ROP4* (Pp6c10_2660, Phytozome); Pp*RSL1* (Pp6c1_20350, Phytozome); Pp*SHI1* (Pp6c21_9000, Phytozome); and Pp*UBIQUITIN-E2* (Pp6c12_2450, Phytozome); Rs*ROP1* (gnl|onekp|JADL_scaffold_2005567 Rhynchostegium_serrulatum, CNGBdb); Rs*ROP2 (gnl|onekp|JADL_scaffold_2005565 Rhynchostegium_serrulatum*, CNGBdb); Sf*ROP1* (Sphfalx06G097600, Phytozome); Sf*ROP2* (Sphfalx13G088000, Phytozome); Sf*ROP3* (Sphfalx14G076800, Phytozome); Sf*ROP4* (Sphfalx18G051700, Phytozome); Tl*ROP* (gnl|onekp|SKQD_scaffold_2079078 Takakia_lepidozioides, CNGBdb).

Supplementary Data

Supplementary Fig. S1. PpROP gene expression in protonemata.

Supplementary Fig. S2. Editing of the genomic Pp*ROP1* locus through homologous recombination and summary of transgenic lines.

Supplementary Fig. S3. Editing of the genomic Pp*ROP2* and Pp*ROP3* loci through homologous recombination.

1016 **Supplementary Fig. S4.** Editing of the genomic Pp*ROP4* locus through homologous
1017 recombination.
1018 **Supplementary Fig. S5.** Knockout of a single Pp*rop* (*rop*^{1xKO}) does not affect
1019 protonemata.
1020 **Supplementary Fig. S6.** PpROPs do not influence the expression of auxin-regulated
1021 gene expression or the auxin content.
1022 **Supplementary Fig. S7.** β-estradiol does not influence Pp*ROP* expression or
1023 protonemal development.
1024 **Supplementary Fig. S8.** Gametophore-like structures of *rop*^{4xKO}/*ROP1*^{pro}:*ROP1*^{Q64L}.
1025 **Supplementary Table S1.** Rate of polarized cell expansion of *rop*4xKO/*ind*^{pro}:*ROP2* at
1026 low induction level.
1027 **Supplementary Table S2.** ROP protein families in mosses: number of members and
1028 amino acid sequence conservation.
1029 **Supplementary Table S3.** *P. patens* lines used in this study.
1030 **Supplementary Table S4.** Culture media used in this study.
1031 **Supplementary Data Set 1.** Oligonucleotides used in this study.
1032 **Supplementary Data Set 2.** Vectors used in this study.
1033 **Supplementary Data Set 3.** Statistical analyses.

1034 **Author contributions**

1035 Designed the research: A.L.B, M.N., and B.K.; Performed research: A.L.B., M.N., J.N.,
1036 T.I.L., D.K., K.L., H.V., S.S.; Data analysis: A.L.B., B.K., M.N., K.L.; Writing – original
1037 draft: M.N.; Writing – review & editing: B.K., M.N.; Visualization: M.N.; Supervision: B.K.
1038 and M.N.; Project administration: B.K.; Funding acquisition: K.L. and B.K. All authors are
1039 in agreement with this MS and approved its content.

1040 **Acknowledgments**

1041 We are thankful to Dr. Mattias Thelander (Swedish University of Agricultural Sciences,
1042 Uppsala, Sweden) for the vector pMT123 and *PINA*^{pro}:*PINA-GFP*, Prof. Mitsuyasu
1043 Hasebe (NIBB, Okazaki, Japan) for the vectors pGX8, p35S-Zeo, and p35S-loxP-BSD,
1044 and Dr. Pierre-François Perroud (IJPB, INRAE, Versailles) for invaluable technical and
1045 conceptual advice. We thank Roger Granbom for excellent technical support.

Funding

K.L. was supported by funding from the Knut and Alice Wallenberg Foundation (KAW 2016.0341 and KAW 2016.0352) and the Swedish Governmental Agency for Innovation Systems (VINNOVA 2016-00504). Confocal microscopy relied on a major equipment grand awarded to B.K. by the German Research Foundation (DFG, INST 90/1074-1 FUGG).

Conflict of interest: The authors declare no conflicts of interest.

References

Altschul, S.F., Gish, W., Miller, W., Myers, E.W., and Lipman, D.J. (1990). Basic local alignment search tool. J. Mol. Biol. **215,** 403-410. 10.1016/S0022-2836(05)80360-2

Andersen, S.U., Buechel, S., Zhao, Z., Ljung, K., Novák, O., Busch, W., Schuster, C., and Lohmann, J.U. (2008). Requirement of B2-type cyclin-dependent kinases for meristem integrity in *Arabidopsis thaliana*. Plant Cell **20,** 88-100. https://doi.org/10.1105/tpc.107.054676

Ashton, N.W., and Cove, D.J. (1977). The isolation and preliminary characterisation of auxotrophic and analogue resistant mutants of the moss, *Physcomitrella patens*. Mol. Gen. Genetics **154,** 87-95. https://doi.org/10.1007/BF00265581

Aspenström, P. (2019). The Intrinsic GDP/GTP Exchange Activities of Cdc42 and Rac1 Are Critical Determinants for Their Specific Effects on Mobilization of the Actin Filament System. Cells **8,** 759. 10.3390/cells8070759

Aspenström, P. (2022). The Role of Fast-Cycling Atypical RHO GTPases in Cancer. Cancers **14,** 1961. https://doi.org/10.3390/cancers14081961

Bao, L., Ren, J., Nguyen, M., Slusarczyk, A.S., Thole, J.M., Martinez, S.P., Huang, J., Fujita, T., and Running, M.P. (2022). The cellular function of ROP GTPase prenylation is important for multicellularity in the moss *Physcomitrium patens*. Development **149**. https://doi.org/10.1242/dev.200279

Berardini, T.Z., Reiser, L., Li, D., Mezheritsky, Y., Muller, R., Strait, E., and Huala, E. (2015). The arabidopsis information resource: Making and mining the "gold standard" annotated reference plant genome. genesis **53,** 474-485. https://doi.org/10.1002/dvg.22877

Berken, A., Thomas, C., and Wittinghofer, A. (2005). A new family of RhoGEFs activates the Rop molecular switch in plants. Nature **436,** 1176-1180. https://doi.org/10.1038/nature03883

Bi, G., Zhao, S., Yao, J., Wang, H., Zhao, M., Sun, Y., Hou, X., Haas, F.B., Varshney, D., Prigge, M., Rensing, S.A., Jiao, Y., Ma, Y., Yan, J., and Dai, J. (2024). Near telomere-to-telomere genome of the model plant Physcomitrium patens. Nat. Plants **10,** 327-343. 10.1038/s41477-023-01614-7

Bishop, A.L., and Hall, A. (2000). Rho GTPases and their effector proteins. Biochem. J. **348,** 241-255. 10.1042/bj3480241

Boureux, A., Vignal, E., Faure, S., and Fort, P. (2007). Evolution of the Rho family of ras-like GTPases in eukaryotes. Mol. Biol. Evol. **24,** 203-216. 10.1093/molbev/msl145

Brun, F., Gonneau, M., Laloue, M., and Nogué, F. (2003). Identification of Physcomitrella patens genes specific of bud and gametophore formation. Plant Sci. **165,** 1267-1274. https://doi.org/10.1016/S0168-9452(03)00335-2

Burkart, G.M., Baskin, T.I., and Bezanilla, M. (2015). A family of ROP proteins that suppress actin dynamics and are essential for polarized growth and cell adhesion. J. Cell Sci. **128,** 2553-2564. https://doi.org/10.1242/jcs.172445

1089 **Cevik, S., Peng, X., Beyer, T., Pir, M.S., Yenisert, F., Woerz, F., Hoffmann, F., Altunkaynak, B., Pir, B.,**
1090 **Boldt, K., Karaman, A., Cakiroglu, M., Oner, S.S., Cao, Y., Ueffing, M., and Kaplan, O.I.** (2023). WDR31
1091 displays functional redundancy with GTPase-activating proteins (GAPs) ELMOD and RP2 in regulating IFT
1092 complex and recruiting the BBSome to cilium. Life Sci. Alliance **6,** e202201844.
1093 https://doi.org/10.26508/lsa.202201844
1094 **Chen, C.Y.H., Cheung, A.Y., and Wu, H.-M.** (2003). Actin-Depolymerizing Factor Mediates Rac/Rop
1095 GTPase–Regulated Pollen Tube Growth. Plant Cell **15,** 237-249. https://doi.org/10.1105/tpc.007153
1096 **Cheng, X., Mwaura, B.W., Chang Stauffer, S.R., and Bezanilla, M.** (2020). A fully functional ROP
1097 fluorescent fusion protein reveals roles for this GTPase in subcellular and tissue-level patterning. Plant
1098 Cell **32,** 3436-3451. https://doi.org/10.1105/tpc.20.00440
1099 **Clark, K., Karsch-Mizrachi, I., Lipman, D.J., Ostell, J., and Sayers, E.W.** (2016). GenBank. Nucleic Acids
1100 Res. **44,** D67-D72. https://doi.org/10.1093/nar/gkv1276
1101 **Coleman, M.L., Marshall, C.J., and Olson, M.F.** (2004). RAS and RHO GTPases in G1-phase cell-cycle
1102 regulation. Nat. Rev. Mol. Cell Biol. **5,** 355-366. 10.1038/nrm1365
1103 **Collonnier, C., Epert, A., Mara, K., Maclot, F., Guyon-Debast, A., Charlot, F., White, C., Schaefer, D.G.,**
1104 **and Nogué, F.** (2017). CRISPR-Cas9-mediated efficient directed mutagenesis and RAD51-dependent and
1105 RAD51-independent gene targeting in the moss *Physcomitrella patens*. Plant Biotechnol. J. **15,** 122-131.
1106 10.1111/pbi.12596
1107 **Cove, D.** (2005). The Moss *Physcomitrella patens*. Annu. Rev. Genet. **39,** 339 - 358.
1108 10.1146/annurev.genet.39.073003.110214
1109 **Cove, D., and Knight, C.** (1993). The moss *Physcomitrella patens,* a model system with potential for the
1110 study of plant reproduction. Plant Cell **5,** 1483-1488. https://doi.org/10.1105/tpc.5.10.1483
1111 **Cove, D.J., Perroud, P.-F., Charron, A.J., McDaniel, S.F., Khandelwal, A., and Quatrano, R.S.** (2009).
1112 Isolation and Regeneration of Protoplasts of the Moss *Physcomitrella patens*. Cold Spring Harbor
1113 Protocols **2009**. https://doi.org/doi:10.1101/pdb.prot5140
1114 **Dean, E.J., Davis, J.C., Davis, R.W., and Petrov, D.A.** (2008). Pervasive and Persistent Redundancy among
1115 Duplicated Genes in Yeast. PLOS Genet. **4,** e1000113. https://doi.org/10.1371/journal.pgen.1000113
1116 **Denninger, P., Reichelt, A., Schmidt, V.A.F., Mehlhorn, D.G., Asseck, L.Y., Stanley, C.E., Keinath, N.F.,**
1117 **Evers, J.-F., Grefen, C., and Grossmann, G.** (2019). Distinct RopGEFs Successively Drive Polarization and
1118 Outgrowth of Root Hairs. Curr. Biol. **29,** 1854-1865. https://doi.org/10.1016/j.cub.2019.04.059
1119 **Eklund, D.M., Svensson, E.M., and Kost, B.** (2010). *Physcomitrella patens:* a model to investigate the role
1120 of RAC/ROP GTPase signalling in tip growth. J. Exp. Bot. **61,** 1917-1937.
1121 https://doi.org/10.1093/jxb/erq080
1122 **Etienne-Manneville, S., and Hall, A.** (2002). Rho GTPases in cell biology. Nature **420,** 629-635.
1123 https://doi.org/10.1038/nature01148
1124 **Fantes, P., and Nurse, P.** (1977). Control of cell size at division in fission yeast by a growth-modulated size
1125 control over nuclear division. Exp. Cell Res. **107,** 377-386. https://doi.org/10.1016/0014-
1126 4827(77)90359-7
1127 **Feiguelman, G., Fu, Y., and Yalovsky, S.** (2018). ROP GTPases Structure-Function and Signaling Pathways.
1128 Plant Physiol. **176,** 57-79. https://doi.org/10.1104/pp.17.01415
1129 **Fu, Y., Gu, Y., Zheng, Z., Wasteneys, G., and Yang, Z.** (2005). Arabidopsis interdigitating cell growth
1130 requires two antagonistic pathways with opposing action on cell morphogenesis. Cell **120,** 687-700.
1131 10.1016/j.cell.2004.12.026
1132 **Gao, B., Chen, M.-X., Li, X.-S., Liang, Y.-Q., Zhang, D.-Y., Wood, A.J., Oliver, M.J., and Zhang, J.-H.** (2022).
1133 Ancestral gene duplications in mosses characterized by integrated phylogenomic analyses. J. Syst. Evol.
1134 **60,** 144-159. https://doi.org/10.1111/jse.12683
1135 **Goodstein, D.M., Shu, S., Howson, R., Neupane, R., Hayes, R.D., Fazo, J., Mitros, T., Dirks, W., Hellsten,**
1136 **U., Putnam, N., and Rokhsar, D.S.** (2012). Phytozome: a comparative platform for green plant
1137 genomics. Nucleic Acids Res. **40,** D1178-D1186. https://doi.org/10.1093/nar/gkr944

1138 **Green, M.R., and Sambrook, J.** (2012). Molecular cloning: A laboratory manual. (Cold Spring Harbor, New
1139 York: Cold Spring Harbor Laboratory Press).
1140 **Grimsley, N.H., Ashton, N.W., and Cove, D.J.** (1977). The production of somatic hybrids by protoplast
1141 fusion in the moss, *Physcomitrella patens*. Mol. Gen. Genet. **154,** 97-100.
1142 https://doi.org/10.1007/bf00265582
1143 **Gu, Y., Vernoud, V., Fu, Y., and Yang, Z.** (2003a). ROP GTPase regulation of pollen tube growth through
1144 the dynamics of tip-localized F-actin. J. Exp. Bot. **54,** 93-101. 10.1093/jxb/erg035
1145 **Gu, Z., Steinmetz, L.M., Gu, X., Scharfe, C., Davis, R.W., and Li, W.-H.** (2003b). Role of duplicate genes in
1146 genetic robustness against null mutations. Nature **421,** 63-66. https://doi.org/10.1038/nature01198
1147 **Hall, A., and Lalli, G.** (2010). Rho and Ras GTPases in axon growth, guidance, and branching. Cold Spring
1148 Harb Perspect Biol **2,** a001818. https://doi.org/10.1101/cshperspect.a001818
1149 **Harrison, C.J., Roeder, A.H.K., Meyerowitz, E.M., and Langdale, J.A.** (2009). Local Cues and Asymmetric
1150 Cell Divisions Underpin Body Plan Transitions in the Moss *Physcomitrella patens*. Curr. Biol. **19,** 461-471.
1151 https://doi.org/10.1016/j.cub.2009.02.050
1152 **Heasman, S.J., and Ridley, A.J.** (2008). Mammalian Rho GTPases: new insights into their functions from
1153 in vivo studies. Nat. Rev. Mol. Cell Biol. **9,** 690-701. 10.1038/nrm2476
1154 **Hiwatashi, Y., Obara, M., Sato, Y., Fujita, T., Murata, T., and Hasebe, M.** (2008). Kinesins are
1155 indispensable for interdigitation of phragmoplast microtubules in the moss *Physcomitrella patens*. Plant
1156 Cell **20,** 3094-3106. https://doi.org/10.1105/tpc.108.061705
1157 **Hodge, R.G., and Ridley, A.J.** (2016). Regulating Rho GTPases and their regulators. Nat. Rev. Mol. Cell
1158 Biol. **17,** 496-510. https://doi.org/10.1038/nrm.2016.67
1159 **Humphries, J.A., Vejlupkova, Z., Luo, A., Meeley, R.B., Sylvester, A.W., Fowler, J.E., and Smith, L.G.**
1160 (2011). ROP GTPases Act with the Receptor-Like Protein PAN1 to Polarize Asymmetric Cell Division in
1161 Maize. Plant Cell **23,** 2273-2284. https//doi.org.10.1105/tpc.111.085597
1162 **Ito, K., Ren, J., and Fujita, T.** (2014). Conserved function of Rho-related Rop/RAC GTPase signaling in
1163 regulation of cell polarity in *Physcomitrella patens*. Gene **544,** 241-247.
1164 https://doi.org/10.1016/j.gene.2014.04.057
1165 **Jaeger, R., and Moody, L.A.** (2021). A fundamental developmental transition in *Physcomitrium patens* is
1166 regulated by evolutionarily conserved mechanisms. Evol. Devel. **23,** 123-136.
1167 https://doi.org/10.1111/ede.12376
1168 **Jang, G., and Dolan, L.** (2011). Auxin promotes the transition from chloronema to caulonema in moss
1169 protonema by positively regulating PpRSL1and PpRSL2 in *Physcomitrella patens*. New Phytol. **192,** 319-
1170 327. https://doi.org/10.1111/j.1469-8137.2011.03805.x
1171 **Jones, A.R., Forero-Vargas, M., Withers, S.P., Smith, R.S., Traas, J., Dewitte, W., and Murray, J.A.H.**
1172 (2017). Cell-size dependent progression of the cell cycle creates homeostasis and flexibility of plant cell
1173 size. Nat. Commun. **8,** 15060. https://doi.org/10.1038/ncomms15060
1174 **Katzen, F.** (2007). Gateway® recombinational cloning: a biological operating system. Expert Opin. Drug
1175 Discov. **2,** 571-589. https://doi.org/10.1517/17460441.2.4.571
1176 **Kawano, Y., Kaneko-Kawano, T., and Shimamoto, K.** (2014). Rho family GTPase-dependent immunity in
1177 plants and animals. Front. Plant Sci. **5**. https://doi.org/10.3389/fpls.2014.00522
1178 **Klahre, U., and Kost, B.** (2006). Tobacco RhoGTPase ACTIVATING PROTEIN1 Spatially Restricts Signaling of
1179 RAC/Rop to the Apex of Pollen Tubes. Plant Cell **18,** 3033-3046.
1180 https://doi.org/10.1105/tpc.106.045336
1181 **Kofuji, R., and Hasebe, M.** (2014). Eight types of stem cells in the life cycle of the moss Physcomitrella
1182 patens. Curr. Opin. Plant Biol. **17,** 13-21. 10.1016/j.pbi.2013.10.007
1183 **Kondrashov, F.A., Rogozin, I.B., Wolf, Y.I., and Koonin, E.V.** (2002). Selection in the evolution of gene
1184 duplications. Genome Biol. **3**. https://doi.org/10.1186/gb-2002-3-2-research0008
1185 **Kost, B.** (2008). Spatial control of Rho (Rac-Rop) signaling in tip-growing plant cells. Trends Cell Biol. **18,**
1186 119-127. 10.1016/j.tcb.2008.01.003

Kost, B. (2010). Regulatory and Cellular Functions of Plant RhoGAPs and RhoGDIs. In Integrated G Proteins Signaling in Plants, S. Yalovsky, F. Baluška, and A. Jones, eds (Berlin, Heidelberg: Springer Berlin Heidelberg), pp. 27-48.

Kubo, M., Imai, A., Nishiyama, T., Ishikawa, M., Sato, Y., Kurata, T., Hiwatashi, Y., Reski, R., and Hasebe, M. (2013). System for Stable β-Estradiol-Inducible Gene Expression in the Moss *Physcomitrella patens*. PLoS ONE **8,** e77356. https://doi.org/10.1371/journal.pone.0077356

Kumar, S., and Ruiz, N. (2023). Bacterial AsmA-Like Proteins: Bridging the Gap in Intermembrane Phospholipid Transport. Contact **6**. https://doi.org/10.1177/25152564231185931

Lang, D., Ullrich, K.K., Murat, F., Fuchs, J., Jenkins, J., Haas, F.B., Piednoel, M., Gundlach, H., Van Bel, M., Meyberg, R., Vives, C., Morata, J., Symeonidi, A., Hiss, M., Muchero, W., Kamisugi, Y., Saleh, O., Blanc, G., Decker, E.L., Van Gessel, N., Grimwood, J., Hayes, R.D., Graham, S.W., Gunter, L.E., McDaniel, S.F., Hoernstein, S.N.W., Larsson, A., Li, F.-W., Perroud, P.-F., Phillips, J., Ranjan, P., Rokshar, D.S., Rothfels, C.J., Schneider, L., Shu, S., Stevenson, D.W., Thümmler, F., Tillich, M., Villarreal Aguilar, J.C., Widiez, T., Wong, G.K.-S., Wymore, A., Zhang, Y., Zimmer, A.D., Quatrano, R.S., Mayer, K.F.X., Goodstein, D., Casacuberta, J.M., Vandepoele, K., Reski, R., Cuming, A.C., Tuskan, G.A., Maumus, F., Salse, J., Schmutz, J., and Rensing, S.A. (2018). The *Physcomitrella patens* chromosome-scale assembly reveals moss genome structure and evolution. Plant J. **93,** 515-533. https://doi.org/10.1111/tpj.13801

Lauster, T., Stöckle, D., Gabor, K., Haller, T., Krieger, N., Lotz, P., Mayakrishnan, R., Späth, E., Zimmermann, S., Livanos, P., and Müller, S. (2022). Arabidopsis pavement cell shape formation involves spatially confined ROPGAP regulators. Curr. Biol. **32,** 532-544.e537. https://doi.org/10.1016/j.cub.2021.12.042

Lavy, M., Bloch, D., Hazak, O., Gutman, I., Poraty, L., Sorek, N., Sternberg, H., and Yalovsky, S. (2007). A novel ROP/RAC effector links cell polarity, root-meristem maintenance, and vesicle trafficking. Curr. Biol. **17,** 947-952. https://doi.org/10.1016/j.cub.2007.04.038

Le Bail, A., Scholz, S., and Kost, B. (2013). Evaluation of reference genes for RT qPCR analyses of structure-specific and hormone regulated gene expression in *Physcomitrella patens* gametophytes. PLoS ONE **8,** e70998. https://10.1371/journal.pone.0070998

Le Bail, A., Schulmeister, S., Perroud, P.F., Ntefidou, M., Rensing, S.A., and Kost, B. (2019). Analysis of the localization of fluorescent PpROP1 and PpROP-GEF4 fusion proteins in moss protonemata based on genomic "knock-in" and estradiol-titratable expression. Front. Plant Sci. **10,** 456. https://doi.org/10.3389/fpls.2019.00456

Leebens-Mack, J., Barker, M.S., Carpenter, E.J., and Deyholos, M.K. (2019). One thousand plant transcriptomes and the phylogenomics of green plants. Nature **574,** 679-685. 10.1038/s41586-019-1693-2

Li, C., Sako, Y., Imai, A., Nishiyama, T., Thompson, K., Kubo, M., Hiwatashi, Y., Kabeya, Y., Karlson, D., Wu, S.-H., Ishikawa, M., Murata, T., Benfey, P.N., Sato, Y., Tamada, Y., and Hasebe, M. (2017). A Lin28 homologue reprograms differentiated cells to stem cells in the moss *Physcomitrella patens*. Nat. Commun. **8,** 14242. https://doi.org/10.1038/ncomms14242

Li, H., Wu, G., Ware, D., Davis, K.R., and Yang, Z. (1998). Arabidopsis Rho-Related GTPases: Differential Gene Expression in Pollen and Polar Localization in Fission Yeast1. Plant Physiol. **118,** 407-417. 10.1104/pp.118.2.407

Li, H., Lin, Y., Heath, R.M., Zhu, M.X., and Yang, Z. (1999). Control of pollen tube tip growth by a Rop GTPase-dependent pathway that leads to tip-localized calcium influx. Plant Cell **11,** 1731-1742. 10.1105/tpc.11.9.1731

Liu, L., Niu, L., Ji, K., Wang, Y., Zhang, C., Pan, M., Wang, W., Schiefelbein, J., Yu, F., and An, L. (2023). AXR1modulates trichome morphogenesis through mediating ROP2 stability in Arabidopsis. Plant J. **116,** 756-772. https://doi.org/10.1111/tpj.16403

Luo, N., Yan, A., Liu, G., Guo, J., Rong, D., Kanaoka, M.M., Xiao, Z., Xu, G., Higashiyama, T., Cui, X., and Yang, Z. (2017). Exocytosis-coordinated mechanisms for tip growth underlie pollen tube growth guidance. Nat. Commun. **8,** 1687. https://doi.org/10.1038/s41467-017-01452-0

Molendijk, A.J., Bischoff, F., S.V.Rajendrakumar, C., Friml, J., Braun, M., Gilroy, S., and Palme, K. (2001). *Arabidopsis thaliana* Rop GTPases are localized to tips of root hairs and control polar growth. EMBO J. **20,** 2779-2788. https://doi.org/10.1093/emboj/20.11.2779

Moody, L.A., Kelly, S., Rabbinowitsch, E., and Langdale, J.A. (2018). Genetic Regulation of the 2D to 3D Growth Transition in the Moss *Physcomitrella patens*. Curr. Biol. **28,** 473-478.e475. https://doi.org/10.1016/j.cub.2017.12.052

Müller, S. (2023). Update: on selected ROP cell polarity mechanisms in plant cell morphogenesis. Plant Physiol. **193,** 26-41. 10.1093/plphys/kiad229

Mulvey, H., and Dolan, L. (2023a). RHO of plant signaling was established early in streptophyte evolution. Curr. Biol. **33,** 5515-5525.e5514. https://doi.org/10.1016/j.cub.2023.11.007

Mulvey, H., and Dolan, L. (2023b). RHO GTPase of plants regulates polarized cell growth and cell division orientation during morphogenesis. Curr. Biol. **33,** 2897-2911.e2896. https://doi.org/https://doi.org/10.1016/j.cub.2023.06.015

Nowak, M.A., Boerlijst, M.C., Cooke, J., and Smith, J.M. (1997). Evolution of genetic redundancy. Nature **388,** 167-171. https://doi.org/10.1038/40618

Ntefidou, M., Eklund, D.M., Le Bail, A., Schulmeister, S., Scherbel, F., Brandl, L., Dörfler, W., Eichstädt, C., Bannmüller, A., Ljung, K., and Kost, B. (2023). *Physcomitrium patens* PpRIC, an ancestral CRIB-domain ROP effector, inhibits auxin-induced differentiation of apical initial cells. Cell Rep. **42**. https://doi.org/10.1016/j.celrep.2023.112130

Okano, Y., Aono, N., Hiwatashi, Y., Murata, T., Nishiyama, T., Ishikawa, T., Kubo, M., and Hasebe, M. (2009). A polycomb repressive complex 2 gene regulates apogamy and gives evolutionary insights into early land plant evolution. Proc. Natl. Acad. Sci. U. S. A. **106,** 16321-16326. https://doi.org/10.1073/pnas.0906997106

Ou, H., and Yi, P. (2022). ROP GTPase-dependent polarity establishment during tip growth in plants. New Phytol. **236,** 49-57. https://doi.org/10.1111/nph.18373

Raval, P.K., Ngan, W.Y., Gallie, J., and Agashe, D. (2023). The layered costs and benefits of translational redundancy. eLife **12,** e81005. https://doi.org/10.7554/eLife.81005

Ren, H., Dang, X., Yang, Y., Huang, D., Liu, M., Gao, X., and Lin, D. (2016). SPIKE1 Activates ROP GTPase to Modulate Petal Growth and Shape. Plant Physiol. **172,** 358-371. 10.1104/pp.16.00788

Rensing, S.A., Goffinet, B., Meyberg, R., Wu, S.-Z., and Bezanilla, M. (2020). The Moss *Physcomitrium* (*Physcomitrella*) *patens*: A Model Organism for Non-Seed Plants. Plant Cell **32,** 1361-1376. https://doi.org/10.1105/tpc.19.00828

Rensing, S.A., Ick, J., Fawcett, J.A., Lang, D., Zimmer, A., Van De Peer, Y., and Reski, R. (2007). An ancient genome duplication contributed to the abundance of metabolic genes in the moss *Physcomitrella patens*. BMC Evol. Biol. **7,** 130. https://doi.org/10.1186/1471-2148-7-130

Reski, R., and Abel, W.O. (1985). Induction of budding on chloronemata and caulonemata of the moss, *Physcomitrella patens*, using isopentenyladenine. Planta **165,** 354-358. https://doi.org/10.1007/bf00392232

Roszak, P., Heo, J.-o., Blob, B., Toyokura, K., Sugiyama, Y., de Luis Balaguer, M.A., Lau, W.W.Y., Hamey, F., Cirrone, J., Madej, E., Bouatta, A.M., Wang, X., Guichard, M., Ursache, R., Tavares, H., Verstaen, K., Wendrich, J., Melnyk, C.W., Oda, Y., Shasha, D., Ahnert, S.E., Saeys, Y., De Rybel, B., Heidstra, R., Scheres, B., Grossmann, G., Mähönen, A.P., Denninger, P., Göttgens, B., Sozzani, R., Birnbaum, K.D., and Helariutta, Y. (2021). Cell-by-cell dissection of phloem development links a maturation gradient to cell specialization. Science **374,** eaba5531. https://doi.org/10.1126/science.aba5531

Ruan, J., Lai, L., Ou, H., and Yi, P. (2023). Two subtypes of GTPase-activating proteins coordinate tip growth and cell size regulation in *Physcomitrium patens*. Nat. Commun. **14,** 7084. https://doi.org/10.1038/s41467-023-42879-y

Schaefer, D., Zryd, J.-P., Knight, C.D., and Cove, D.J. (1991). Stable transformation of the moss *Physcomitrella patens*. Mol. Gen. Genet. **226,** 418-424. https://doi.org/10.1007/BF00260654

Schaefer, D.G., and Zrÿd, J.-P. (1997). Efficient gene targeting in the moss *Physcomitrella patens*. Plant J. **11,** 1195-1206. https://doi.org/10.1046/j.1365-313x.1997.11061195.x

Schindelin, J., Arganda-Carreras, I., Frise, E., Kaynig, V., Longair, M., Pietzsch, T., Preibisch, S., Rueden, C., Saalfeld, S., Schmid, B., Tinevez, J.-Y., White, D.J., Hartenstein, V., Eliceiri, K., Tomancak, P., and Cardona, A. (2012). Fiji: an open-source platform for biological-image analysis. Nat. Methods **9,** 676-682. https://doi.org/10.1038/nmeth.2019

Schumaker, K.S., and Dietrich, M.A. (1997). Programmed Changes in Form during Moss Development. Plant Cell **9,** 1099-1107

Stephan, O., Cottier, S., Fahlén, S., Montes-Rodriguez, A., Sun, J., Eklund, D.M., Klahre, U., and Kost, B. (2014). RISAP Is a TGN-associated RAC5 effector regulating membrane traffic during polar cell growth in tobacco. Plant Cell **26,** 4426-4447. https://doi.org/10.1105/tpc.114.131078

The UniProt Consortium. (2024). UniProt: the Universal Protein Knowledgebase in 2025. Nucleic Acids Res., gkae1010. 10.1093/nar/gkae1010

Thelander, M., Olsson, T., and Ronne, H. (2004). Snf1-related protein kinase 1 is needed for growth in a normal day–night light cycle. EMBO J. **23,** 1900-1910. https://doi.org/10.1038/sj.emboj.7600182

Thelander, M., Nilsson, A., Olsson, T., Johansson, M., Girod, P.-A., Schaefer, D.G., Zrÿd, J.-P., and Ronne, H. (2007). The moss genes PpSKI1 and PpSKI2 encode nuclear SnRK1 interacting proteins with homologues in vascular plants. Plant Mol. Biol. **64,** 559-573. https://doi.org/10.1007/s11103-007-9176-5

Thole, J.M., Perroud, P.F., Quatrano, R.S., and Running, M.P. (2014). Prenylation is required for polar cell elongation, cell adhesion, and differentiation in Physcomitrella patens. Plant J. **78,** 441-451. 10.1111/tpj.12484

Viaene, T., Landberg, K., Thelander, M., Medvecka, E., Pederson, E., Feraru, E., Cooper, Endymion D., Karimi, M., Delwiche, Charles F., Ljung, K., Geisler, M., Sundberg, E., and Friml, J. (2014). Directional auxin transport mechanisms in early diverging land plants. Curr. Biol. **24,** 2786-2791. https://doi.org/10.1016/j.cub.2014.09.056

Vidali, L., Augustine, R.C., Kleinman, K.P., and Bezanilla, M. (2007). Profilin is essential for tip growth in the moss *Physcomitrella patens*. Plant Cell **19,** 3705-3722. https://doi.org/10.1105/tpc.107.053413

Vidali, L., Burkart, G.M., Augustine, R.C., Kerdavid, E., Tüzel, E., and Bezanilla, M. (2010). Myosin XI is essential for tip growth in *Physcomitrella patens*. Plant Cell **22,** 1868-1882. https://doi.org/10.1105/tpc.109.073288

Vieten, A., Vanneste, S., WiśNiewska, J., Benková, E., Benjamins, R., Beeckman, T., Luschnig, C., and Friml, J.I. (2005). Functional redundancy of PIN proteins is accompanied by auxin-dependent cross-regulation of PIN expression. Development **132,** 4521-4531. https://doi.org/10.1242/dev.02027

Winge, P., Brembu, T., Kristensen, R., and Bones, A.M. (2000). Genetic Structure and Evolution of RAC-GTPases in Arabidopsis thaliana. Genetics **156,** 1959-1971

Yalovsky, S., Bloch, D., Sorek, N., and Kost, B. (2008). Regulation of membrane trafficking, cytoskeleton dynamics, and cell polarity by ROP/RAC GTPases. Plant Physiol. **147,** 1527-1543. 10.1104/pp.108.122150

Yi, P., and Goshima, G. (2020). Rho of plants GTPases and cytoskeletal elements control nuclear positioning and asymmetric cell division during *Physcomitrella patens* branching. Curr. Biol. **30,** 2860-2868. https://doi.org/10.1016/j.cub.2020.05.022

1328 **Figure legends**

1329 **Figure 1. Knockout of two Pp*ROP*s (*rop*^{2xKO}) promotes caulonema differentiation.**
1330 Graphs and images based on 5-day-old protonemata or 5-week-old colonies
1331 regenerated from protoplasts with the indicated genotypes of double Pp*ROP* knockout
1332 mutants and WT using culture conditions listed in Supplementary Table S4. **A)** Average
1333 subapical cell length of chloronema and caulonema cells in 5-day-old protonemata. n =
1334 50 cells were analyzed per genotype. The experiment was performed three times with
1335 consistent results. **B)** Bright field images of 5-day-old chloronemal and caulonemal
1336 filament tips. Asterisks indicate the cell wall between neighboring cells. Scale bars: 25
1337 µm. **C)** Average percentage of caulonema differentiation in 5-day-old protonemal
1338 filaments with at least three cells as determined by microscopic observation. n = 60
1339 colonies per genotype were measured in 3 independent experiments. **D-G)** Average size
1340 (area) of 5-day-old protonemata **(D)** or 5-week-old colonies **(E)** as determined based on
1341 microscopic imaging of chlorophyll autofluorescence **(F**, 5-day-old**)** or pictures recorded
1342 using a stereo microscope **(G**, 5-week-old**)**. The mean value of WT was used as a
1343 calibrator (relative area = 1). n = 105 colonies per genotype were measured in 3
1344 independent experiments (**D**), or n = 42 colonies per genotype were measured. The
1345 experiment was performed three times with consistent results (**E**). Scale bars: 400 µm
1346 **(F)**, 10 mm **(G)**. (**A, C-E)** Error bars: standard deviation (SD), dots represent individual
1347 data points. Statistical analysis by one-way ANOVA/Tukey's test (pairwise comparisons
1348 to WT and relevant pairwise comparisons are displayed, all others see Supplementary
1349 Data Set S3): ^{ns} $P > 0.05$ (not significant), * $P \leq 0.05$, ** $P \leq 0.01$, *** $P \leq 0.001$, **** $P \leq$
1350 0.0001.

1351 **Figure 2. Knockout of three Pp*ROP*s (*rop*^{3xKO}) inhibits tip growth of protonemata**
1352 **and rhizoids.** Graphs and images based on 5-day-old protonemata or 5-week-old
1353 colonies regenerated from protoplasts with the indicated genotypes of triple Pp*ROP*
1354 knockout mutants and WT cultivated on media listed in Supplementary Table S4. **A)**
1355 Bright field micrographs of 5-day-old chloronemal and caulonemal filament tips.
1356 Asterisks indicate the cell wall between neighboring cells. Scale bars: 25 µm. **B)**
1357 Average subapical cell length of chloronemal and caulonemal cells in 5-day-old
1358 protonemata. n = 50 cells per genotype were measured. The experiment was repeated

1359 three times with consistent results. **C)** Average percentage of caulonema differentiation
1360 in 5-day-old protonemal filaments with at least three cells as determined by microscopic
1361 observation. n = 60 colonies per genotype were measured in 3 independent
1362 experiments. **D, E, G, H)** Average size (area) of 5-day-old protonemata **(D)** or 5-week-
1363 old colonies **(E)** as determined based on microscopic imaging of chlorophyll
1364 autofluorescence **(G)** or pictures recorded using a stereo microscope **(H)**. Scale bars:
1365 400 µm **(G)**, 10 mm **(H)**. The mean value of WT was used as a calibrator (relative area =
1366 1). n = 105 colonies per genotype were measured in 3 independent experiments **(D),** or
1367 n = 45 colonies per genotype were measured. The experiment was repeated three times
1368 with consistent results **(E)**. **F** and **I)** Average length of rhizoids of 5-week-old
1369 gametophores **(F)** based on pictures recorded using a stereo microscope (arrows
1370 indicate the end of rhizoids) **(I)**. Scale bars: 5 mm. n = 21 rhizoids per genotype were
1371 measured. The experiment was repeated three times with consistent results. **B-F)** Error
1372 bars: standard deviation (SD), dots represent individual data points. Statistical analysis
1373 by two-way ANOVA/Tukey's test **(B)** or one-way ANOVA/Tukey's test **(C-F)**
1374 (comparisons to WT are displayed, all others see Supplementary Data Set S3): ^{ns} $P >$
1375 0.05 (not significant), * $P \leq 0.05$, **** $P \leq 0.0001$.

1376 **Figure 3. Pp*ROP*s are not altered in their gene expression in *rop*^{3xKO} mutants and**
1377 **redundantly complement the *rop*^{4xKO} mutant. A** and **B)** qRT-qPCR of expression
1378 levels of Pp*ROP*s in 1-week-old protonemata cultivated through homogenization
1379 (Supplementary Table S4) with the indicated genotype: *rop*^{3xKO} mutants **(A)**, *rop*^{4xKO}
1380 mutant complemented with the coding and 3' UTR sequence of Pp*ROP1* (Pp*ROP4*
1381 identical amino acid sequence) or Pp*ROP2* or Pp*ROP3* downstream of the Pp*ROP1*
1382 promoter (*rop*^{4xKO}/*ROP1*^{pro}:*ROPX*) **(B)** were compared to WT. Absolute transcript levels
1383 were determined based on standard curves using the value obtained for one WT
1384 replicate of Pp*ROP1* as a calibrator (relative expression = 1). Bars: mean of three
1385 biological and two technical replicates, error bars: standard error of the mean. The
1386 experiment was performed two times with consistent results. **C-E)** Average size (area) of
1387 5-day-old protonemata **(C)** or 4-week-old colonies **(D)** regenerated from protoplasts with
1388 the indicated genotypes: i) WT, ii) *rop3/2/4*, iii) *rop*^{4xKO}/*ROP1*^{pro}:*ROPX* as determined
1389 based on microscopic imaging of chlorophyll autofluorescence **(E,** 5 days**)** or pictures

1390 recorded using a stereo microscope **(E,** 4 weeks**)**. The mean value of WT was used as a
1391 calibrator (relative area = 1). n = 100 **(C)** or n = 80 **(D)** colonies per genotype were
1392 measured in 3 independent experiments. Error bars: standard deviation (SD), dots
1393 represent individual data points. Scale bars: 250 µm (**E** upper row, 5 days), 5 mm (**E**
1394 lower row, 4 weeks). Statistical analysis by two-way ANOVA/Bonferroni's test **(A)** or one-
1395 way ANOVA/Tukey's test **(B**-**D)** (pairwise comparisons to WT and relevant pairwise
1396 comparisons are displayed, all others provided in Supplementary Data Set S3): ^{ns} $P >$
1397 0.05 (not significant), * $P \leq 0.05$, **** $P \leq 0.0001$.

1398 **Figure 4. Loss of all Pp*ROP*s affects cell division and eliminates tip growth.**
1399 Analysis of the *rop*^{4xKO} phenotype was performed using protonemata or 5-week-old
1400 colonies cultivated on media listed in Supplementary Table S4 with the indicated
1401 genotypes: i) WT, ii) *rop3/4/1,* iii) *rop3/4/1/2, rop3/2/4/1* (*rop*^{4xKO}), iv) *rop*^{4xKO}/*ind*^{pro}:*ROP2*
1402 uninduced (conditional complementation of *rop*^{4xKO} with the coding and 3' UTR
1403 sequence of Pp*ROP2* downstream of the inducible β-estradiol promoter). **A-C)** 1-week-
1404 old protonemata cultivated through homogenization. **A)** Bright field micrographs of
1405 *rop*^{4xKO} mutants. Scale bars: 100 µm. **B)** Confocal imaging of the cell division plane
1406 using projections of serial confocal optical sections of protonemata stained with
1407 propidium iodide. Scale bars: 25 µm. **C)** qRT-PCR of relative Pp*ROP2* transcript levels
1408 determined according to the $2^{-\Delta CCT}$ method, using the value obtained for one WT
1409 replicate as a calibrator (relative expression = 1). Bars: mean of three biological and two
1410 technical replicates. The experiment was repeated two times with consistent results. **D-**
1411 **G)** Analysis of the *rop*^{4xKO} phenotype using 4 or 5-day-old protonemata or 5-week-old
1412 colonies regenerated from protoplasts with the indicated genotypes. *rop*^{4xKO}/*ind*^{pro}:*ROP2*
1413 protoplasts were regenerated without β-estradiol resembling the *rop*^{4xKO} phenotype. **D)**
1414 Bright field images from 5-day-old protonemata (top panel) and images of 5-week-old
1415 colonies (lower panel) were recorded using a stereo microscope. Scale bars: 100 µm
1416 (upper panel), 10 mm (lower panel, black bar), 500 µm (lower panel, white bars). **E)**
1417 Average size (area) of 5-day-old protonemata regenerated from protoplasts as
1418 determined based on microscopic imaging of chlorophyll autofluorescence using the
1419 mean value of WT as calibrator (relative area = 1). n = 50 colonies per genotype
1420 measured in 3 independent experiments. **F** and **G)** Cell division rate in 4-day-old

1421 protonemata was analyzed through projections of serial confocal optical sections
1422 displaying DAPI staining (white) and chlorophyll autofluorescence (red) (scale bars: 100
1423 µm) **(F)** and determination of the average nuclei number **(G)**. n = 50 colonies per
1424 genotype measured in 3 independent experiments. **C, E, G)** Error bars: standard error of
1425 the mean (SEM) **(C)**, standard deviation (SD) **(E** and **G)**, dots represent individual data
1426 points. Statistical analysis by one-way ANOVA/Tukey's test (pairwise comparisons to WT
1427 and relevant pairwise comparisons are displayed, all others see Supplementary Data
1428 Set S3): ^{ns} $P > 0.05$ (not significant), *** $P \leq 0.001$, **** $P \leq 0.0001$.

1429 **Figure 5. Titratable Pp*ROP2* expression rescues *rop*^{4xKO}.** Protonemata or 4-week-
1430 colonies were regenerated from protoplasts using media solidified with agar except
1431 where otherwise noted (see Supplementary Table S4) with the indicated genotypes: i)
1432 WT, ii) *rop*^{4xKO}/*ind*^{pro}:*ROP2* (conditional complementation of *rop*^{4xKO} with the coding and
1433 3' UTR sequence of Pp*ROP2* downstream of the inducible β-estradiol promoter) treated
1434 with representative β-estradiol concentrations. **A)** Bright field images of 5-day-old
1435 protonemata and images using a stereo microscope of 4-week-old colonies.
1436 *rop*^{4xKO}/*ind*^{pro}:*ROP2* did not develop gametophores (4 weeks) in the absence or with
1437 minimal PpROP2 expression (0 µM, 2x10^{-5} µM β-estradiol). Treatment with 2x10^{-4} µM β-
1438 estradiol generated gametophore-like structures only in liquid BCD medium (asterisk)
1439 and at ≥ 4x10^{-4} µM β-estradiol gametophores developed on BCD medium solidified with
1440 agar. Closed triangles indicate protonemata, open triangles indicate rhizoids. Scale bars:
1441 200 µm (1st top row), 100 µm (2nd row), 5 mm (3rd row), 1 mm (4th row), 1 mm (5th row,
1442 black bar), 500 µm (5th row, white bars). **B)** Relative transcript levels of Pp*ROP2* were
1443 determined in 7-day-old protonemata (WT, *rop*^{4xKO}/*ind*^{pro}:*ROP2* treated with 9x10^{-4} µM β-
1444 estradiol) or 10-day-old protonemata (*rop*^{4xKO}/*ind*^{pro}:*ROP2* treated with ≤ 4x10^{-4} µM β-
1445 estradiol) according to the $2^{-\Delta\Delta Ct}$ method, using the value obtained for one WT replicate
1446 as calibrator (relative expression = 1). Bars: mean of three biological and two technical
1447 replicates. The experiment was repeated two times with consistent results. **C** and **D)**
1448 Average subapical cell length of chloronemata **(C)** or average percentage of caulonema
1449 differentiation as determined by microscopic observation **(D)** in 5-day-old protonemata. n
1450 = 22 cells **(C)** or n = 30 colonies **(D)** per genotype measured in 3 independent
1451 experiments. **E)** Average size (area) of 5-day-old or 4-week-old colonies using the mean

1452 value of WT as calibrator (relative area = 1). n = 60 colonies per genotype measured in
1453 three independent experiments (5 days). n = 22 colonies per genotype, the experiment
1454 was performed three times with consistent results (4 weeks). **B-E)** Error bars: standard
1455 error of the mean (SEM) **(B)**, standard deviation (SD) **(C-E)**. Dots represent individual
1456 data points. Statistical analysis by one-way ANOVA/Tukey's test (pairwise comparisons
1457 to WT are displayed, all others see Supplementary Data Set S3): ^{ns} $P > 0.05$ (not
1458 significant), * $P \leq 0.05$, ** $P \leq 0.01$, *** $P \leq 0.001$, **** $P \leq 0.0001$.

1459 **Figure 6. Pp*ROP* overexpression deregulates tip growth and caulonema**
1460 **differentiation.** 1-week old protonemata cultivated through homogenization **(A)** or 5-
1461 day-old protonemata or 4-week colonies regenerated from protoplasts **(B-H)** using
1462 media listed in Supplementary Table S4 with the indicated genotypes: i) WT, ii)
1463 WT/i*nd*^{pro}:*ROP1* (overexpression of the Pp*ROP1* coding sequence and 3' UTR in WT
1464 using the inducible β-estradiol promoter. **A)** Relative transcript levels of Pp*ROP1* were
1465 determined according to the $2^{-\Delta CCT}$ method using the value obtained for one WT
1466 replicate as calibrator (relative expression level = 1). Bars: mean of three biological and
1467 two technical replicates. The experiment was repeated two times with consistent results.
1468 **B-D)** Average percentage of caulonema differentiation as determined by microscopic
1469 observation **(B)** or average subapical chloronemal cell length **(C)** or cell width **(D)** in
1470 filaments with at least three cells of 5-day-old protonemata. n = 42 cells per genotype
1471 measured in 3 independent experiments. **E)** Bright field micrographs of filament tips of
1472 5-day-old protonemata with the indicated genotypes. Asterisks indicate the cell wall
1473 between neighboring cells, dotted rectangles indicate the magnified apical region. Scale
1474 bars: 25 µm. **F-H)** Average size (area) of 5-day-old protonemata **(F)** or 4-week-old
1475 colonies **(G)** using the mean value of WT as calibrator (relative area = 1) were
1476 determined based on microscopic imaging of chlorophyll autofluorescence **(H**, 1st top
1477 row; 5 days**)** or pictures recorded using a stereo microscope **(H**, 2nd and 3rd rows; 4
1478 weeks**)**. Scale bars: 500 µm (1st top row), 5 mm (2nd row), 1 mm (3rd row). n = 35 **(F)** or n
1479 = 23 **(G)** colonies per genotype. The experiment was repeated two times, and the results
1480 from one representative experiment are shown here. **A-D, F, G)** Error bars: standard
1481 error of the mean (SEM) **(A)**, standard deviation (SD) **(B-D, F, G)**. Dots represent

individual data points. Statistical analysis by one-way ANOVA/Tukey's test (pairwise comparisons are displayed): ^{ns} $P > 0.05$ (not significant) **** $P \leq 0.0001$.

Figure 7. GTP/GDP cycling is essential for most PpROP functions but not gametophore initiation. Graphs and images based on protonemata or gametophores or colonies using culture conditions (Supplementary Table S4) with the indicated genotypes: i) WT, ii) *rop2/3/4*, iii) *rop*^{4xKO} iv) *rop*^{4xKO}/*ROP1*^{pro}:*ROP1*^{Q64L} (complementation of *rop*^{4xKO} with the Pp*ROP1* coding and 3' UTR sequence containing a constitutive active mutation [Q64L] downstream of the endogenous Pp*ROP1* promoter), v) *rop*^{4xKO}/*ROP1*^{pro}:*ROP1*^{F31L} (complementation of *rop*^{4xKO} with the Pp*ROP1* coding and the 3' UTR sequence containing a fast cycling mutation [F31L] downstream of the endogenous Pp*ROP1* promoter). **A)** Relative transcript levels of Pp*ROP1* in 1-week-old protonemata cultivated through homogenization according to the $2^{-\Delta CCT}$ method, using the value obtained for one WT replicate as a calibrator (relative expression = 1). Bars: mean of three biological and two technical replicates. The experiment was repeated two times with consistent results. **B-E)** 5-day-old protonemata or 5-week-old colonies regenerated from protoplasts (WT, *rop2/3/4*, *rop*^{4xKO}/*ROP1*^{pro}:*ROP1*^{F31L}) or cultivated through homogenization (*rop*^{4xKO}, *rop*^{4xKO}/*ROP1*^{pro}:*ROP1*^{Q64L}). **B)** Images of 5-day-old protonemata recorded using bright field microscopy (upper row) and images of 5-week-old colonies obtained using a stereo microscope (WT, *rop2/3/4*, *rop*^{4xKO}/*ROP1*^{pro}:*ROP1*^{F31L}) or bright field microscopy (*rop*^{4xKO}, *rop*^{4xKO}/*ROP1*^{pro}:*ROP1*^{Q64L}) (lower row). Scale bars: 100 µm (upper row), 10 mm (black bars, lower row), 400 µm (white bars, lower row). **C)** Images of 5-week-old gametophores cultivated on solid BCD medium except *rop*^{4xKO}/*ROP1*^{pro}:*ROP1*^{Q64L} that developed gametophore-like structures only in liquid BCD medium (asterisk) were recorded using a stereo microscope. Arrow indicates a gametophore-like structure used for magnification using bright field microscopy (dotted rectangle). Scale bars: 2 mm (black bars) 200 µm (white bars). **D)** Average size (area) of 5-day-old protonemata or 5-week-old colonies normalized to the mean value of WT (relative area = 1). n = 30 colonies per genotype; the experiment was repeated three times with consistent results (5 days) or n = 81 colonies per genotype measured in 3 independent experiments (5 weeks). **E)** Average percentage of caulonema differentiation in 5-day-old protonemal

1513 filaments with at least three cells was determined by microscopic observation. n = 10
1514 colonies per genotype. The experiment was repeated three times with consistent results.
1515 **A**, **D, E)** Error bars: standard error of the mean (SEM) **(A)**, standard deviation (SD) **(D**
1516 and **E),** dots represent individual data points. Statistical analysis by one-way
1517 ANOVA/Tukey's test (pairwise comparisons to WT and relevant pairwise comparisons
1518 are displayed, all others see Supplementary Data Set S3). ^{ns} $P > 0.05$ (not significant), *
1519 $P \leq 0.05$, ** $P \leq 0.01$, *** $P \leq 0.001$, **** $P \leq 0.0001$.

1520 **Figure 8. At*ROP7* or Hs*RHOA* overexpression partially rescues Pp*ROP*s.** 1-week-
1521 old protonemata or 4-week-old colonies were cultivated through homogenization using
1522 media described in Supplementary Table S4 with the indicated genotypes: i) WT, ii)
1523 *rop1/2/3*, iii) *rop*^{4xKO}/*ind*^{pro}:At*ROP7* or *rop*^{4xKO}/*ind*^{pro}:Hs*RHOA* (complementation of
1524 *rop*^{4xKO} with the coding sequence of At*ROP7* or Hs*RHOA* downstream of the β-estradiol
1525 inducible promoter). **A)** Absolute transcript levels of Pp*ROP4*, At*ROP7,* or Hs*RHOA*
1526 were determined in 1-week-old protonemata with the indicated genotype based on
1527 standard curves, using the value obtained for one WT replicate of Pp*ROP4* as calibrator
1528 (relative expression = 1). Bars: mean of three biological and two technical replicates.
1529 Error bars: standard error of the mean. The experiment was repeated two times with
1530 consistent results. Statistical analysis by one-way ANOVA/Tukey's test (pairwise
1531 comparisons to WT and relevant pairwise comparisons are displayed, all others see
1532 Supplementary Data Set S3): ^{ns} $P > 0.05$ (not significant), * $P \leq 0.05$, ** $P \leq 0.01$, *** $P \leq$
1533 0.001, **** $P \leq 0.0001$. **B** and **C)** Bright field micrographs of 1-week-old protonemata **(B)**,
1534 or images of 4-week-old gametophores recorded using a stereo microscope (WT,
1535 *rop1/2/3*) or gametophore-like structures using a bright field microscope
1536 (*rop*^{4xKO}/*ind*^{pro}:At*ROP7*, *rop*^{4xKO}/*ind*^{pro}:Hs*RHOA*) **(C)**. Scale bars: 50 µm **(B)**, 2 mm (black
1537 bars), 200 µm (white bars) **(C)**.

1538 **Figure 9. Overview of PpROP functions.** Schematic drawing summarizing PpROP
1539 functions in protonemata and gametophores of *P. patens* with the indicated genotypes: i)
1540 WT (black font), ii) WT/*ind*^{pro}:*ROP1* (Pp*ROP1* overexpresion in WT controlled by the
1541 inducible β-estradiol promoter) (Kubo et al., 2013) (black font), iii) *rop*^{1xKO}*, rop*^{2xKO}*,*
1542 *rop*^{3xKO}, *rop*^{4xKO} (Pp*ROP* knockout mutants) (red font), iv) *rop*^{4xKO}/*ROP1*^{pro}:*ROP1*^{Q64L},
1543 *rop*^{4xKO}/*ROP1*^{pro}:*ROP1*^{F31L} (complementation of *rop*^{4xKO} with the coding and 3' UTR

1544 sequence of Pp*ROP1* containing a constitutive active [Q64L] or fast cycling mutation
1545 [F31L] downstream of the Pp*ROP1* promoter) (black font), v) *rop*^{4xKO}*/ind*^{pro}:At*ROP7* or
1546 *rop*^{4xKO}*/ind*^{pro}:Hs*RHOA* (complementation of *rop*^{4xKO} with the coding sequence of
1547 At*ROP7* or Hs*RHOA* downstream of the inducible β-estradiol promoter) (black font), vi)
1548 *rop*^{4xKO}*/ind*^{pro}:*ROP2* (complementation of *rop*^{4xKO} with the coding and 3' UTR sequence
1549 of Pp*ROP2* downstream of the inducible β-estradiol promoter) (blue font). nd: not
1550 determined.

1551 **Supplementary data legends**

1552 **Supplementary Figure S1. Pp*ROP* gene expression in protonemata** (supports **Figs.**
1553 **1-5, 7**, **Supplementary Fig. S5**). Absolute transcripts levels of Pp*ROP*s in 1-week-old
1554 protonemata of WT cultivated through homogenization on BCDA medium
1555 (Supplementary Table S4) were determined based on standard curves, using the value
1556 obtained for one WT replicate of Pp*ROP1* as calibrator (relative expression = 1). Bars
1557 represent means of three biological and two technical replicates. Error bars: standard
1558 error of the mean (SEM). Statistical analysis by one-way ANOVA/Tukey's test
1559 (Supplementary Data Set S3): ^{ns} $P > 0.05$ (not significant); * $P \leq 0.05$.

1560 **Supplementary Figure S2. Editing of the genomic Pp*ROP1* locus through**
1561 **homologous recombination and summary of transgenic lines** (supports **Figs. 1-8,**
1562 **Supplementary Figs. S5, S6, S8**). **A)** Schematic representation of the Pp*ROP1* genetic
1563 locus and plasmid maps used to generate transgenic lines (Supplementary Table S3),
1564 drawn to scale. pSLU33 was used to generate *rop1* knockout by replacing the genomic
1565 fragment containing all exons and introns of Pp*ROP1* with the expression cassette,
1566 conferring resistance to hygromycin. pFAU508 (*ROP1*^{pro}:*ROP1*), pFAU509
1567 (*ROP1*^{pro}:*ROP2*), pFAU517 (*ROP1*^{pro}:*ROP3*), pFAU306 (*ROP1*^{pro}:*ROP1*^{Q64L}) or
1568 pFAU421 (*ROP1*^{pro}:*ROP1*^{F31L}) were used to generate *rop*^{4xKO} complementation lines by
1569 replacing all exons and introns of Pp*ROP1* in *rop3/2/4* with the coding and 3' UTR
1570 sequence of a Pp*ROP* variant. **A** and **D**) Green boxes: exons (numbered) or coding
1571 sequences, gray boxes: UTR sequences, blue boxes: regions used for homologous
1572 recombination targeting, white boxes: resistance markers, arrows: primers used for
1573 genotyping or RT-qPCR (Supplementary Data Set S1), three dots: sequence not
1574 displayed to scale to save space, green numbers: nucleotide position in the Pp*ROP1*

1575 coding region. **B)** Confirmation of transgenic lines through genotyping PCR using
1576 genomic DNA with the indicated primers. **C)** Summary of *rop* knockouts indicating the
1577 order in which they were generated from left to right (upper table). Summary of *rop*^{4xKO}
1578 complementation lines generated by replacement of the remaining Pp*ROP* in the
1579 indicated *rop*^{3xKO} genetic background (red font) with the coding sequence of an
1580 *ROP*/*RHO* gene expressed by the endogenous Pp*ROP1* promoter or the inducible β-
1581 estradiol-inducible promoter (Kubo et al., 2013) (bottom table). **D)** Vector map of
1582 pFAU461 used to overexpress *P*p*ROP1* in WT (WT/*ind*^{pro}:*ROP1*) by inserting the coding
1583 and 3' UTR sequence of Pp*ROP1* downstream of the inducible β-estradiol-inducible
1584 promoter in the PIG1 neutral region through homologous recombination. **E)** Confirmation
1585 of WT/*ind*^{pro}:*ROP1* transgenic line through genotyping PCR using genomic DNA with the
1586 indicated primers.

1587 **Supplementary Figure S3. Editing of the genomic Pp*ROP2* and Pp*ROP3* loci**
1588 **through homologous recombination** (supports **Figs. 1-5**, **7, Supplementary Figs.**
1589 **S5, S6**). **A** and **C)** Schematic representation of the Pp*ROP2* **(A)** and Pp*ROP3* **(C)**
1590 genetic loci and plasmid maps used to generate transgenic lines (Supplementary Table
1591 S3), drawn to scale. Green boxes: exons (numbered) or coding sequences, gray boxes:
1592 UTR sequences, blue boxes: regions used for homologous recombination targeting,
1593 white boxes: resistance markers, arrows: primers used for genotyping or RT-qPCR
1594 (Supplementary Data Set S1), three dots: sequence not displayed to scale to save
1595 space, green numbers: nucleotide position in the Pp*ROP2* **(A)** or Pp*ROP3* **(C)** coding
1596 sequence. **A)** pSLU34 was used to generate *rop2* knockout by replacing the genomic
1597 fragment containing all Pp*ROP2* exons and introns with the expression cassette,
1598 conferring resistance to zeocin. **C)** pSLU35 was used to generate *rop3* knockout by
1599 replacing the genomic fragment containing all Pp*ROP3* exons and introns with the
1600 expression cassette, conferring resistance to blasticidin. pFAU431 was used to
1601 complement *rop*^{4xKO} by replacing all exons and introns of the Pp*ROP3* locus with the
1602 coding and 3′ UTR sequence of Pp*ROP2* expressed under the control of the β-estradiol-
1603 inducible system (Kubo et al., 2013) generating *rop*^{4xKO}/*ind*^{pro}:*ROP2*. The lexA operator
1604 and 35S promoter are depicted, but not the GX8 promoter or XVE regions. **B** and **D)**

1605 Confirmation of transgenic lines through genotyping PCR using genomic DNA with the
1606 indicated primers.

1607 **Supplementary Figure S4. Editing of the genomic Pp*ROP4* locus through**
1608 **homologous recombination** (supports **Figs. 1**-**5**, **7**, **8, Supplementary Figs. S5, S6**).
1609 **A)** Schematic representation of the Pp*ROP4* genetic locus and plasmid maps used to
1610 generate transgenic lines (Supplementary Table S3), drawn to scale. pSLU36 was used
1611 to generate *rop4* knockout by replacing the genomic fragment containing all Pp*ROP4*
1612 exons and introns with the expression cassette, conferring resistance to G418. pFAU398
1613 (ind^{pro}:At*ROP7*) or pFAU402 (ind^{pro}:Hs*RHOA*) were used to complement rop^{4xKO} by
1614 replacing all exons and introns of Pp*ROP4* in *rop3/1/2* with the coding sequence of
1615 At*ROP7* or Hs*RHOA* expressed under the control of the β-estradiol-inducible system
1616 (Kubo et al., 2013), generating rop^{4xKO}/ind^{pro}:At*ROP7* or rop^{4xKO}/ind^{pro}:Hs*RHOA*,
1617 respectively. Green boxes: exons (numbered) or coding sequences, gray boxes: UTR
1618 sequences, blue boxes: regions used for homologous recombination targeting, white
1619 boxes: resistance markers, arrows: primers (Supplementary Data Set S1) used for
1620 genotyping or RT-qPCR, three dots: sequence not displayed to scale to save space,
1621 green numbers: nucleotide position in the Pp*ROP4* coding sequence. **B)** Confirmation of
1622 transgenic lines through genotyping PCR using genomic DNA with the indicated primers.
1623 **Supplementary Figure S5**. **Knockout of a single Pp*ROP* (rop^{1xKO}) does not affect**
1624 **protonemata** (supports **Fig. 1**). **A-F)** Graphs and images based on 5-day-old
1625 protonemata or 5-week-old colonies regenerated from protoplasts were cultivated using
1626 media listed in Supplementary Table S4. **A)** Average subapical cell length of
1627 chloronemata and caulonemata in 5-day-old protonemata. n = 50 cells per genotype.
1628 The experiment was repeated three times with consistent results. **B)** Bright field
1629 micrographs of chloronemal and caulonemal filament tips. Asterisks: cell wall between
1630 apical and subapical cells. Scale bars: 25 µm. **C)** Average percentage of caulonema
1631 differentiation in 5-day-old protonema filaments with at least three cells as determined by
1632 microscopic observation. n = 60 colonies per genotype measured in 3 independent
1633 experiments. **D-F)** Average size of 5-day-old protonemata **(D)** or 5-week-old colonies **(E)**
1634 determined using micrographs of chlorophyll autofluorescence **(F**, upper row**)** or bright
1635 field images **(F**, lower row**)** recorded with a stereo microscope. n = 120 colonies per

1636 genotype measured in 3 independent experiments **(D)** or n = 41 colonies per genotype.
1637 The experiment was performed three times with consistent results **(E)**. Scale bars: 400
1638 µm **(F,** upper row**),** 10 mm **(F,** lower row**)**. **A, C-E)** Error bars: standard deviation (SD),
1639 dots represent individual data points. Statistical analysis by two-way ANOVA/Tukey's
1640 test **(A)** or one-way ANOVA/Tukey's test **(C-E)**. Pairwise comparisons to WT are
1641 displayed, all others see Supplementary Data Set S3: ^{ns} $P > 0.05$ (not significant); * $P \leq$
1642 0.05.

1643 **Supplementary Figure S6**. **PpROPs do not influence the expression of auxin-**
1644 **regulated genes or the auxin content** (supports **Fig. 2**). **A-C)** Graphs and images
1645 based on 1-week-old protonemata with the indicated genotype cultivated using media
1646 described in Supplementary Table S4. **A)** Free IAA content of WT and *rop*^{2xKO} lines were
1647 analyzed by gas chromatography-tandem mass spectrometry. Bars: means of n = 11
1648 independent measurements, error bars: standard deviation, dots represent individual
1649 data points. **B)** Confocal microscopy imaging of PpPINA-GFP (Pp*PINA*^{pro}:Pp*PINA-GFP*)
1650 (Viaene et al., 2014) in WT and *rop1/2*. Asterisks indicate the cell wall between the
1651 apical and subapical cell. Scale bars: 25 µm. **C)** RT-qPCR was used to assess the
1652 expression of several auxin-responsive genes related to auxin signaling according to the
1653 $2^{-\Delta CCT}$ method, using the value obtained for one WT replicate as a calibrator (relative
1654 expression = 1). Bars: mean of three biological and two technical replicates, error bars:
1655 standard error of the mean (SEM). **A** and **C)** Statistical analysis by one-way
1656 ANOVA/Tukey's test (pairwise comparisons to WT are displayed, all others see
1657 Supplementary Data Set S3): ^{ns} $P > 0.05$ (not significant).

1658 **Supplementary Figure S7. β-Estradiol does not influence Pp*ROP* expression or**
1659 **protonemal development** (supports **Figs. 5, 6, 8**). Graphs based on protonemata or 4-
1660 week-old colonies of WT cultivated using media listed in Supplementary Table S4. 1 µM
1661 β-estradiol was added to the media from a 10 mM stock solution dissolved in DMSO. **A)**
1662 Relative expression level of Pp*ROP1* in 1-week-old protonemata cultivated through
1663 homogenization was determined according to the $2^{-\Delta CCT}$ method, using the value
1664 obtained for one WT replicate as calibrator (relative expression = 1). Bars: mean of three
1665 biological and two technical replicates; error bars: standard error of the mean (SEM).

1666 The experiment was repeated two times with consistent results. **B-F)** Nuclei count and
1667 growth parameters were assessed using protoplasts regenerated for 2 days on PRMB
1668 medium without β-estradiol, followed by 2 days **(B)** or 3 days **(C-E)** on BCDA medium or
1669 4 weeks **(F)** on BCD medium supplemented with 1 µM β-estradiol. **B)** Nuclei were
1670 counted in 4-day-old protonemata stained with DAPI using confocal fluorescence
1671 microscopy. n = 8 colonies per genotype. The experiment was repeated three times with
1672 consistent results. **C** and **D)** Average subapical cell length of chloronema cells **(C)** or
1673 average percentage of caulonema differentiation in 5-day-old protonemal filaments with
1674 at least three cells as determined by microscopic observation **(D)**. n = 42 cells per
1675 genotype were analyzed in 3 independent experiments **(C),** or n = 20 colonies per
1676 genotype were analyzed. The experiment was repeated three times with consistent
1677 results **(D)**. **E** and **F)** Average size (area) of 5-day-old **(E)** or 4-week-old **(F)** colonies
1678 determined based on microscopic imaging of chlorophyll autofluorescence **(E)** or bright
1679 field micrographs **(F)** using a stereo microscope. The mean value of WT was used as a
1680 calibrator (relative area = 1). n = 55 protonemata **(F)** or n = 60 colonies **(E)** per genotype
1681 were analyzed in 3 independent experiments. **A-F**) Error bars: standard error of the
1682 mean (SEM) **(A),** standard deviation (SD) **(C-F)**; dots represent individual data points.
1683 Statistical analysis (Supplementary Data Set S3) by unpaired Student's *t*-test: ^{ns} $P >$
1684 0.05 (not significant).

1685 **Supplementary Figure S8. Gametophore-like structures of**
1686 ***rop*^{4xKO}/*ROP1*^{pro}:*ROP1*^{Q64L}** (supports **Fig. 7**). 5-week-old cultures were cultivated in
1687 liquid BCD medium (Supplementary Table S4). Maximum projections of serial optical
1688 sections of cell walls stained with propidium iodide were imaged using confocal
1689 microscopy. Scale bars: 100 µm.
1690

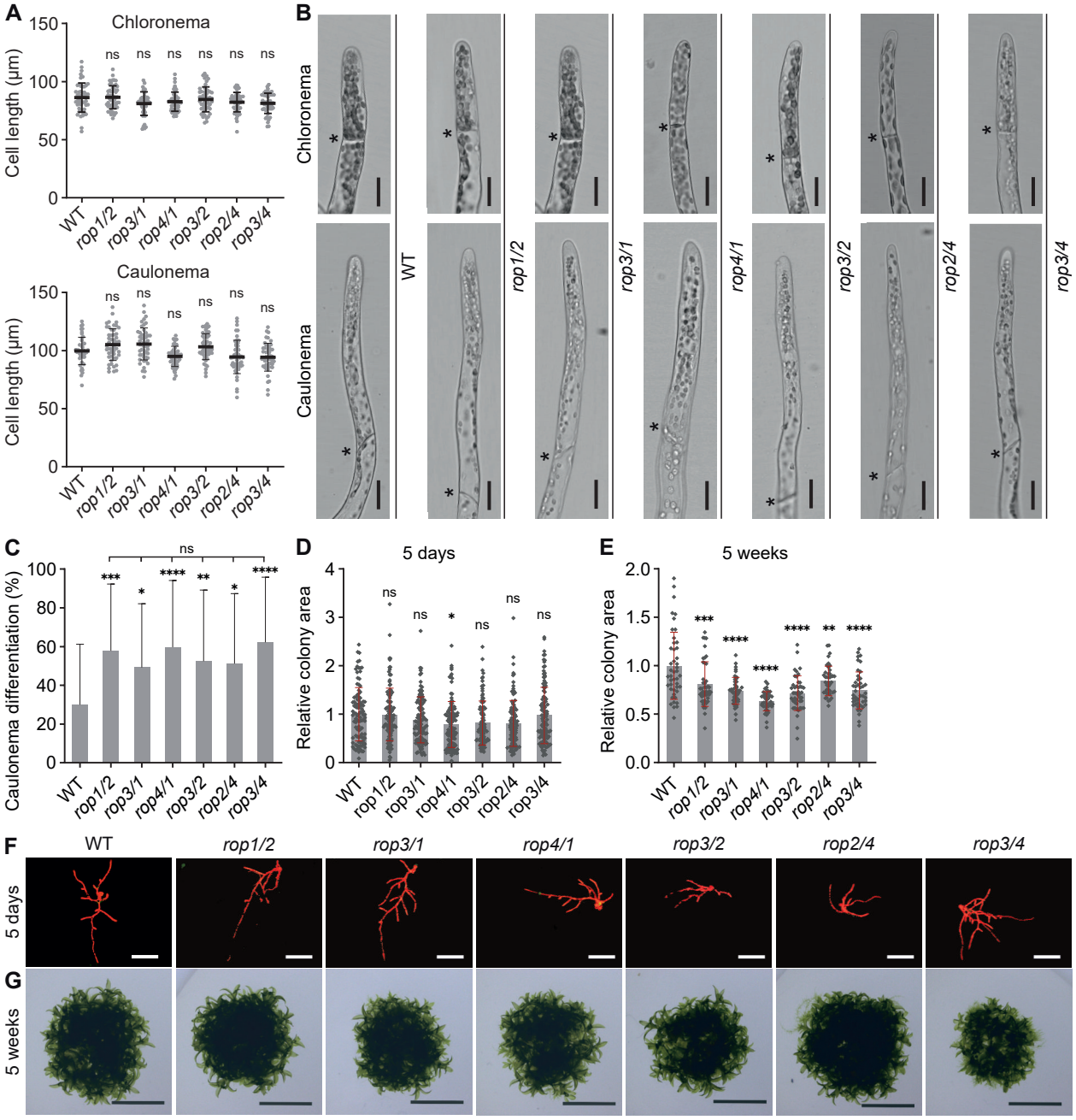

Figure 1. Knockout of two Pp*ROP*s (*rop*^{2xKO}) promotes caulonema differentiation. Graphs and images based on 5-day-old protonemata or 5-week-old colonies regenerated from protoplasts with the indicated genotypes of double Pp*ROP* knockout mutants and WT using culture conditions listed in Supplementary Table S4. **A)** Average subapical cell length of chloronema and caulonema cells in 5-day-old protonemata. n = 50 cells were analyzed per genotype. The experiment was performed three times with consistent results. **B)** Bright field images of 5-day-old chloronemal and caulonemal filament tips. Asterisks indicate the cell wall between neighboring cells. Scale bars: 25 µm. **C)** Average percentage of caulonema differentiation in 5-day-old protonemal filaments with at least three cells as determined by microscopic observation. n = 60 colonies per genotype were measured in 3 independent experiments. **D–G)** Average size (area) of 5-day-old protonemata **(D)** or 5-week-old colonies **(E)** as determined based on microscopic imaging of chlorophyll autofluorescence **(F**, 5-day-old**)** or pictures recorded using a stereo microscope **(G**, 5-week-old**)**. The mean value of WT was used as a calibrator (relative area = 1). n = 105 colonies per genotype were measured in 3 independent experiments (**D**), or n = 42 colonies per genotype were measured. The experiment was performed three times with consistent results (**E**). Scale bars: 400 µm **(F)**, 10 mm **(G)**. (**A, C–E)** Error bars: standard deviation (SD), dots represent individual data points. Statistical analysis by one-way ANOVA/Tukey's test (pairwise comparisons to WT and relevant pairwise comparisons are displayed, all others see Supplementary Data Set S2): ^{ns} $P > 0.05$ (not significant), * $P \leq 0.05$, ** $P \leq 0.01$, *** $P \leq 0.001$, **** $P \leq 0.0001$.

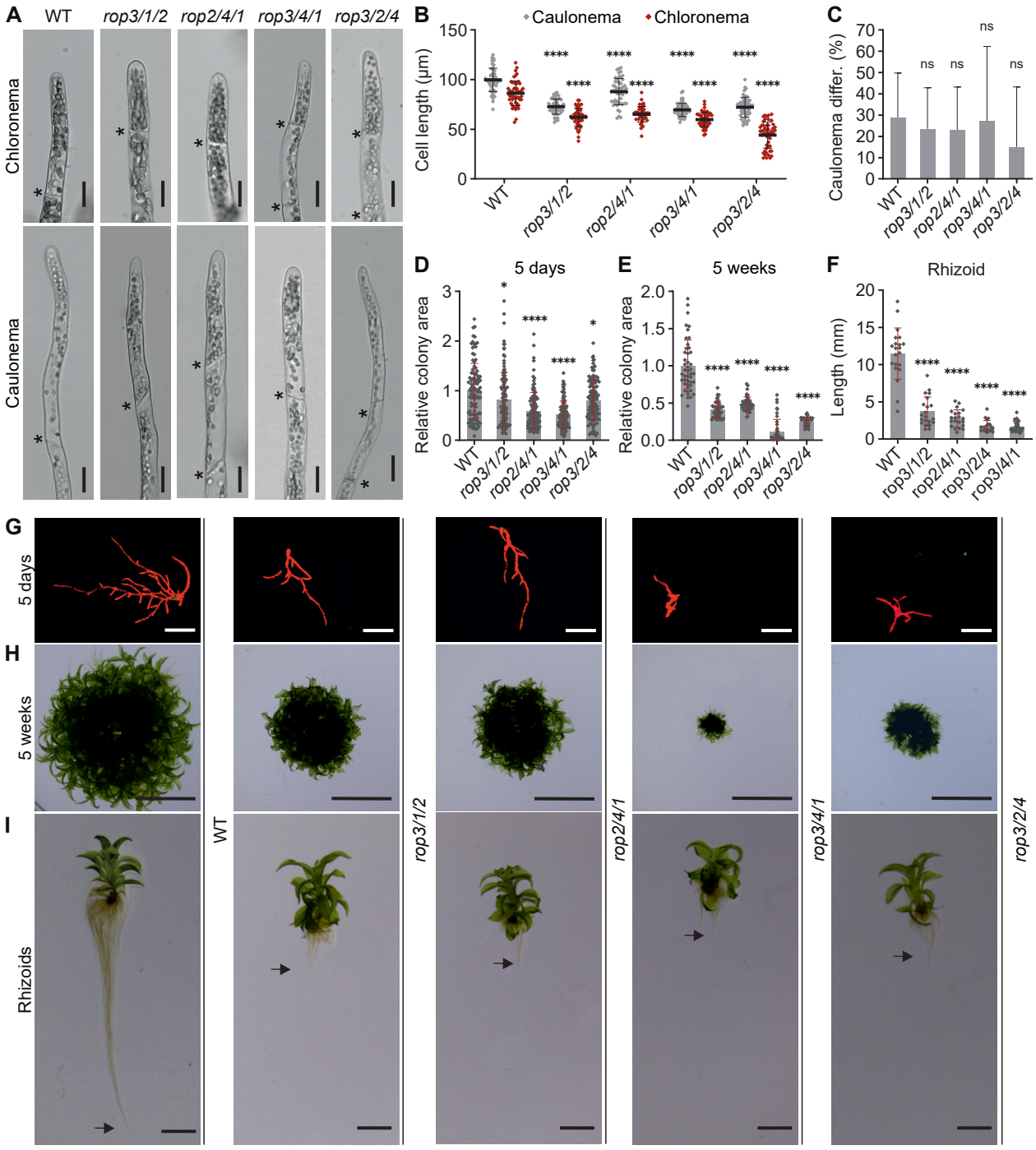

Figure 2. Knockout of three Pp*ROP*s (*rop*^{3xKO}) inhibits tip growth of protonemata and rhizoids. Graphs and images based on 5-day-old protonemata or 5-week-old colonies regenerated from protoplasts with the indicated genotypes of triple Pp*ROP* knockout mutants and WT cultivated on media listed in Supplementary Table S4. **A)** Bright field micrographs of 5-day-old chloronemal and caulonemal filament tips. Asterisks indicate the cell wall between neighboring cells. Scale bars: 25 µm. **B)** Average subapical cell length of chloronemal and caulonemal cells in 5-day-old protonemata. n = 50 cells per genotype were measured. The experiment was repeated three times with consistent results. **C)** Average percentage of caulonema differentiation in 5-day-old protonemal filaments with at least three cells as determined by microscopic observation. n = 60 colonies per genotype were measured in 3 independent experiments. **D, E, G, H)** Average size (area) of 5-day-old protonemata **(D)** or 5-week-old colonies **(E)** as determined based on microscopic imaging of chlorophyll autofluorescence **(G)** or pictures recorded using a stereo microscope **(H)**. Scale bars: 400 µm **(G)**, 10 mm **(H)**. The mean value of WT was used as a calibrator (relative area = 1). n = 105 colonies per genotype were measured in 3 independent experiments **(D),** or n = 45 colonies per genotype were measured. The experiment was repeated three times with consistent results **(E)**. **F** and **I)** Average length of rhizoids of 5-week-old gametophores **(F)** based on pictures recorded using a stereo microscope (arrows indicate the end of rhizoids) **(I)**. Scale bars: 5 mm. n = 21 rhizoids per genotype were measured. The experiment was repeated three times with consistent results. **B–F)** Error bars: standard deviation (SD), dots represent individual data points. Statistical analysis by two-way ANOVA/Tukey's test **(B)** or one-way ANOVA/Tukey's test **(C–F)** (comparisons to WT are displayed, all others see Supplementary Data Set S2): ^{ns} $P > 0.05$ (not significant), * $P \leq 0.05$, **** $P \leq 0.0001$.

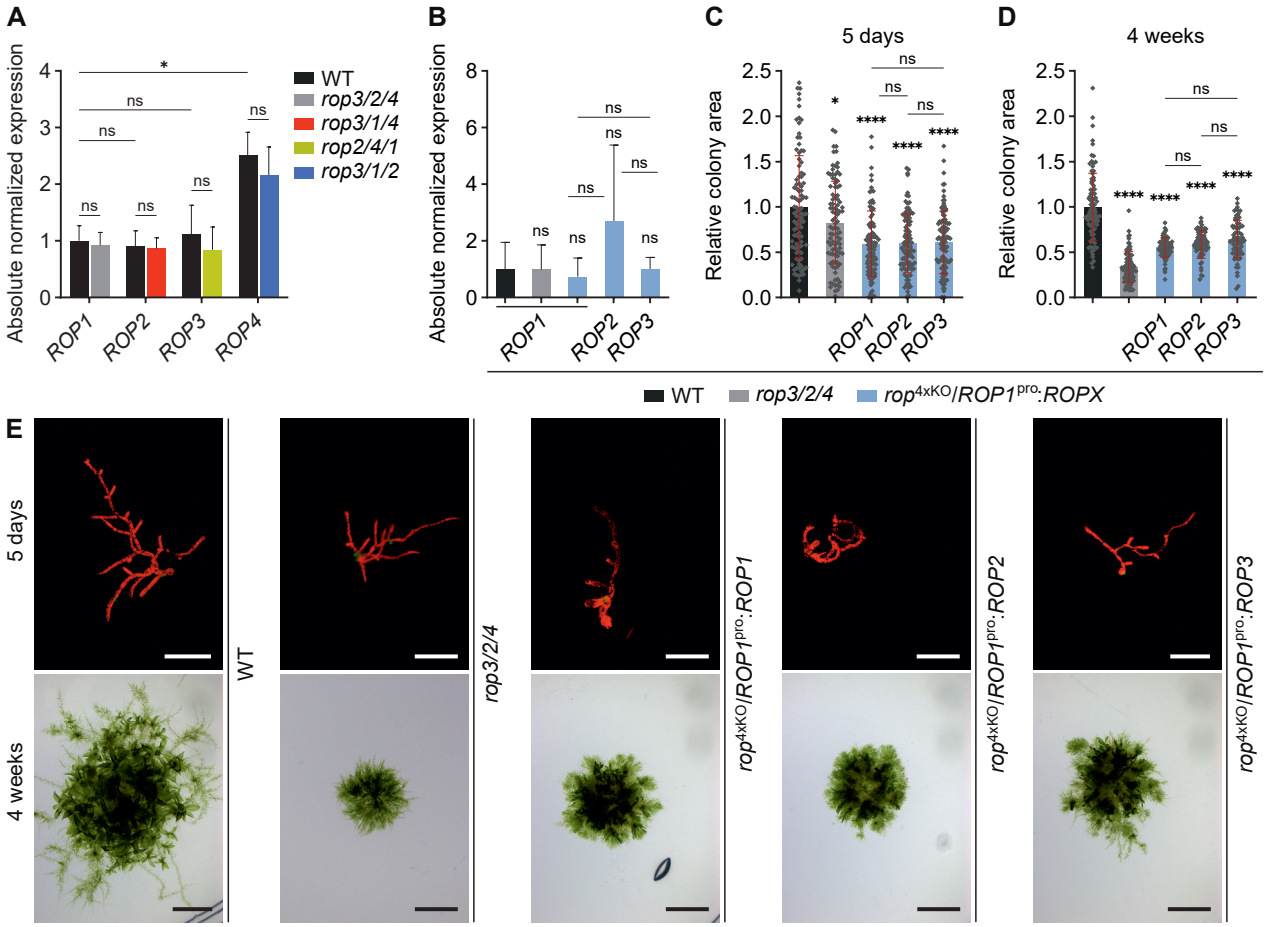

Figure 3. Pp*ROP*s are not altered in their gene expression in *rop*^{3xKO} mutants and redundantly complement the *rop*^{4xKO} mutant. A and **B)** qRT-qPCR of expression levels of Pp*ROP*s in 1-week-old protonemata cultivated through homogenization (Supplementary Table S4) with the indicated genotype: *rop*^{3xKO} mutants **(A)**, *rop*^{4xKO} mutant complemented with the coding and 3' UTR sequence of Pp*ROP1* (Pp*ROP4* identical amino acid sequence) or Pp*ROP2* or Pp*ROP3* downstream of the Pp*ROP1* promoter (*rop*^{4xKO}/*ROP1*$^{pro.}$:*ROPX*) **(B)** were compared to WT. Absolute transcript levels were determined based on standard curves using the value obtained for one WT replicate of Pp*ROP1* as a calibrator (relative expression = 1). Bars: mean of three biological and two technical replicates, error bars: standard error of the mean. The experiment was performed two times with consistent results. **C–E)** Average size (area) of 5-day-old protonemata **(C)** or 4-week-old colonies **(D)** regenerated from protoplasts with the indicated genotypes: i) WT, ii) *rop3/2/4*, iii) *rop*^{4xKO}/*ROP1*$^{pro.}$:*ROPX* as determined based on microscopic imaging of chlorophyll autofluorescence **(E,** 5 days**)** or pictures recorded using a stereo microscope **(E,** 4 weeks**)**. The mean value of WT was used as calibrator (relative area = 1). n = 100 **(C)** or n = 80 **(D)** colonies per genotype were measured in 3 independent experiments. Error bars: standard deviation (SD), dots represent individual data points. Scale bars: 250 µm (**E** upper row, 5 days), 5 mm (**E** lower row, 4 weeks). Statistical analysis by two-way ANOVA/Bonferroni's test **(A)** or one-way ANOVA/Tukey's test **(B–D)** (pairwise comparisons to WT and relevant pairwise comparisons are displayed, all others provided in Supplementary Data Set S2): ^{ns} $P > 0.05$ (not significant), * $P \leq 0.05$, **** $P \leq 0.0001$.

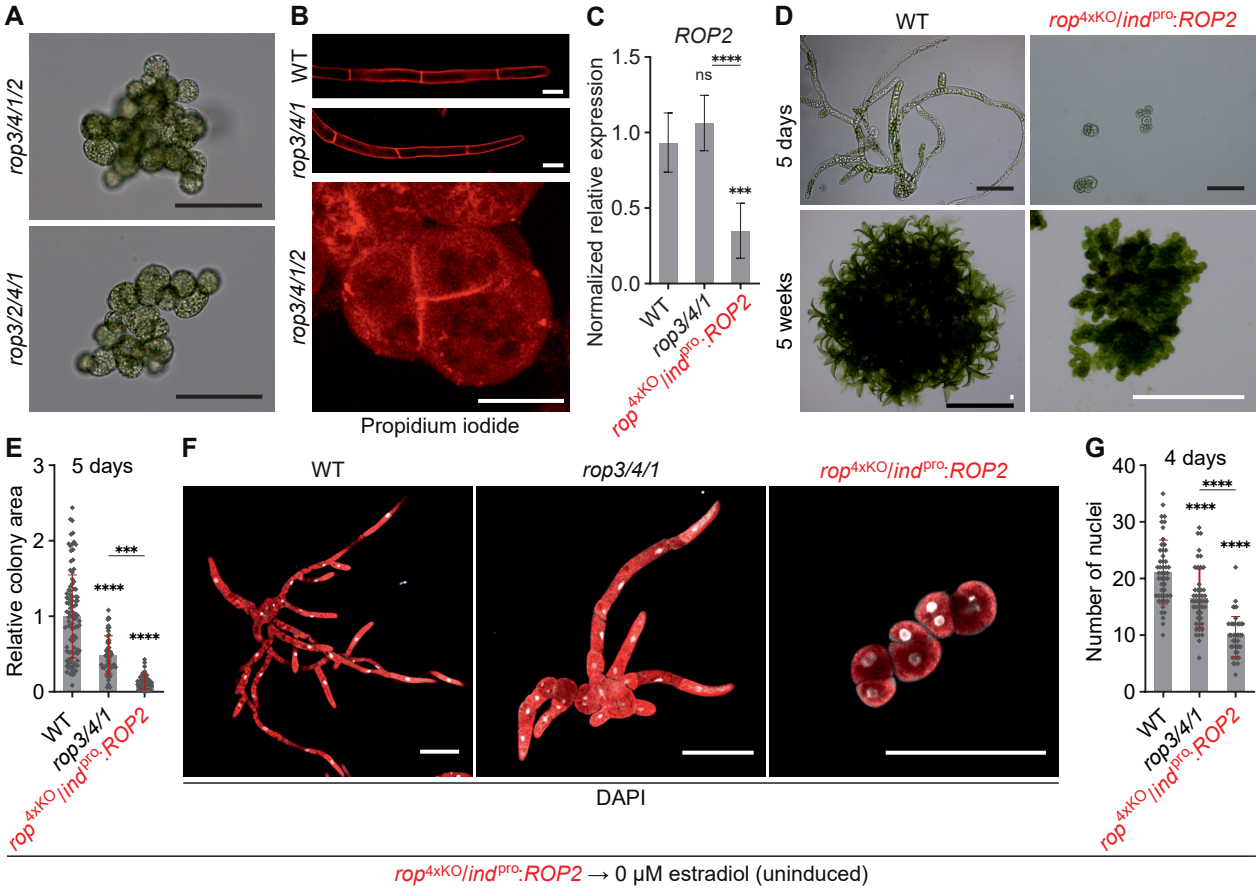

Figure 4. Loss of all Pp*ROP*s affects cell division and eliminates tip growth. Analysis of the *rop*^{4xKO} phenotype was performed using protonemata or 5-week-old colonies cultivated on media listed in Supplementary Table S4 with the indicated genotypes: i) WT, ii) *rop3/4/1,* iii) *rop3/4/1/2, rop3/2/4/1* (*rop*^{4xKO}), iv) *rop*^{4xKO}/*ind*^{pro}:*ROP2* uninduced (conditional complementation of *rop*^{4xKO} with the coding and 3' UTR sequence of Pp*ROP2* downstream of the inducible β-estradiol promoter). **A–C)** 1-week-old protonemata cultivated through homogenization. **A)** Bright field micrographs of *rop*^{4xKO} mutants. Scale bars: 100 µm. **B)** Confocal imaging of the cell division plane using projections of serial confocal optical sections of protonemata stained with propidium iodide. Scale bars: 25 µm. **C)** qRT-PCR of relative Pp*ROP2* transcript levels determined according to the $2^{-\Delta CCT}$ method, using the value obtained for one WT replicate as a calibrator (relative expression = 1). Bars: mean of three biological and two technical replicates. The experiment was repeated two times with consistent results. **D–G)** Analysis of the *rop*^{4xKO} phenotype using 4 or 5-day-old protonemata or 5-week-old colonies regenerated from protoplasts with the indicated genotypes. *rop*^{4xKO}/*ind*^{pro}:*ROP2* protoplasts were regenerated without β-estradiol resembling the *rop*^{4xKO} phenotype. **D)** Bright field images from 5-day-old protonemata (top panel) and images of 5-week-old colonies (lower panel) were recorded using a stereo microscope. Scale bars: 100 µm (upper panel), 10 mm (lower panel, black bar), 500 µm (lower panel, white bars). **E)** Average size (area) of 5-day-old protonemata regenerated from protoplasts as determined based on microscopic imaging of chlorophyll autofluorescence using the mean value of WT as calibrator (relative area = 1). n = 50 colonies per genotype measured in 3 independent experiments. **F** and **G)** Cell division rate in 4-day-old protonemata was analyzed through projections of serial confocal optical sections displaying DAPI staining (white) and chlorophyll autofluorescence (red) (scale bars: 100 µm) **(F)** and determination of the average nuclei number **(G)**. n = 50 colonies per genotype measured in 3 independent experiments. **C, E, G)** Error bars: standard error of the mean (SEM) **(C)**, standard deviation (SD) **(E** and **G)**, dots represent individual data points. Statistical analysis by one-way ANOVA/Tukey's test (pairwise comparisons to WT and relevant pairwise comparisons are displayed, all others see Supplementary Data Set S2): ^{ns} $P > 0.05$ (not significant), *** $P \leq 0.001$, **** $P \leq 0.0001$.

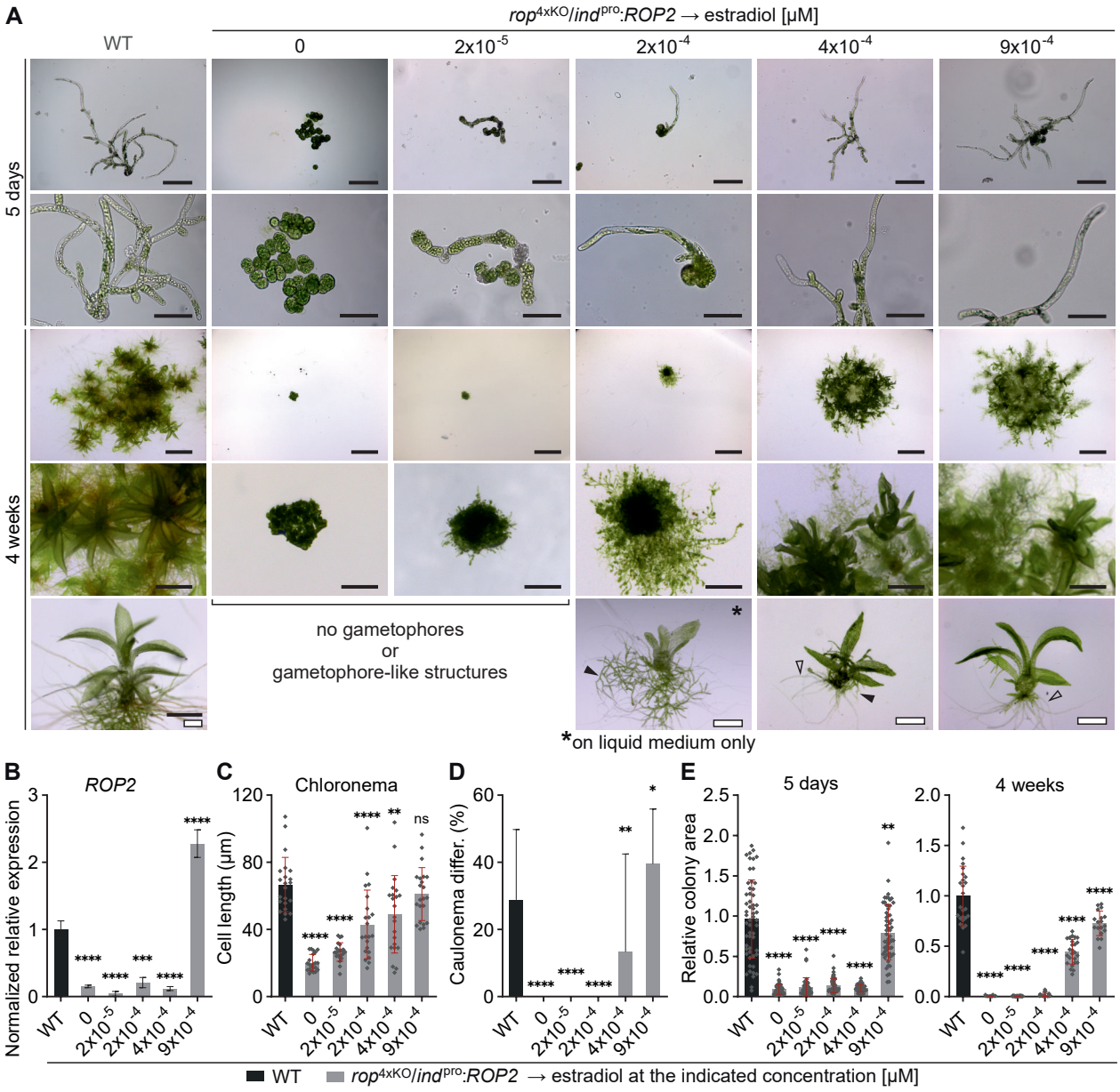

Figure 5. Titratable Pp*ROP2* expression rescues *rop*^{4xKO}. Protonemata or 4-week-colonies were regenerated from protoplasts using media solidified with agar except where otherwise noted (see Supplementary Table S4) with the indicated genotypes: i) WT, ii) *rop*^{4xKO}/*ind*^{pro}:*ROP2* (conditional complementation of *rop*^{4xKO} with the coding and 3' UTR sequence of Pp*ROP2* downstream of the inducible β-estradiol promoter) treated with representative β-estradiol concentrations. **A)** Bright field images of 5-day-old protonemata and images using a stereo microscope of 4-week-old colonies. *rop*^{4xKO}/*ind*^{pro}:*ROP2* did not develop gametophores (4 weeks) in the absence or with minimal PpROP2 expression (0 µM, 2x10^{-5} µM β-estradiol). Treatment with 2x10^{-4} µM β-estradiol generated gametophore-like structures only in liquid BCD medium (asterisk) and at ≥ 4x10^{-4} µM β-estradiol gametophores developed on BCD medium solidified with agar. Closed triangles indicate protonemata, open triangles indicate rhizoids. Scale bars: 200 µm (1st top row), 100 µm (2nd row), 5 mm (3rd row), 1 mm (4th row), 1 mm (5th row, black bar), 500 µm (5th row, white bars). **B)** Relative transcript levels of Pp*ROP2* were determined in 7-day-old protonemata (WT, *rop*^{4xKO}/*ind*^{pro}:*ROP2* treated with 9x10^{-4} µM β-estradiol) or 10-day-old protonemata (*rop*^{4xKO}/*ind*^{pro}:*ROP2* treated with ≤ 4x10^{-4} µM β-estradiol) according to the $2^{-\Delta\Delta Ct}$ method, using the value obtained for one WT replicate as calibrator (relative expression = 1). Bars: mean of three biological and two technical replicates. The experiment was repeated two times with consistent results. **C** and **D)** Average subapical cell length of chloronema **(C)** or average percentage of caulonema differentiation as determined by microscopic observation **(D)** in 5-day-old protonemata. n = 22 cells **(C)** or n = 30 colonies **(D)** per genotype measured in 3 independent experiments. **E)** Average size (area) of 5-day-old or 4-week-old colonies using the mean value of WT as calibrator (relative area = 1). n = 60 colonies per genotype measured in three independent experiments (5 days). n = 22 colonies per genotype; the experiment was performed three times with consistent results (4 weeks). **B–E)** Error bars: standard error of the mean (SEM) **(B)**, standard deviation (SD) **(C–E)**. Dots represent individual data points. Statistical analysis by one-way ANOVA/Tukey's test (pairwise comparisons to WT are displayed, all others see Supplementary Data Set S2): ^{ns} $P > 0.05$ (not significant), * $P \leq 0.05$, ** $P \leq 0.01$, *** $P \leq 0.001$, **** $P \leq 0.0001$.

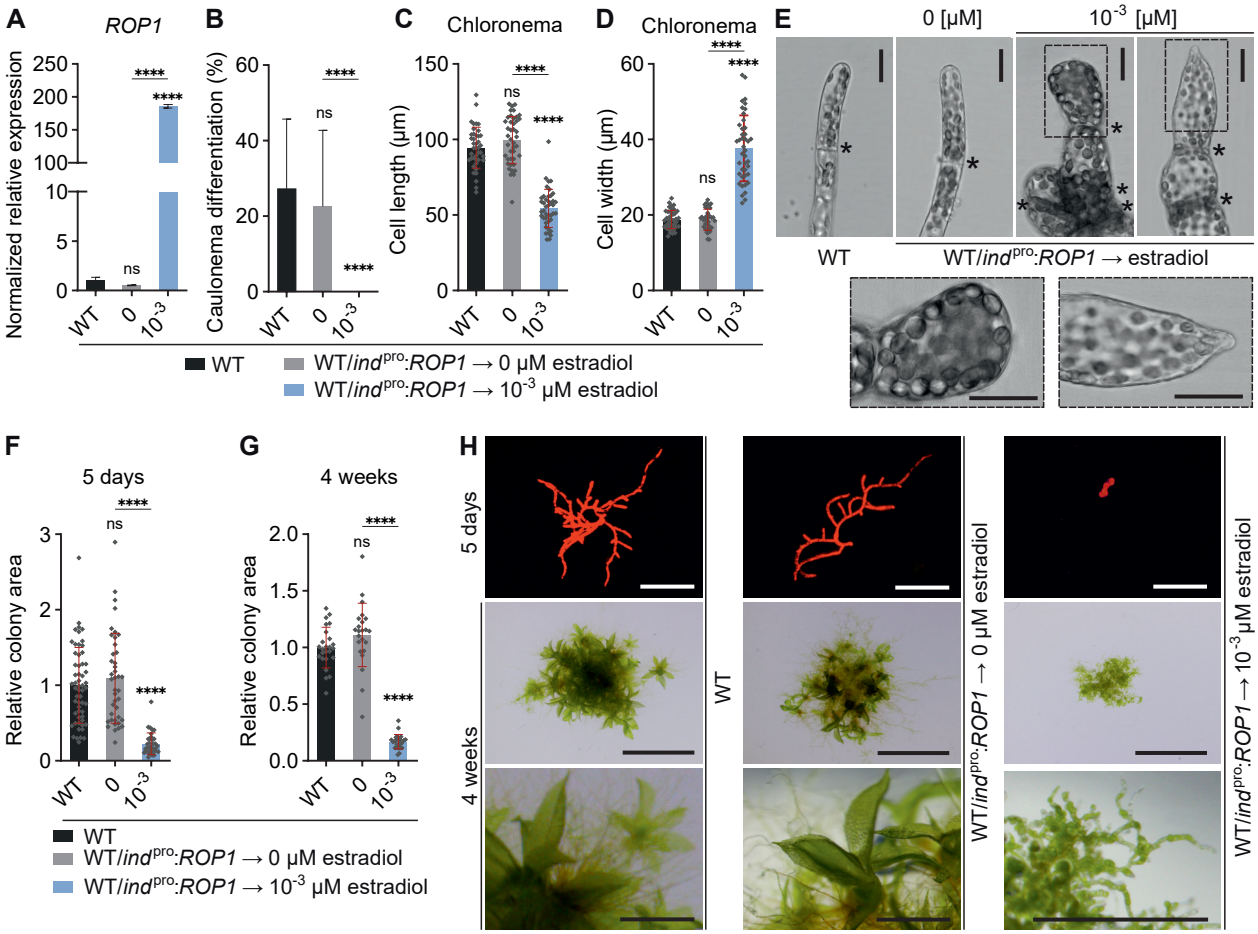

Figure 6. Pp*ROP* overexpression deregulates tip growth and caulonema differentiation. 1-week old protonemata cultivated through homogenization **(A)** or 5-day-old protonemata or 4-week colonies regenerated from protoplasts **(B–H)** using media listed in Supplementary Table S4 with the indicated genotypes: i) WT, ii) WT/*ind*^{pro}:*ROP1* (overexpression of the Pp*ROP1* coding sequence and 3' UTR in WT using the inducible β-estradiol promoter. **A)** Relative transcript levels of Pp*ROP1* were determined according to the $2^{-\Delta CCT}$ method using the value obtained for one WT replicate as calibrator (relative expression level = 1). Bars: mean of three biological and two technical replicates. The experiment was repeated two times with consistent results. **B–D)** Average percentage of caulonema differentiation as determined by microscopic observation **(B)** or average subapical chloronemal cell length **(C)** or cell width **(D)** in filaments with at least three cells of 5-day-old protonemata. n = 42 cells per genotype measured in 3 independent experiments. **E)** Bright field micrographs of filament tips of 5-day-old protonemata with the indicated genotypes. Asterisks indicate the cell wall between neighboring cells, dotted rectangles indicate the magnified apical region. Scale bars: 25 µm. **F–H)** Average size (area) of 5-day-old protonemata **(F)** or 4-week-old colonies **(G)** using the mean value of WT as calibrator (relative area = 1) were determined based on microscopic imaging of chlorophyll autofluorescence **(H**, 1st top row; 5 days**)** or pictures recorded using a stereo microscope **(H**, 2nd and 3rd rows; 4 weeks**)**. Scale bars: 500 µm (1st top row), 5 mm (2nd row), 1 mm (3rd row). n = 35 **(F)** or n = 23 **(G)** colonies per genotype. The experiment was repeated two times, and the results from one representative experiment are shown here. **A–D, F, G)** Error bars: standard error of the mean (SEM) **(A)**, standard deviation (SD) **(B–D, F, G)**. Dots represent individual data points. Statistical analysis by one-way ANOVA/Tukey's test (pairwise comparisons are displayed): ^{ns} $P > 0.05$ (not significant) **** $P \leq 0.0001$..

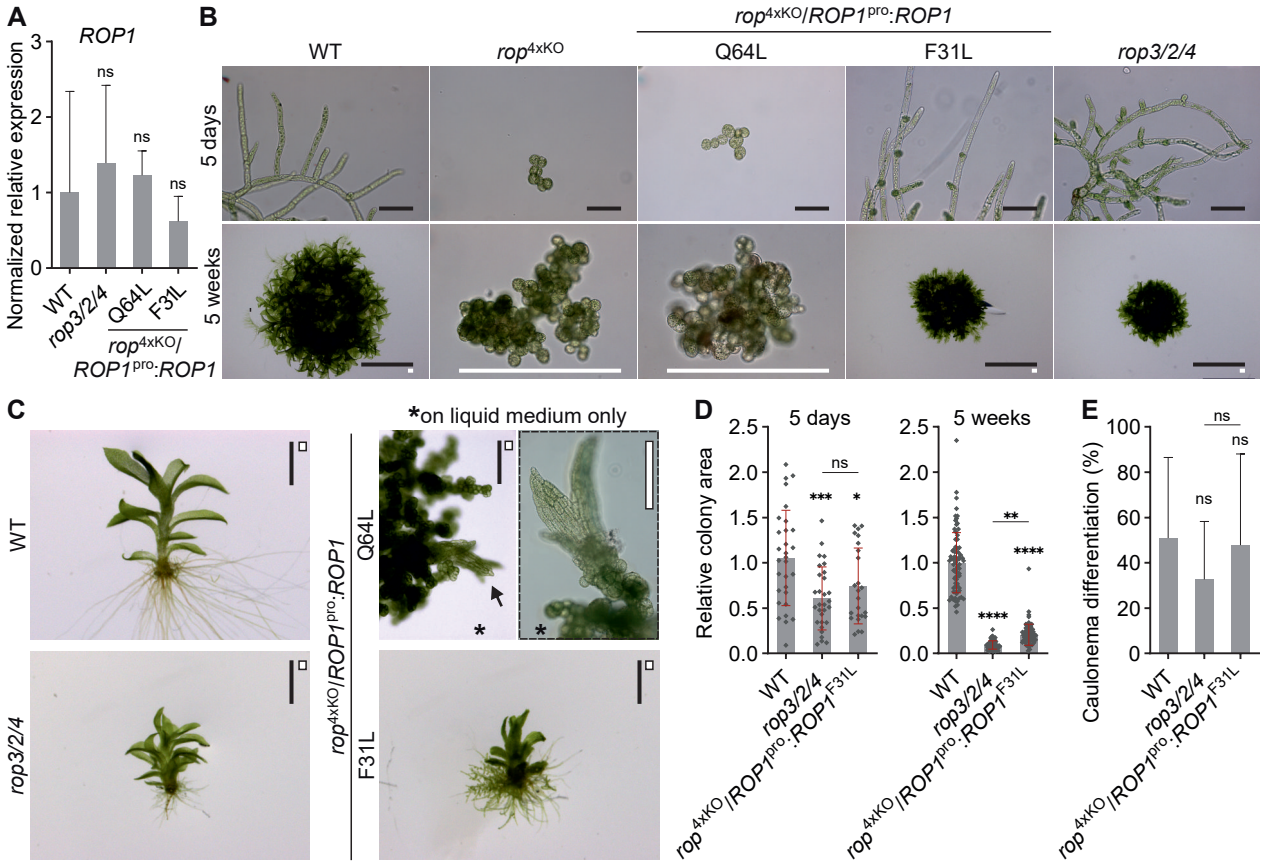

Figure 7. GTP/GDP cycling is essential for most PpROP functions but not gametophore initiation. Graphs and images based on protonemata or gametophores or colonies using culture conditions (Supplementary Table S4) with the indicated genotypes: i) WT, ii) *rop2/3/4*, iii) *rop*^{4xKO} iv) *rop*^{4xKO}/*ROP1*^{pro}:*ROP1*^{Q64L} (complementation of *rop*^{4xKO} with the Pp*ROP1* coding and 3' UTR sequence containing a constitutive active mutation [Q64L] downstream of the endogenous Pp*ROP1* promoter), v) *rop*^{4xKO}/*ROP1*^{pro}:*ROP1*^{F31L} (complementation of *rop*^{4xKO} with the Pp*ROP1* coding and the 3' UTR sequence containing a fast cycling mutation [F31L] downstream of the endogenous Pp*ROP1* promoter). **A)** Relative transcript levels of Pp*ROP1* in 1-week-old protonemata cultivated through homogenization according to the $2^{-\Delta CCT}$ method, using the value obtained for one WT replicate as a calibrator (relative expression = 1). Bars: mean of three biological and two technical replicates. The experiment was repeated two times with consistent results. **B–E)** 5-day-old protonemata or 5-week-old colonies regenerated from protoplasts (WT, *rop2/3/4*, *rop*^{4xKO}/*ROP1*^{pro}:*ROP1*^{F31L}) or cultivated through homogenization (*rop*^{4xKO}, *rop*^{4xKO}/*ROP1*^{pro}:*ROP1*^{Q64L}). **B)** Images of 5-day-old protonemata recorded using bright field microscopy (upper row) and images of 5-week-old colonies obtained using a stereo microscope (WT, *rop2/3/4*, *rop*^{4xKO}/*ROP1*^{pro}:*ROP1*^{F31L}) or bright field microscopy (*rop*^{4xKO}, *rop*^{4xKO}/*ROP1*^{pro}:*ROP1*^{Q64L}) (lower row). Scale bars: 100 µm (upper row), 10 mm (black bars, lower row), 400 µm (white bars, lower row). **C)** Images of 5-week-old gametophores cultivated on solid BCD medium except *rop*^{4xKO}/*ROP1*^{pro}:*ROP1*^{Q64L} that developed gametophore-like structures only in liquid BCD medium (asterisk) were recorded using a stereo microscope. Arrow indicates a gametophore-like structure used for magnification using bright field microscopy (dotted rectangle). Scale bars: 2 mm (black bars) 200 µm (white bars). **D)** Average size (area) of 5-day-old protonemata or 5-week-old colonies normalized to the mean value of WT (relative area = 1). n = 30 colonies per genotype; the experiment was repeated three times with consistent results (5 days) or n = 81 colonies per genotype measured in 3 independent experiments (5 weeks). **E)** Average percentage of caulonema differentiation in 5-day-old protonemal filaments with at least three cells was determined by microscopic observation. n = 10 colonies per genotype. The experiment was repeated three times with consistent results. **A**, **D, E)** Error bars: standard error of the mean (SEM) **(A)**, standard deviation (SD) **(D** and **E),** dots represent individual data points. Statistical analysis by one-way ANOVA/Tukey's test (pairwise comparisons to WT and relevant pairwise comparisons are displayed, all others see Supplementary Data Set S2). ^{ns} $P > 0.05$ (not significant), * $P \leq 0.05$, ** $P \leq 0.01$, *** $P \leq 0.001$, **** $P \leq 0.0001$.

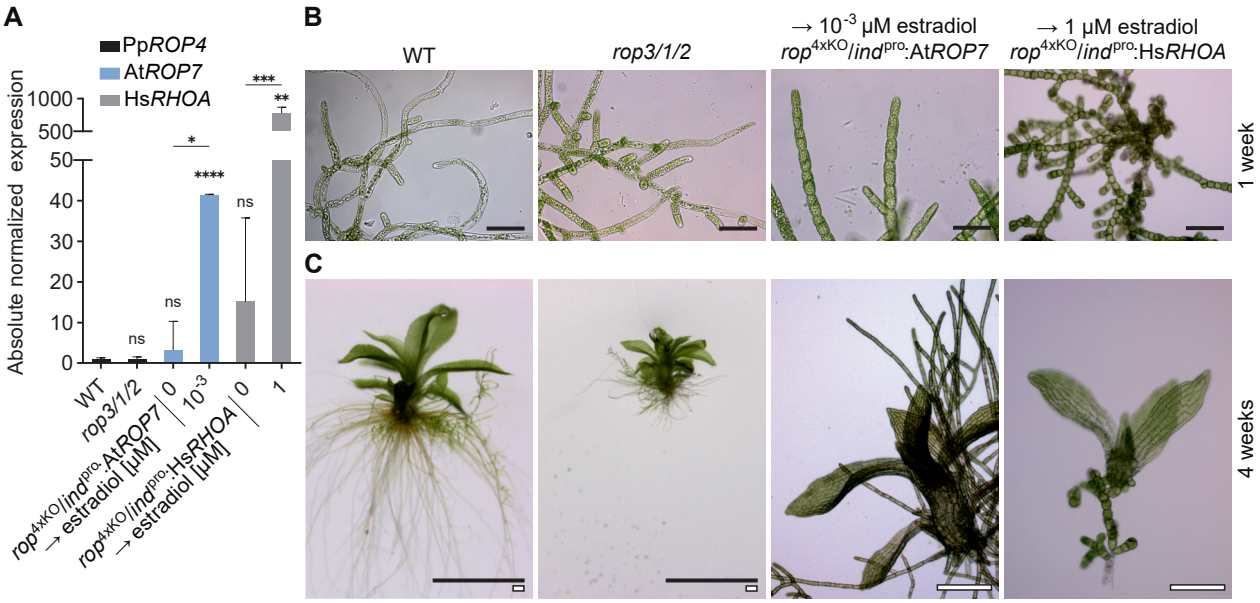

Figure 8. At*ROP7* or Hs*RHOA* overexpression partially rescues Pp*ROP*s. 1-week-old protonemata or 4-week-old colonies were cultivated through homogenization using media described in Supplementary Table S4 with the indicated genotypes: i) WT, ii) *rop1/2/3*, iii) *rop*^{4xKO}/*ind*^{pro}:At*ROP7* or *rop*^{4xKO}/*ind*^{pro}:Hs*RHOA* (complementation of *rop*^{4xKO} with the coding sequence of At*ROP7*, or Hs*RHOA* downstream of the β-estradiol inducible promoter). **A)** Absolute transcript levels of Pp*ROP4*, At*ROP7* or Hs*RHOA* were determined in 1-week-old protonemata with the indicated genotype based on standard curves, using the value obtained for one WT replicate of Pp*ROP4* as calibrator (relative expression = 1). Bars: mean of three biological and two technical replicates. Error bars: standard error of the mean. The experiment was repeated two times with consistent results. Statistical analysis by one-way ANOVA/Tukey's test (pairwise comparisons to WT and relevant pairwise comparisons are displayed, all others see Supplementary Data Set S2): ^{ns} $P > 0.05$ (not significant), * $P \leq 0.05$, ** $P \leq 0.01$, *** $P \leq 0.001$, **** $P \leq 0.0001$. **B** and **C)** Bright field micrographs of 1-week-old protonemata **(B)** and images of 4-week-old gametophores recorded using a stereo microscope (WT, *rop1/2/3*) or gametophore-like structures using a bright field microscope (*rop*^{4xKO}/*ind*^{pro}:At*ROP7*, *rop*^{4xKO}/*ind*^{pro}:Hs*RHOA*) **(C)**. Scale bars: 50 µm **(B)**, 2 mm (black bars), 200 µm (white bars).

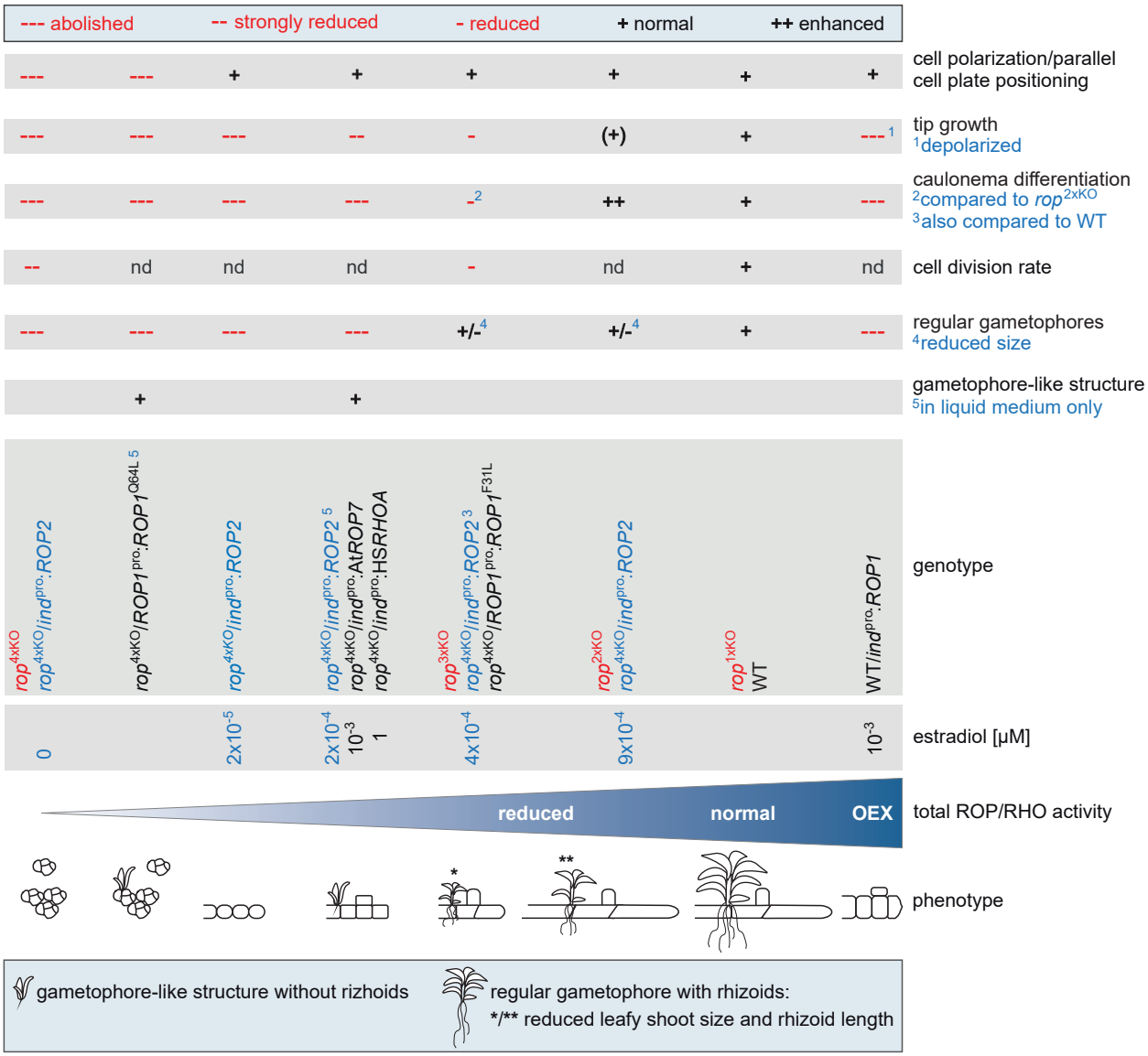

Figure 9. Overview of PpROP functions. Schematic drawing summarizing PpROP functions in protonemata and gametophores of *P. patens* with the indicated genotypes: i) WT (black font), ii) WT/*ind*^{pro}:*ROP1* (Pp*ROP1* overexpresion in WT controlled by the inducible β-estradiol promoter) (black font), iii) *rop*^{1xKO}, *rop*^{2xKO}, *rop*^{3xKO}, *rop*^{4xKO} (Pp*ROP* knockout mutants) (red font), iv) *rop*^{4xKO}/*ROP1*^{pro}:*ROP1*^{Q64L}, *rop*^{4xKO}/*ROP1*^{pro}:*ROP1*^{F31L} (complementation of *rop*^{4xKO} with the coding and 3' UTR sequence of Pp*ROP1* containing a constitutive active [Q64L] or fast cycling mutation [F31L] downstream of the Pp*ROP1* promoter) (black font), v) *rop*^{4xKO}/*ind*^{pro}:At*ROP7* or *rop*^{4xKO}/*ind*^{pro}:Hs*RHOA* (complementation of *rop*^{4xKO} with the coding sequence of At*ROP7* or Hs*RHOA* downstream of the inducible β-estradiol promoter) (black font), vi) *rop*^{4xKO}/*ind*^{pro}:*ROP2* (complementation of *rop*^{4xKO} with the coding and 3' UTR sequence of Pp*ROP2* downstream of the inducible β-estradiol promoter) (blue font). nd: not determined.

Parsed Citations

Altschul, S.F., Gish, W., Miller, W., Myers, E.W., and Lipman, D.J. (1990). Basic local alignment search tool. J. Mol. Biol. 215, 403-410. 10.1016/S0022-2836(05)80360-2
Google Scholar: Author Only Title Only Author and Title

Andersen, S.U., Buechel, S., Zhao, Z., Ljung, K., Novák, O., Busch, W., Schuster, C., and Lohmann, J.U. (2008). Requirement of B2-type cyclin-dependent kinases for meristem integrity in Arabidopsis thaliana. Plant Cell 20, 88-100. https://doi.org/10.1105/tpc.107.054676
Google Scholar: Author Only Title Only Author and Title

Ashton, N.W., and Cove, D.J. (1977). The isolation and preliminary characterisation of auxotrophic and analogue resistant mutants of the moss, Physcomitrella patens. Mol. Gen. Genetics 154, 87-95. https://doi.org/10.1007/BF00265581
Google Scholar: Author Only Title Only Author and Title

Aspenström, P. (2019). The Intrinsic GDP/GTP Exchange Activities of Cdc42 and Rac1 Are Critical Determinants for Their Specific Effects on Mobilization of the Actin Filament System. Cells 8, 759. 10.3390/cells8070759
Google Scholar: Author Only Title Only Author and Title

Aspenström, P. (2022). The Role of Fast-Cycling Atypical RHO GTPases in Cancer. Cancers 14, 1961. https://doi.org/10.3390/cancers14081961
Google Scholar: Author Only Title Only Author and Title

Bao, L., Ren, J., Nguyen, M., Slusarczyk, A.S., Thole, J.M., Martinez, S.P., Huang, J., Fujita, T., and Running, M.P. (2022). The cellular function of ROP GTPase prenylation is important for multicellularity in the moss Physcomitrium patens. Development 149. https://doi.org/10.1242/dev.200279
Google Scholar: Author Only Title Only Author and Title

Berardini, T.Z., Reiser, L., Li, D., Mezheritsky, Y., Muller, R., Strait, E., and Huala, E. (2015). The arabidopsis information resource: Making and mining the "gold standard" annotated reference plant genome. genesis 53, 474-485. https://doi.org/10.1002/dvg.22877
Google Scholar: Author Only Title Only Author and Title

Berken, A., Thomas, C., and Wittinghofer, A. (2005). A new family of RhoGEFs activates the Rop molecular switch in plants. Nature 436, 1176-1180. https://doi.org/10.1038/nature03883
Google Scholar: Author Only Title Only Author and Title

Bi, G., Zhao, S., Yao, J., Wang, H., Zhao, M., Sun, Y., Hou, X., Haas, F.B., Varshney, D., Prigge, M., Rensing, S.A., Jiao, Y., Ma, Y., Yan, J., and Dai, J. (2024). Near telomere-to-telomere genome of the model plant Physcomitrium patens. Nat. Plants 10, 327-343. 10.1038/s41477-023-01614-7
Google Scholar: Author Only Title Only Author and Title

Bishop, A.L., and Hall, A. (2000). Rho GTPases and their effector proteins. Biochem. J. 348, 241-255. 10.1042/bj3480241
Google Scholar: Author Only Title Only Author and Title

Boureux, A., Vignal, E., Faure, S., and Fort, P. (2007). Evolution of the Rho family of ras-like GTPases in eukaryotes. Mol. Biol. Evol. 24, 203-216. 10.1093/molbev/msl145
Google Scholar: Author Only Title Only Author and Title

Brun, F., Gonneau, M., Laloue, M., and Nogué, F. (2003). Identification of Physcomitrella patens genes specific of bud and gametophore formation. Plant Sci. 165, 1267-1274. https://doi.org/10.1016/S0168-9452(03)00335-2
Google Scholar: Author Only Title Only Author and Title

Burkart, G.M., Baskin, T.I., and Bezanilla, M. (2015). A family of ROP proteins that suppress actin dynamics and are essential for polarized growth and cell adhesion. J. Cell Sci. 128, 2553-2564. https://doi.org/10.1242/jcs.172445
Google Scholar: Author Only Title Only Author and Title

Cevik, S., Peng, X., Beyer, T., Pir, M.S., Yenisert, F., Woerz, F., Hoffmann, F., Altunkaynak, B., Pir, B., Boldt, K., Karaman, A., Cakiroglu, M., Oner, S.S., Cao, Y., Ueffing, M., and Kaplan, O.I. (2023). WDR31 displays functional redundancy with GTPase-activating proteins (GAPs) ELMOD and RP2 in regulating IFT complex and recruiting the BBSome to cilium. Life Sci. Alliance 6, e202201844. https://doi.org/10.26508/lsa.202201844
Google Scholar: Author Only Title Only Author and Title

Chen, C.Y.H., Cheung, A.Y., and Wu, H.-M. (2003). Actin-Depolymerizing Factor Mediates Rac/Rop GTPase–Regulated Pollen Tube Growth. Plant Cell 15, 237-249. https://doi.org/10.1105/tpc.007153
Google Scholar: Author Only Title Only Author and Title

Cheng, X., Mwaura, B.W., Chang Stauffer, S.R., and Bezanilla, M. (2020). A fully functional ROP fluorescent fusion protein reveals roles for this GTPase in subcellular and tissue-level patterning. Plant Cell 32, 3436-3451. https://doi.org/10.1105/tpc.20.00440
Google Scholar: Author Only Title Only Author and Title

Clark, K., Karsch-Mizrachi, I., Lipman, D.J., Ostell, J., and Sayers, E.W. (2016). GenBank. Nucleic Acids Res. 44, D67-D72. https://doi.org/10.1093/nar/gkv1276
Google Scholar: Author Only Title Only Author and Title

Coleman, M.L., Marshall, C.J., and Olson, M.F. (2004). RAS and RHO GTPases in G1-phase cell-cycle regulation. Nat. Rev. Mol. Cell Biol. 5, 355-366. 10.1038/nrm1365
Google Scholar: Author Only Title Only Author and Title

Collonnier, C., Epert, A., Mara, K., Maclot, F., Guyon-Debast, A., Charlot, F., White, C., Schaefer, D.G., and Nogué, F. (2017). CRISPR-Cas9-mediated efficient directed mutagenesis and RAD51-dependent and RAD51-independent gene targeting in the moss Physcomitrella patens. Plant Biotechnol. J. 15, 122-131. 10.1111/pbi.12596
Google Scholar: Author Only Title Only Author and Title

Cove, D. (2005). The Moss Physcomitrella patens. Annu. Rev. Genet. 39, 339 - 358. 10.1146/annurev.genet.39.073003.110214
Google Scholar: Author Only Title Only Author and Title

Cove, D., and Knight, C. (1993). The moss Physcomitrella patens, a model system with potential for the study of plant reproduction. Plant Cell 5, 1483-1488. https://doi.org/10.1105/tpc.5.10.1483
Google Scholar: Author Only Title Only Author and Title

Cove, D.J., Perroud, P.-F., Charron, A.J., McDaniel, S.F., Khandelwal, A., and Quatrano, R.S. (2009). Isolation and Regeneration of Protoplasts of the Moss Physcomitrella patens. Cold Spring Harbor Protocols 2009. https://doi.org/doi:10.1101/pdb.prot5140
Google Scholar: Author Only Title Only Author and Title

Dean, E.J., Davis, J.C., Davis, R.W., and Petrov, D.A. (2008). Pervasive and Persistent Redundancy among Duplicated Genes in Yeast. PLOS Genet. 4, e1000113. https://doi.org/10.1371/journal.pgen.1000113
Google Scholar: Author Only Title Only Author and Title

Denninger, P., Reichelt, A., Schmidt, V.A.F., Mehlhorn, D.G., Asseck, L.Y., Stanley, C.E., Keinath, N.F., Evers, J.-F., Grefen, C., and Grossmann, G. (2019). Distinct RopGEFs Successively Drive Polarization and Outgrowth of Root Hairs. Curr. Biol. 29, 1854-1865. https://doi.org/10.1016/j.cub.2019.04.059
Google Scholar: Author Only Title Only Author and Title

Eklund, D.M., Svensson, E.M., and Kost, B. (2010). Physcomitrella patens: a model to investigate the role of RAC/ROP GTPase signalling in tip growth. J. Exp. Bot. 61, 1917-1937. https://doi.org/10.1093/jxb/erq080
Google Scholar: Author Only Title Only Author and Title

Etienne-Manneville, S., and Hall, A. (2002). Rho GTPases in cell biology. Nature 420, 629-635. https://doi.org/10.1038/nature01148
Google Scholar: Author Only Title Only Author and Title

Fantes, P., and Nurse, P. (1977). Control of cell size at division in fission yeast by a growth-modulated size control over nuclear division. Exp. Cell Res. 107, 377-386. https://doi.org/10.1016/0014-4827(77)90359-7
Google Scholar: Author Only Title Only Author and Title

Feiguelman, G., Fu, Y., and Yalovsky, S. (2018). ROP GTPases Structure-Function and Signaling Pathways. Plant Physiol. 176, 57-79. https://doi.org/10.1104/pp.17.01415
Google Scholar: Author Only Title Only Author and Title

Fu, Y., Gu, Y., Zheng, Z., Wasteneys, G., and Yang, Z. (2005). Arabidopsis interdigitating cell growth requires two antagonistic pathways with opposing action on cell morphogenesis. Cell 120, 687-700. 10.1016/j.cell.2004.12.026
Google Scholar: Author Only Title Only Author and Title

Gao, B., Chen, M.-X., Li, X.-S., Liang, Y.-Q., Zhang, D.-Y., Wood, A.J., Oliver, M.J., and Zhang, J.-H. (2022). Ancestral gene duplications in mosses characterized by integrated phylogenomic analyses. J. Syst. Evol. 60, 144-159. https://doi.org/10.1111/jse.12683
Google Scholar: Author Only Title Only Author and Title

Goodstein, D.M., Shu, S., Howson, R., Neupane, R., Hayes, R.D., Fazo, J., Mitros, T., Dirks, W., Hellsten, U., Putnam, N., and Rokhsar, D.S. (2012). Phytozome: a comparative platform for green plant genomics. Nucleic Acids Res. 40, D1178-D1186. https://doi.org/10.1093/nar/gkr944
Google Scholar: Author Only Title Only Author and Title

Green, M.R., and Sambrook, J. (2012). Molecular cloning: A laboratory manual. (Cold Spring Harbor, New York: Cold Spring Harbor Laboratory Press).
Google Scholar: Author Only Title Only Author and Title

Grimsley, N.H., Ashton, N.W., and Cove, D.J. (1977). The production of somatic hybrids by protoplast fusion in the moss, Physcomitrella patens. Mol. Gen. Genet. 154, 97-100. https://doi.org/10.1007/bf00265582
Google Scholar: Author Only Title Only Author and Title

Gu, Y., Vernoud, V., Fu, Y., and Yang, Z. (2003a). ROP GTPase regulation of pollen tube growth through the dynamics of tip-localized F-actin. J. Exp. Bot. 54, 93-101. 10.1093/jxb/erg035
Google Scholar: Author Only Author and Title

Gu, Z., Steinmetz, L.M., Gu, X., Scharfe, C., Davis, R.W., and Li, W.-H. (2003b). Role of duplicate genes in genetic robustness against null mutations. Nature 421, 63-66. https://doi.org/10.1038/nature01198
Google Scholar: Author Only Author and Title

Hall, A., and Lalli, G. (2010). Rho and Ras GTPases in axon growth, guidance, and branching. Cold Spring Harb Perspect Biol 2, a001818. https://doi.org/10.1101/cshperspect.a001818
Google Scholar: Author Only Title Only Author and Title

Harrison, C.J., Roeder, A.H.K., Meyerowitz, E.M., and Langdale, J.A. (2009). Local Cues and Asymmetric Cell Divisions Underpin Body Plan Transitions in the Moss Physcomitrella patens. Curr. Biol. 19, 461-471. https://doi.org/10.1016/j.cub.2009.02.050
Google Scholar: Author Only Title Only Author and Title

Heasman, S.J., and Ridley, A.J. (2008). Mammalian Rho GTPases: new insights into their functions from in vivo studies. Nat. Rev. Mol. Cell Biol. 9, 690-701. 10.1038/nrm2476
Google Scholar: Author Only Title Only Author and Title

Hiwatashi, Y., Obara, M., Sato, Y., Fujita, T., Murata, T., and Hasebe, M. (2008). Kinesins are indispensable for interdigitation of phragmoplast microtubules in the moss Physcomitrella patens. Plant Cell 20, 3094-3106. https://doi.org/10.1105/tpc.108.061705
Google Scholar: Author Only Title Only Author and Title

Hodge, R.G., and Ridley, A.J. (2016). Regulating Rho GTPases and their regulators. Nat. Rev. Mol. Cell Biol. 17, 496-510. https://doi.org/10.1038/nrm.2016.67
Google Scholar: Author Only Title Only Author and Title

Humphries, J.A., Vejlupkova, Z., Luo, A., Meeley, R.B., Sylvester, A.W., Fowler, J.E., and Smith, L.G. (2011). ROP GTPases Act with the Receptor-Like Protein PAN1 to Polarize Asymmetric Cell Division in Maize. Plant Cell 23, 2273-2284. https//doi.org.10.1105/tpc.111.085597
Google Scholar: Author Only Title Only Author and Title

Ito, K., Ren, J., and Fujita, T. (2014). Conserved function of Rho-related Rop/RAC GTPase signaling in regulation of cell polarity in Physcomitrella patens. Gene 544, 241-247. https://doi.org/10.1016/j.gene.2014.04.057
Google Scholar: Author Only Title Only Author and Title

Jaeger, R., and Moody, L.A. (2021). A fundamental developmental transition in Physcomitrium patens is regulated by evolutionarily conserved mechanisms. Evol. Devel. 23, 123-136. https://doi.org/10.1111/ede.12376
Google Scholar: Author Only Title Only Author and Title

Jang, G., and Dolan, L. (2011). Auxin promotes the transition from chloronema to caulonema in moss protonema by positively regulating PpRSL1and PpRSL2 in Physcomitrella patens. New Phytol. 192, 319-327. https://doi.org/10.1111/j.1469-8137.2011.03805.x
Google Scholar: Author Only Title Only Author and Title

Jones, A.R., Forero-Vargas, M., Withers, S.P., Smith, R.S., Traas, J., Dewitte, W., and Murray, J.A.H. (2017). Cell-size dependent progression of the cell cycle creates homeostasis and flexibility of plant cell size. Nat. Commun. 8, 15060. https://doi.org/10.1038/ncomms15060
Google Scholar: Author Only Title Only Author and Title

Katzen, F. (2007). Gateway® recombinational cloning: a biological operating system. Expert Opin. Drug Discov. 2, 571-589. https://doi.org/10.1517/17460441.2.4.571
Google Scholar: Author Only Title Only Author and Title

Kawano, Y., Kaneko-Kawano, T., and Shimamoto, K. (2014). Rho family GTPase-dependent immunity in plants and animals. Front. Plant Sci. 5. https://doi.org/10.3389/fpls.2014.00522
Google Scholar: Author Only Title Only Author and Title

Klahre, U., and Kost, B. (2006). Tobacco RhoGTPase ACTIVATING PROTEIN1 Spatially Restricts Signaling of RAC/Rop to the Apex of Pollen Tubes. Plant Cell 18, 3033-3046. https://doi.org/10.1105/tpc.106.045336
Google Scholar: Author Only Title Only Author and Title

Kofuji, R., and Hasebe, M. (2014). Eight types of stem cells in the life cycle of the moss Physcomitrella patens. Curr. Opin. Plant Biol. 17, 13-21. 10.1016/j.pbi.2013.10.007
Google Scholar: Author Only Title Only Author and Title

Kondrashov, F.A., Rogozin, I.B., Wolf, Y.I., and Koonin, E.V. (2002). Selection in the evolution of gene duplications. Genome Biol. 3. https://doi.org/10.1186/gb-2002-3-2-research0008
Google Scholar: Author Only Author and Title

Kost, B. (2008). Spatial control of Rho (Rac-Rop) signaling in tip-growing plant cells. Trends Cell Biol. 18, 119-127. 10.1016/j.tcb.2008.01.003
Google Scholar: Author Only Title Only Author and Title

Kost, B. (2010). Regulatory and Cellular Functions of Plant RhoGAPs and RhoGDIs. In Integrated G Proteins Signaling in Plants, S. Yalovsky, F. Baluška, and A. Jones, eds (Berlin, Heidelberg: Springer Berlin Heidelberg), pp. 27-48.
Google Scholar: Author Only Title Only Author and Title

Kubo, M., Imai, A., Nishiyama, T., Ishikawa, M., Sato, Y., Kurata, T., Hiwatashi, Y., Reski, R., and Hasebe, M. (2013). System for Stable β-Estradiol-Inducible Gene Expression in the Moss Physcomitrella patens. PLoS ONE 8, e77356. https://doi.org/10.1371/journal.pone.0077356
Google Scholar: Author Only Title Only Author and Title

Kumar, S., and Ruiz, N. (2023). Bacterial AsmA-Like Proteins: Bridging the Gap in Intermembrane Phospholipid Transport. Contact 6. https://doi.org/10.1177/25152564231185931
Google Scholar: Author Only Title Only Author and Title

Lang, D., Ullrich, K.K., Murat, F., Fuchs, J., Jenkins, J., Haas, F.B., Piednoel, M., Gundlach, H., Van Bel, M., Meyberg, R., Vives, C., Morata, J., Symeonidi, A., Hiss, M., Muchero, W., Kamisugi, Y., Saleh, O., Blanc, G., Decker, E.L., Van Gessel, N., Grimwood, J., Hayes, R.D., Graham, S.W., Gunter, L.E., McDaniel, S.F., Hoernstein, S.N.W., Larsson, A., Li, F.-W., Perroud, P.-F., Phillips, J., Ranjan, P., Rokshar, D.S., Rothfels, C.J., Schneider, L., Shu, S., Stevenson, D.W., Thümmler, F., Tillich, M., Villarreal Aguilar, J.C., Widiez, T., Wong, G.K.-S., Wymore, A., Zhang, Y., Zimmer, A.D., Quatrano, R.S., Mayer, K.F.X., Goodstein, D., Casacuberta, J.M., Vandepoele, K., Reski, R., Cuming, A.C., Tuskan, G.A., Maumus, F., Salse, J., Schmutz, J., and Rensing, S.A. (2018). The Physcomitrella patens chromosome-scale assembly reveals moss genome structure and evolution. Plant J. 93, 515-533. https://doi.org/10.1111/tpj.13801
Google Scholar: Author Only Title Only Author and Title

Lauster, T., Stöckle, D., Gabor, K., Haller, T., Krieger, N., Lotz, P., Mayakrishnan, R., Späth, E., Zimmermann, S., Livanos, P., and Müller, S. (2022). Arabidopsis pavement cell shape formation involves spatially confined ROPGAP regulators. Curr. Biol. 32, 532-544.e537. https://doi.org/10.1016/j.cub.2021.12.042
Google Scholar: Author Only Title Only Author and Title

Lavy, M., Bloch, D., Hazak, O., Gutman, I., Poraty, L., Sorek, N., Sternberg, H., and Yalovsky, S. (2007). A novel ROP/RAC effector links cell polarity, root-meristem maintenance, and vesicle trafficking. Curr. Biol. 17, 947-952. https://doi.org/10.1016/j.cub.2007.04.038
Google Scholar: Author Only Title Only Author and Title

Le Bail, A., Scholz, S., and Kost, B. (2013). Evaluation of reference genes for RT qPCR analyses of structure-specific and hormone regulated gene expression in Physcomitrella patens gametophytes. PLoS ONE 8, e70998. https://10.1371/journal.pone.0070998
Google Scholar: Author Only Title Only Author and Title

Le Bail, A., Schulmeister, S., Perroud, P.F., Ntefidou, M., Rensing, S.A., and Kost, B. (2019). Analysis of the localization of fluorescent PpROP1 and PpROP-GEF4 fusion proteins in moss protonemata based on genomic "knock-in" and estradiol-titratable expression. Front. Plant Sci. 10, 456. https://doi.org/10.3389/fpls.2019.00456
Google Scholar: Author Only Title Only Author and Title

Leebens-Mack, J., Barker, M.S., Carpenter, E.J., and Deyholos, M.K. (2019). One thousand plant transcriptomes and the phylogenomics of green plants. Nature 574, 679-685. 10.1038/s41586-019-1693-2
Google Scholar: Author Only Title Only Author and Title

Li, C., Sako, Y., Imai, A., Nishiyama, T., Thompson, K., Kubo, M., Hiwatashi, Y., Kabeya, Y., Karlson, D., Wu, S.-H., Ishikawa, M., Murata, T., Benfey, P.N., Sato, Y., Tamada, Y., and Hasebe, M. (2017). A Lin28 homologue reprograms differentiated cells to stem cells in the moss Physcomitrella patens. Nat. Commun. 8, 14242. https://doi.org/10.1038/ncomms14242
Google Scholar: Author Only Title Only Author and Title

Li, H., Wu, G., Ware, D., Davis, K.R., and Yang, Z. (1998). Arabidopsis Rho-Related GTPases: Differential Gene Expression in Pollen and Polar Localization in Fission Yeast1. Plant Physiol. 118, 407-417. 10.1104/pp.118.2.407
Google Scholar: Author Only Title Only Author and Title

Li, H., Lin, Y., Heath, R.M., Zhu, M.X., and Yang, Z. (1999). Control of pollen tube tip growth by a Rop GTPase-dependent pathway that leads to tip-localized calcium influx. Plant Cell 11, 1731-1742. 10.1105/tpc.11.9.1731
Google Scholar: Author Only Title Only Author and Title

Liu, L., Niu, L., Ji, K., Wang, Y., Zhang, C., Pan, M., Wang, W., Schiefelbein, J., Yu, F., and An, L. (2023). AXR1modulates trichome morphogenesis through mediating ROP2 stability in Arabidopsis. Plant J. 116, 756-772. https://doi.org/10.1111/tpj.16403
Google Scholar: Author Only Title Only Author and Title

Luo, N., Yan, A., Liu, G., Guo, J., Rong, D., Kanaoka, M.M., Xiao, Z., Xu, G., Higashiyama, T., Cui, X., and Yang, Z. (2017). Exocytosis-coordinated mechanisms for tip growth underlie pollen tube growth guidance. Nat. Commun. 8, 1687.

https://doi.org/10.1038/s41467-017-01452-0
Google Scholar: Author Only Title Only Author and Title

Molendijk, A.J., Bischoff, F., S.V.Rajendrakumar, C., Friml, J., Braun, M., Gilroy, S., and Palme, K. (2001). Arabidopsis thaliana Rop GTPases are localized to tips of root hairs and control polar growth. EMBO J. 20, 2779-2788. https://doi.org/10.1093/emboj/20.11.2779
Google Scholar: Author Only Title Only Author and Title

Moody, L.A., Kelly, S., Rabbinowitsch, E., and Langdale, J.A. (2018). Genetic Regulation of the 2D to 3D Growth Transition in the Moss Physcomitrella patens. Curr. Biol. 28, 473-478.e475. https://doi.org/10.1016/j.cub.2017.12.052
Google Scholar: Author Only Title Only Author and Title

Müller, S. (2023). Update: on selected ROP cell polarity mechanisms in plant cell morphogenesis. Plant Physiol. 193, 26-41. 10.1093/plphys/kiad229
Google Scholar: Author Only Title Only Author and Title

Mulvey, H., and Dolan, L. (2023a). RHO of plant signaling was established early in streptophyte evolution. Curr. Biol. 33, 5515-5525.e5514. https://doi.org/10.1016/j.cub.2023.11.007
Google Scholar: Author Only Title Only Author and Title

Mulvey, H., and Dolan, L. (2023b). RHO GTPase of plants regulates polarized cell growth and cell division orientation during morphogenesis. Curr. Biol. 33, 2897-2911.e2896. https://doi.org/https://doi.org/10.1016/j.cub.2023.06.015
Google Scholar: Author Only Title Only Author and Title

Nowak, M.A., Boerlijst, M.C., Cooke, J., and Smith, J.M. (1997). Evolution of genetic redundancy. Nature 388, 167-171. https://doi.org/10.1038/40618
Google Scholar: Author Only Title Only Author and Title

Ntefidou, M., Eklund, D.M., Le Bail, A., Schulmeister, S., Scherbel, F., Brandl, L., Dörfler, W., Eichstädt, C., Bannmüller, A., Ljung, K., and Kost, B. (2023). Physcomitrium patens PpRIC, an ancestral CRIB-domain ROP effector, inhibits auxin-induced differentiation of apical initial cells. Cell Rep. 42. https://doi.org/10.1016/j.celrep.2023.112130
Google Scholar: Author Only Title Only Author and Title

Okano, Y., Aono, N., Hiwatashi, Y., Murata, T., Nishiyama, T., Ishikawa, T., Kubo, M., and Hasebe, M. (2009). A polycomb repressive complex 2 gene regulates apogamy and gives evolutionary insights into early land plant evolution. Proc. Natl. Acad. Sci. U. S. A. 106, 16321-16326. https://doi.org/10.1073/pnas.0906997106
Google Scholar: Author Only Title Only Author and Title

Ou, H., and Yi, P. (2022). ROP GTPase-dependent polarity establishment during tip growth in plants. New Phytol. 236, 49-57. https://doi.org/10.1111/nph.18373
Google Scholar: Author Only Title Only Author and Title

Raval, P.K., Ngan, W.Y., Gallie, J., and Agashe, D. (2023). The layered costs and benefits of translational redundancy. eLife 12, e81005. https://doi.org/10.7554/eLife.81005
Google Scholar: Author Only Title Only Author and Title

Ren, H., Dang, X., Yang, Y., Huang, D., Liu, M., Gao, X., and Lin, D. (2016). SPIKE1 Activates ROP GTPase to Modulate Petal Growth and Shape. Plant Physiol. 172, 358-371. 10.1104/pp.16.00788
Google Scholar: Author Only Title Only Author and Title

Rensing, S.A., Goffinet, B., Meyberg, R., Wu, S.-Z., and Bezanilla, M. (2020). The Moss Physcomitrium (Physcomitrella) patens: A Model Organism for Non-Seed Plants. Plant Cell 32, 1361-1376. https://doi.org/10.1105/tpc.19.00828
Google Scholar: Author Only Title Only Author and Title

Rensing, S.A., Ick, J., Fawcett, J.A., Lang, D., Zimmer, A., Van De Peer, Y., and Reski, R. (2007). An ancient genome duplication contributed to the abundance of metabolic genes in the moss Physcomitrella patens. BMC Evol. Biol. 7, 130. https://doi.org/10.1186/1471-2148-7-130
Google Scholar: Author Only Title Only Author and Title

Reski, R., and Abel, W.O. (1985). Induction of budding on chloronemata and caulonemata of the moss, Physcomitrella patens, using isopentenyladenine. Planta 165, 354-358. https://doi.org/10.1007/bf00392232
Google Scholar: Author Only Title Only Author and Title

Roszak, P., Heo, J.-o., Blob, B., Toyokura, K., Sugiyama, Y., de Luis Balaguer, M.A., Lau, W.W.Y., Hamey, F., Cirrone, J., Madej, E., Bouatta, A.M., Wang, X., Guichard, M., Ursache, R., Tavares, H., Verstaen, K., Wendrich, J., Melnyk, C.W., Oda, Y., Shasha, D., Ahnert, S.E., Saeys, Y., De Rybel, B., Heidstra, R., Scheres, B., Grossmann, G., Mähönen, A.P., Denninger, P., Göttgens, B., Sozzani, R., Birnbaum, K.D., and Helariutta, Y. (2021). Cell-by-cell dissection of phloem development links a maturation gradient to cell specialization. Science 374, eaba5531. https://doi.org/10.1126/science.aba5531
Google Scholar: Author Only Title Only Author and Title

Ruan, J., Lai, L., Ou, H., and Yi, P. (2023). Two subtypes of GTPase-activating proteins coordinate tip growth and cell size regulation in Physcomitrium patens. Nat. Commun. 14, 7084. https://doi.org/10.1038/s41467-023-42879-y
Google Scholar: Author Only Title Only Author and Title

Schaefer, D., Zryd, J.-P., Knight, C.D., and Cove, D.J. (1991). Stable transformation of the moss Physcomitrella patens. Mol. Gen. Genet. 226, 418-424. https://doi.org/10.1007/BF00260654
Google Scholar: Author Only Title Only Author and Title

Schaefer, D.G., and Zrÿd, J.-P. (1997). Efficient gene targeting in the moss Physcomitrella patens. Plant J. 11, 1195-1206. https://doi.org/10.1046/j.1365-313x.1997.11061195.x
Google Scholar: Author Only Title Only Author and Title

Schindelin, J., Arganda-Carreras, I., Frise, E., Kaynig, V., Longair, M., Pietzsch, T., Preibisch, S., Rueden, C., Saalfeld, S., Schmid, B., Tinevez, J.-Y., White, D.J., Hartenstein, V., Eliceiri, K., Tomancak, P., and Cardona, A. (2012). Fiji: an open-source platform for biological-image analysis. Nat. Methods 9, 676-682. https://doi.org/10.1038/nmeth.2019
Google Scholar: Author Only Title Only Author and Title

Schumaker, K.S., and Dietrich, M.A. (1997). Programmed Changes in Form during Moss Development. Plant Cell 9, 1099-1107
Google Scholar: Author Only Title Only Author and Title

Stephan, O., Cottier, S., Fahlén, S., Montes-Rodriguez, A., Sun, J., Eklund, D.M., Klahre, U., and Kost, B. (2014). RISAP Is a TGN-associated RAC5 effector regulating membrane traffic during polar cell growth in tobacco. Plant Cell 26, 4426-4447. https://doi.org/10.1105/tpc.114.131078
Google Scholar: Author Only Title Only Author and Title

The UniProt Consortium. (2024). UniProt: the Universal Protein Knowledgebase in 2025. Nucleic Acids Res., gkae1010. 10.1093/nar/gkae1010
Google Scholar: Author Only Title Only Author and Title

Thelander, M., Olsson, T., and Ronne, H. (2004). Snf1-related protein kinase 1 is needed for growth in a normal day–night light cycle. EMBO J. 23, 1900-1910. https://doi.org/10.1038/sj.emboj.7600182
Google Scholar: Author Only Title Only Author and Title

Thelander, M., Nilsson, A., Olsson, T., Johansson, M., Girod, P.-A., Schaefer, D.G., Zrÿd, J.-P., and Ronne, H. (2007). The moss genes PpSKI1 and PpSKI2 encode nuclear SnRK1 interacting proteins with homologues in vascular plants. Plant Mol. Biol. 64, 559-573. https://doi.org/10.1007/s11103-007-9176-5
Google Scholar: Author Only Title Only Author and Title

Thole, J.M., Perroud, P.F., Quatrano, R.S., and Running, M.P. (2014). Prenylation is required for polar cell elongation, cell adhesion, and differentiation in Physcomitrella patens. Plant J. 78, 441-451. 10.1111/tpj.12484
Google Scholar: Author Only Title Only Author and Title

Viaene, T., Landberg, K., Thelander, M., Medvecka, E., Pederson, E., Feraru, E., Cooper, Endymion D., Karimi, M., Delwiche, Charles F., Ljung, K., Geisler, M., Sundberg, E., and Friml, J. (2014). Directional auxin transport mechanisms in early diverging land plants. Curr. Biol. 24, 2786-2791. https://doi.org/10.1016/j.cub.2014.09.056
Google Scholar: Author Only Title Only Author and Title

Vidali, L., Augustine, R.C., Kleinman, K.P., and Bezanilla, M. (2007). Profilin is essential for tip growth in the moss Physcomitrella patens. Plant Cell 19, 3705-3722. https://doi.org/10.1105/tpc.107.053413
Google Scholar: Author Only Title Only Author and Title

Vidali, L., Burkart, G.M., Augustine, R.C., Kerdavid, E., Tüzel, E., and Bezanilla, M. (2010). Myosin XI is essential for tip growth in Physcomitrella patens. Plant Cell 22, 1868-1882. https://doi.org/10.1105/tpc.109.073288
Google Scholar: Author Only Title Only Author and Title

Vieten, A., Vanneste, S., WiśNiewska, J., Benková, E., Benjamins, R., Beeckman, T., Luschnig, C., and Friml, J.I. (2005). Functional redundancy of PIN proteins is accompanied by auxin-dependent cross-regulation of PIN expression. Development 132, 4521-4531. https://doi.org/10.1242/dev.02027
Google Scholar: Author Only Title Only Author and Title

Winge, P., Brembu, T., Kristensen, R., and Bones, A.M. (2000). Genetic Structure and Evolution of RAC-GTPases in Arabidopsis thaliana. Genetics 156, 1959-1971
Google Scholar: Author Only Title Only Author and Title

Yalovsky, S., Bloch, D., Sorek, N., and Kost, B. (2008). Regulation of membrane trafficking, cytoskeleton dynamics, and cell polarity by ROP/RAC GTPases. Plant Physiol. 147, 1527-1543. 10.1104/pp.108.122150
Google Scholar: Author Only Title Only Author and Title

Yi, P., and Goshima, G. (2020). Rho of plants GTPases and cytoskeletal elements control nuclear positioning and asymmetric cell division during Physcomitrella patens branching. Curr. Biol. 30, 2860-2868. https://doi.org/10.1016/j.cub.2020.05.022

Google Scholar: Author Only Title Only Author and Title